Transport of adsorbates at metal surfaces: from thermal migration to hot precursors

J.V. Barth

Institut de Physique Expérimentale, Ecole Polytechnique Fédérale de Lausanne, CH-1015 Lausanne, Switzerland

ELSEVIER

Amsterdam–Lausanne–New York–Oxford–Shannon–Tokyo

Contents

ELSEVIER

Surface Science Reports 40 (2000) 75–149

surface science reports

www.elsevier.nl/locate/surfrep

Transport of adsorbates at metal surfaces: from thermal migration to hot precursors

J.V. Barth*

Institut de Physique Expérimentale, Ecole Polytechnique Fédérale de Lausanne, CH-1015 Lausanne, Switzerland

Manuscript received in final form 28 March 2000

Abstract

Theoretical aspects and evolution of surface diffusion studies are discussed with an emphasis on non-metallic adsorbates at metal surfaces. A survey of the existing literature is presented with the main experimental results tabulated. (The tables and their updates are available online at http://ipent.epfl.ch/gr_kern/jv_barth/SD_tables.html) Conception, theoretical and experimental work on transient mobility in the adsorption of gases on metal surfaces are summarized. © 2000 Elsevier Science B.V. All rights reserved.

1. Introduction

The transport of atoms or molecules at solid metal surfaces plays a vital role in a multitude of surface physical and chemical processes: in heterogenous catalysis reaction partners usually adsorb and diffuse at the surface before the products form. Surface mobility is a prerequisite in associative thermal desorption. The equilibration of surface phases or the growth of regular films implies lateral motions of the respective adsorbed species. The formation of nanostructures at surfaces via self-assembly or diffusion limited aggregation requires a balancing of the mobility characteristics and the corresponding lateral interactions. Finally, the adsorption process of atoms or molecules per se may involve transient motions.

Surface mobility thus comprises several aspects.

On the one hand it is the aleatoric thermal mobility of adsorbed particles, which has been macroscopically observed as early as 1785 for the case of powdered charcoal floating on an alcohol surface [1]. This is a Brownian motion [2,3] in two dimensions, as illustrated in Fig. 1.

The basic physical principles of Brownian motion have been elucidated early this century (cf. [4–6]). In the absence of external forces it is a stochastic process reflecting the never ceasing energy fluctuations of a system in thermal equilibrium. When the particles are adsorbed on a homogenous surface and do not interact with each other, this leads to simple random walks.

* Fax: +41-21-693-3604

E-mail address: johannes.barth@epfl.ch (J.V. Barth).

0167-5729/00/$ – see front matter
PII: S0167-5729(00)00002-9

Nomenclature

a	surface lattice constant
Å	Ångström (1×10^{-10} m)
d	dimensionality
D	diffusion coefficient
D_0	pre-exponential factor (prefactor)
D^*	tracer diffusion coefficient
$\tilde{D}$	collective diffusion coefficient
$\overline{D}$	jump diffusion coefficient
eV	electron volt ($1\,\text{eV} = 1.6 \times 10^{-19}\,\text{J} = 23.06\,\text{kcal mol}^{-1} = 96.5\,\text{kJ mol}^{-1} = 8065\,\text{cm}^{-1}$)
E_b	bonding energy of an adsorbate
E_d	energy barrier in collective diffusion
E_m	energy barrier in tracer diffusion
f.c.c.	face-centered cubic
h	Planck constant (4.1×10^{-15} eV s)
j	diffusion flux
k_B	Boltzmann constant ($8.62 \times 10^{-15}\,\text{eV K}^{-1}$)
L	Langmuir ($1\,\text{L} = 1 \times 10^{-6}$ Torr s)
m	adsorbate mass
n	number of adsorbates in an ensemble
t	time
T	temperature

Greek letters

β	$(k_B T)^{-1}$
η	friction coefficient
Φ	thermodynamic factor
Γ	hopping frequency
$\langle\lambda\rangle$	mean jump length
μ	chemical potential
Θ, θ	coverage
ω_0	particle vibrational frequency in adsorption well

Abbreviations

AES	Auger electron spectroscopy
DFT	density functional theory
FEM	field emission microscopy
FIM	field ion microscopy
HAS	helium atom scattering
HREELS	high-resolution electron energy-loss spectroscopy
IRAS	infra-red absorption spectroscopy
LEED	low-energy electron scattering
LITD	laser-induced thermal desorption

LOD	linear optical diffraction
MC	Monte Carlo
MD	molecular dynamics
NMR	nuclear magnetic resonance
PEEM	photoemission electron microscopy
PES	potential energy surface
QHAS	quasielastic helium atom scattering
SHD	second-harmonic diffraction
STM	scanning tunneling microscopy
TDS	thermal desorption spectroscopy
TST	transition-state theory
UHV	ultra-high vacuum

On the other hand, a directed flux of adsorbates can be induced by the variation of their density or chemical potential at the surface. In this case one is dealing with a gradient-driven transport phenomenon for a system which is not in thermodynamic equilibrium. In its simplest form it can be described by Fick's law, where the concentration gradient is the driving force [8]. With increasing time, the resulting surface diffusion will lead to a smearing out of an initial concentration profile, as illustrated by the observations reproduced in Fig. 2. When eventually thermodynamic equilibrium is attained, there is a uniform adsorbate distribution on the surface and no further net surface mass transport takes place; nevertheless the aleatoric thermal mobility persists.

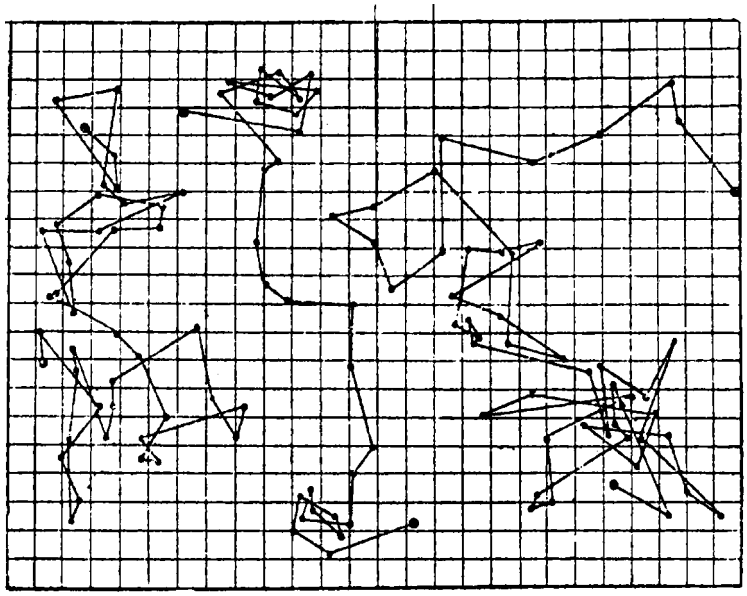

Fig. 1. Two-dimensional projection of gamboge particles performing random motions in an aqueous solution; the positions were determined in equal intervals of time (grid length scale $\approx 3\,\mu m$; from [7]).

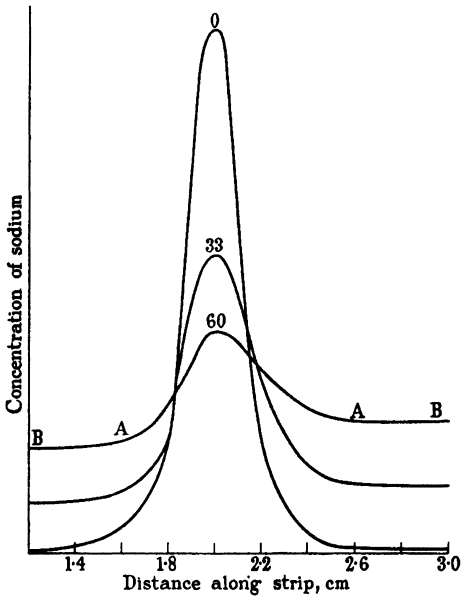

Fig. 2. Decay of a concentration gradient with time for Na atoms adsorbed on the surface of a tungsten ribbon, as monitored by spatially resolved photoelectric current measurements; from [9].

In both cases there is a strong temperature dependence. The higher the temperature, the more active the adsorbate motion and faster the gradient decay.

For the above situations the individual atoms or molecules are considered to be thermalized with the surface, i.e., on solid surfaces they experience the corrugation of the respective atomic lattice and are accomodated at distinct, energetically favorable sites, provided that the thermal energies are small. Surface mobility is thus closely related to diffusion phenomena in the bulk of solids, which have been extensively investigated (cf. [10–13]).

A further channel for transport of atoms or molecules at surfaces is related to the adsorption dynamics and the corresponding dissipation of the binding energy. This possible lateral motion of atoms or molecules in the process of thermalization is called ‘transient mobility’, since it is terminated upon equilibration. It may reflect the existence of a highly mobile precursor, which is only temporarily occupied. Such a precursor state is illustrated by the one-dimensional potential energy diagram in Fig. 3 for the activated dissociative adsorption of a molecule. An intermediate state for a molecule AB can be populated before the breaking of the molecular bond and the accomodation of the atomic species at the surface [14].

The objective of the present paper is to review surface and transient mobility of non-metallic adsorbates at metal surfaces in the light of recent developments in the field. Albeit comprehensive reviews [15–24], book sections [25,26], conference proceedings [27–29] and notably a seminal report [30] on surface diffusion exist, a fair number of new findings and technical developments have been reported since their publication, and the mobility of transient species at metal surfaces could be elucidated. Putting the results into perspective along with a critical discussion is believed to be beneficial for a better understanding of these topics.

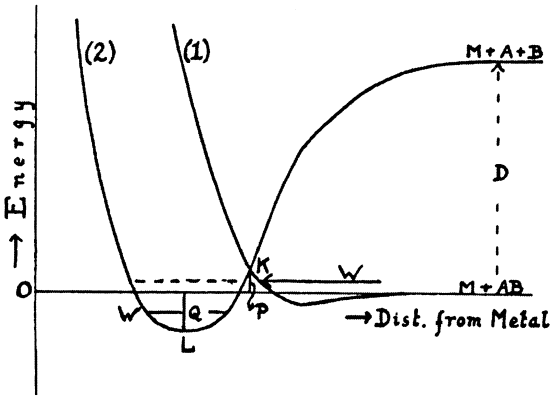

Fig. 3. One-dimensional potential energy diagram for the activated dissociative adsorption of a diatomic molecule AB. Curves (1) and (2) represent the interaction of the molecule and two widely separated atoms with the metal surface, respectively. They cross at K, where the corresponding energy barrier P is indicated. W is the energy of an incoming molecule, W' the sum of the two vibrational energies of the two atoms after adsorption, Q the depth of the atomic adsorption well. From [14].

2. Theoretical aspects of surface migration

Atoms coming from the gas phase into contact with a metal surface thermalize with the phonon heat bath of the crystal upon adsorption, i.e., the substrate thermal energy can be associated with the adsorbate. The adsorbate similarly experiences the periodic substrate atomic lattice, which is illustrated in Fig. 4. The binding energy is subject to lateral variation with local minima corresponding to energetically favorable positions. These adsorption sites are separated by energy barriers being significantly smaller than the energy barrier for desorption. The minimum energy difference between adjacent sites is the migration energy barrier E_m. In the case of anisotropic surfaces, direction dependent migration barriers along principal crystal axes can be present.

The excitation and damping of the thermal motion of an adsorbate is predominantly mediated by the coupling to the substrate phonon bath. The typical frequency of the phonons is $\sim 10^{12}-10^{13}\,s^{-1}$, with surface atom vibrational amplitudes of ~ 0.1 Å at room temperature. The magnitude of the thermal energies with respect to the migration energy barrier is decisive for the possible lateral motion of adsorbates on the surface (for the special case of quantum mechanical tunneling of adsorbates through the barrier, cf. Section 4.1.1).

It is helpful to discriminate two situations:

1. $k_BT \ll E_m$: when the thermal energies are small, the adsorbates are confined to the adsorption sites, corresponding generally to high-symmetry positions on the surface. A temperature can be identified where the adatoms can be considered immobile with respect to a timescale of interest. For temperatures exceeding this value, surface migration is driven by the continous energy exchange between adsorbate and substrate. The corresponding energy fluctuations result in random jumps from one energy minimum to another, i.e., a stochastic hopping mechanism is operative. Most of the time the adsorbates remain in the adsorption well, where they are vibrating, and only rarely the energy necessary to overcome the migration barrier is accumulated. Hence it is frequently assumed that subsequent jumps are uncorrelated, i.e., that hopping is a Markov process. Upon averaging over many events, a hopping rate can be defined.

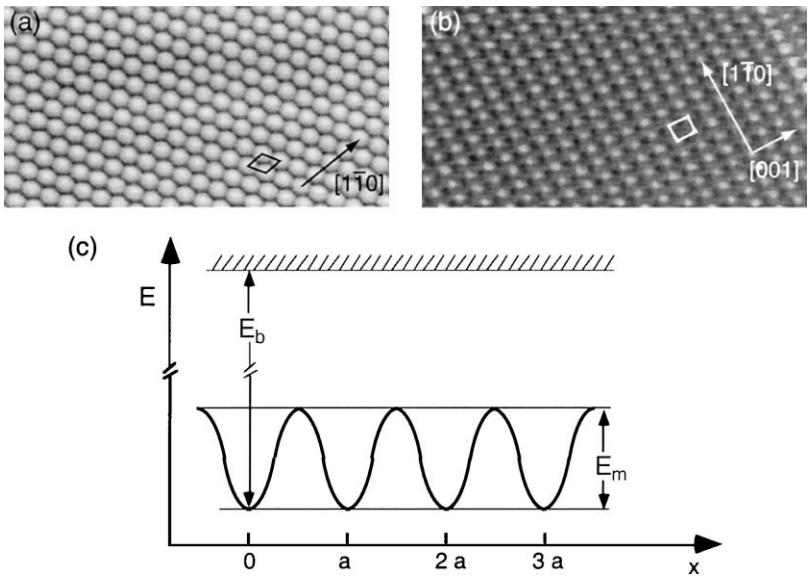

Fig. 4. STM images resolving (a) the hexagonal atomic structure of the close-packed f.c.c.(1 1 1) surface and (b) the anisotropic f.c.c.(1 1 0) surface of Ag. The surface unit cells and high symmetry directions are marked. (c) Schematic one-dimensional potential energy surface experienced by an adsorbate along a high-symmetry surface direction (E_m: migration energy barrier; E_b: bonding energy; a: surface lattice constant).

2. Range $k_BT \sim E_m$ to $k_BT \gg E_m$: with thermal energies close to or exceeding the migration energy barrier, the effect of the lateral surface corrugation on the adsorbate motion becomes smaller or even negligible. Surface migration is thus less restricted and the adatoms transport rather freely on the surface without confinement to specific sites. Consequently, the definition of a hopping rate is senseless. This situation can be described as two-dimensional Brownian motion. The corresponding diffusion coefficient for high thermal energies is expected to obey [4,21,31,32]:

$$D = \frac{k_BT}{m\gamma}, \tag{2.1}$$

where γ is the friction associated with the unconfined particle random motion. The correlation between D and the associated mobility B describing the behavior of the adsorbate in an external force field is provided by the Einstein relation $B = D/k_BT$. The same equation is encountered in the case of Brownian motion in a fluid with viscosity coefficient γ. Note that in most cases thermal desorption becomes appreciable when the thermal energy approaches the migration barrier, and hence desorption and diffusion coproceed. The migration barrier is usually an order of magnitude smaller than the bonding energy.

D will be considered in the following as a scalar; for the general description a diffusion tensor must be invoked (cf. [21,30]):

$$\underline{\underline{D}} = \begin{pmatrix} D_{xx} & D_{xy} \\ D_{yx} & D_{yy} \end{pmatrix}.$$

Most surface science experiments dealing with surface migration have been performed in the range where the condition $k_B T \ll E_m$ holds. Theoretical work suggests that the '$\ll$' condition is fulfilled for $k_B T < \frac{1}{5} E_m$ (cf. [21,33]). Only preliminary insight has been gained into the nature of surface diffusion in the transition regime (e.g., [21,34,35]).

It must be underlined that the results obtained in the hopping regime are not a priori of general validity and care has to be taken in the extrapolation of, say, the migration characteristics of CO on a catalytically active metal determined at low temperatures to obtain those under reaction conditions in an industrial process.

2.1. The isolated adsorbate in the hopping model

In the hopping model, the migration of an isolated adatom corresponds to an aleatoric walk from adsorption site to adsorption site. Upon denoting the starting point of the motion at $t = 0$ as $\boldsymbol{r}_0 \equiv (x_0, y_0)$, the mean jump length along the x, y directions as $\langle \lambda_x \rangle$, $\langle \lambda_y \rangle$ and the corresponding hopping frequencies as Γ_x, Γ_y, the mean square displacement of the atom is

$$\langle (\boldsymbol{r}(t) - \boldsymbol{r}_0)^2 \rangle \equiv \langle (\Delta \boldsymbol{r})^2 \rangle = (\Gamma_x \langle \lambda_x \rangle^2 + \Gamma_y \langle \lambda_y \rangle^2) t, \tag{2.2}$$

which reduces for an isotropic surface to

$$\langle (\Delta \boldsymbol{r})^2 \rangle = \Gamma_h \langle \lambda \rangle^2 t. \tag{2.3}$$

A characteristic property of surface migration is that $\langle (\Delta \boldsymbol{r})^2 \rangle$ varies linearly with time. Note that the very definition of a hopping frequency Γ_h tacitly implies statistic averaging over many hopping events. The time difference between the individual jumps of a specific particle varies stochastically. The corresponding *tracer diffusion coefficient* is defined as

$$D^* = \lim_{t \to \infty} \frac{\langle (\Delta \boldsymbol{r})^2 \rangle}{2dt}, \tag{2.4}$$

where d is the dimensionality of the diffusion process ($d = 1, 2$ at surfaces). From (2.3) and (2.4) it follows that D^* can be expressed in terms of the hopping rate Γ_h and the mean jump length $\langle \lambda \rangle$

$$D^* = \frac{1}{2d} \langle \lambda \rangle^2 \Gamma_h. \tag{2.5}$$

Experimental evidence demonstrates that quite generally the tracer diffusion coefficient obeys an Arrhenius law and accordingly the data are interpreted in terms of the equation

$$D^* = \frac{1}{2d} \langle \lambda \rangle^2 \nu_0 \exp[-\beta E_m] \equiv D_0^* \exp[-\beta E_m], \tag{2.6}$$

where ν_0 is designated as the *attempt frequency*, D_0^* as the *pre-exponential factor* (or *prefactor*) of the tracer diffusion, $\beta = [k_B T]^{-1}$. A unique migration barrier is posed. Eq. (2.6) is a fundamental relation in surface migration.

When nearest-neighbor jumps prevail, $\langle \lambda \rangle$ is equal to the surface lattice constant a. Since $a \sim 3$ Å and since the attempt frequency can be associated with the vibrational frequency of the adsorbate in the adsorption well (typically 10^{13} s^{-1} [36]), the pre-exponential factor is expected to be $\sim 10^{-3}$ cm^2 s^{-1}, which is frequently considered as an universal value.

An important parameter is the probability P_ξ for finding an atom at a specific site ξ after a time interval τ, which was localized at $\xi = 0$ for $\tau = 0$. In the case $\langle\lambda\rangle = a$, P_ξ reads in one dimension [37]

$$P_\xi(\tau) = \exp[-\Gamma_h\tau] I_\xi(\Gamma_h\tau), \tag{2.7}$$

where ξ is expressed in units of a, and I_ξ is the modified Bessel function of the first kind of order ξ [38]. This allows for the determination of the hopping rate from a measured adsorbate displacement distribution. In the simplest case, Γ_h is obtained from the probability P_0 that the adsorbate does not move in the time interval τ, given by

$$P_0(\tau) = \exp[-\Gamma_h\tau]. \tag{2.8}$$

In the spatial continuum limit and for long time intervals the analogous probability distribution P_r is a Gaussian (e.g., [4]), which reads for two-dimensional isotropic diffusion

$$P_r(\tau)\,\mathrm{d}^2r = \frac{1}{\sqrt{\pi a^2\Gamma_h\tau}}\exp\left[-\frac{r^2}{a^2\Gamma_h\tau}\right]\mathrm{d}^2r = \frac{1}{\sqrt{4\pi D^*\tau}}\exp\left[-\frac{r^2}{4D^*\tau}\right]\mathrm{d}^2r, \tag{2.9}$$

where (2.5) was used to substitute for D^*. Expressions for P with more complicated hopping mechanisms in one and two dimensions can be found in Refs. [16,39,40].

As an illustration for hopping migration of an adsorbate on low-index f.c.c. surfaces, consider the model in Fig. 5. Defining the hopping rate in one direction as Γ_s, the diffusivity in two dimensions can be determined. Next-neighbor hopping is assumed.

The mean square displacement along a direction labeled x is

$$\langle(\Delta x)^2\rangle = t\sum_{\alpha=1}^{\varsigma}\Gamma_s x_\alpha^2, \tag{2.10}$$

and hence the one-dimensional tracer diffusion coefficient

$$D_x^* = \frac{1}{2}\sum_{\alpha=1}^{\varsigma}\Gamma_s x_\alpha^2, \tag{2.11}$$

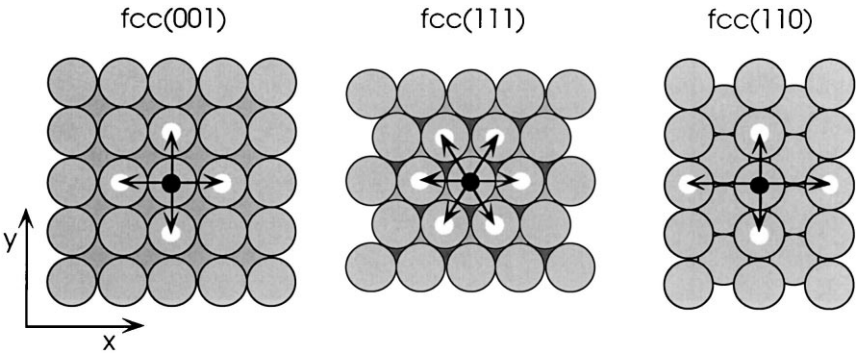

Fig. 5. Ball model for next-neighbor hopping on the f.c.c.(0 0 1), f.c.c.(1 1 1) and f.c.c.(1 1 0) surface. Arrows mark the possible jumps from an adsorbate at the origin. For the f.c.c.(1 1 1) symmetry two inequivalent hollow sites exist (marked light and dark gray, respectively).

where x_α is the projection length of the jump vector on the x-direction, and ζ the number of attainable sites. The total hopping frequency is accordingly $\Gamma_h = \zeta\Gamma_s$.

Due to the symmetry of the f.c.c.(0 0 1) surface, $D_x^* = D_y^* \equiv D^*$. Since $\zeta = 4$ for two-dimensional hopping, $D^* = a^2\Gamma_s = \frac{1}{4}a^2\Gamma_h$.

For the f.c.c.(1 1 1) surface, $D_x^* = D_y^* = \frac{3}{2}a^2\Gamma_s \equiv D^*$. Since $\zeta = 6$, $D^* = \frac{1}{4}a^2\Gamma_h$.

When the adsorbate binds at the hollow sites, and these are energetically degenerate, the jump length is reduced to $a/\sqrt{3}$ with $\zeta = 3$. Hence $D_x^* = D_y^* = \frac{1}{4}a^2\Gamma_s$ and $D^* = \frac{1}{12}a^2\Gamma_h$.

The f.c.c.(1 1 0) surface has a rectangular unit cell. Thus distinct energy barriers for hopping along the principal directions exist and anisotropic diffusion associated with different directional hopping rates Γ_{sx} and Γ_{sy} is expected. The diffusivities along the principal directions are $D_x^* = a^2\Gamma_{sx} = \frac{1}{2}a^2\Gamma_x$ and $D_y^* = b^2\Gamma_{sy} = \frac{1}{2}b^2\Gamma_y$ (since $\zeta = 2$; a and b are the lattice constants along the x and y directions, respectively).

The application of this concept for other geometries is straightforward [13].

Theoretical ansätze justifying the Arrhenius relation in (2.6) and thus providing Γ_s are as follows.

2.1.1. Transition state theory

An expression for the hopping frequency can be obtained by means of transition state theory (TST), which is based on a semiclassical description of the problem [20,21,41–43]. In TST a thermodynamical equilibrium distribution of adsorbates in the transition state at the saddle point of the energy barrier separating the energy minima of neighboring adsorption sites is posed. Implicitly assumed are (i) next-neighbor hopping (due to strong coupling between adsorbate and substrate), i.e., $\langle\lambda\rangle = a$, and (ii) the transition state is a point of no return, a classical mechanics statement which excludes dynamical effects such as recrossing and quantum mechanical tunneling through the barrier. The corresponding rate Γ_s is determined to

$$\Gamma_s = \frac{k_B T}{h}\frac{Z^{\neq}}{Z_0}\exp[-\beta E_m] \tag{2.12}$$

or, equivalently

$$\Gamma_s = \frac{k_B T}{h}\exp\left[\frac{\Delta S^{\neq}}{k_B}\right]\exp[-\beta E_m], \tag{2.13}$$

where Z_0 and $Z^{\neq}$ are the partition functions of the ground and transition state, respectively, and $\Delta S^{\neq} \equiv S^{\neq} - S_0$ denotes the corresponding formal entropy change. When it can be neglected, the prefactor reduces to $k_B T/h$, which amounts to $6.3 \times 10^{12}\,s^{-1}$ at 300 K. For the simple case of a one-dimensional system without coupling to a bath the rate reduces as [42]

$$\Gamma_s \approx \frac{\omega_0}{2\pi}\exp[-\beta E_m], \tag{2.14}$$

where $\omega_0 = \sqrt{U''(x_0)/m}$ is the particle vibration frequency at the well bottom, as illustrated in Fig. 6.

This is formally similar to a useful estimate for the TST hopping rate, which can be formulated with the frustrated translational mode ν_T, i.e., the vibrational mode of the adsorbate parallel to the surface. When $h\nu_T \ll k_B T$, Γ_s can be approximated as (e.g., [44])

$$\Gamma_s \approx \nu_T \exp[-\beta E_m]. \tag{2.15}$$

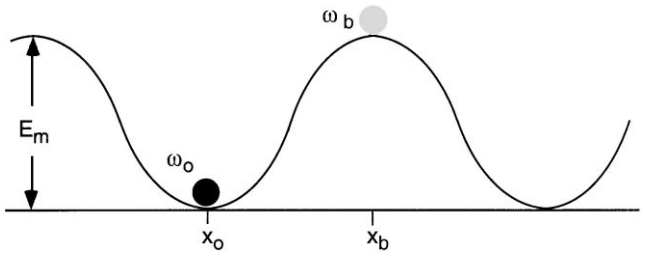

Fig. 6. One-dimensional representation of the escape from a particle confined to a binding site at x_0 by the migration energy barrier E_m at x_b. ω_0 and ω_b are the angular vibration frequencies associated with the minimum and the saddle point of the potential energy.

2.1.2. Langevin dynamics

It has been shown that the TST result principally represents an upper bound for the true hopping rate (see [42]). A starting point for a wider treatment is the Langevin equation [45], which reads for the one-dimensional motion of a particle with mass m in the periodic potential $U(x)$

$$m\partial_t v = -\partial_x U(x) - \eta m v + \xi(t), \tag{2.16}$$

where $v = \partial_t x$. The motion is subject to a dynamical damping with a friction coefficient η and excited by a stochastic force $\xi(t)$, which satisfies the fluctuation–dissipation theorem:

$$\langle \xi(t) \rangle = 0, \qquad \langle \xi(t)\xi(t') \rangle = 2m\eta k_B T \delta(t - t'). \tag{2.17}$$

The physical idea is to incorporate the random excitations driving the stochastic motion in the Langevin force. The excitation force has a mean value of zero. Its temperature-dependent noise strength $2m\eta k_B T$ ensures that the average energy of the adsorbate obeys the classical statistical physics equipartition law ($\langle E \rangle = \frac{1}{2} k_B T$ per degree of freedom). The excitations are opposed by the continous damping force $\eta m v$. It has been pointed out that these are drastic assumptions since it is supposed that for the former 'the discontinuity of events taking place is essential', while for the latter 'it is trivial and can be ignored' [4].

The time evolution of the particle's probability density $P = P(x, v, t)$ is then given by the related Fokker–Planck equation, the Klein–Kramers equation [42,46–48]

$$\partial_t P(x, v, t) = \left(-\partial_x v - \partial_v \frac{F(x) - m\eta v}{m} + \frac{\eta k_B T}{m} \partial_v^2 \right) P(x, v, t), \tag{2.18}$$

where $F(x) = -\partial_x U(x)$. Kramers employed this equation to model the escape rate from a potential well, which for the case of moderate to strong friction under the condition $\eta/\omega_b > k_B T/E_m$ was determined as [42,47]

$$\Gamma_s = \frac{\sqrt{\frac{1}{4}\eta^2 + \omega_b^2} - \frac{1}{2}\eta}{\omega_b} \frac{\omega_0}{2\pi} \exp[-\beta E_m], \tag{2.19}$$

where $\omega_b = \sqrt{U''(x_b)/m}$ denotes the vibration frequency at the barrier (cf. Fig. 6). Interesting are the limits of moderate friction, for which the TST result formulated in Eq. (2.8) is recovered, and that for

strong friction (Smoluchowski limit)

$$\Gamma_s \approx \frac{\omega_0 \omega_b}{2\pi\eta} \exp[-\beta E_m]. \tag{2.20}$$

On the other hand, in the case of $\eta/\omega_b < k_B T/E_m$ and weak friction ($\eta \to 0$), the rate is given by [42,47]

$$\Gamma_s \approx \eta\beta E_m \frac{\omega_0}{2\pi\omega_b} \exp[-\beta E_m]. \tag{2.21}$$

A striking consequence of the rate behavior derived for the limiting cases is that for both strong and weak friction the transition rate is proportional to the damping coefficient, i.e., Γ_s is reduced either with decreasing and increasing η. This implies a turnover behavior of the rate with varying friction. The rate maximum is found at $\eta/\omega_b \approx k_B T/E_m$, where the TST result is approached [33,42].

Comprehensive treatises on the Fokker–Planck equation and Kramer's reaction rate theory can be found in Refs. [4,5,42,48–51]. Over the last years several groups studied surface migration in this framework or generalizations thereof [25,33,52–68].

An important feature of the Kramers approach is that the TST restriction of next-neighbor hopping is lifted when the damping is weak. Since, according to Eq. (2.5), both jump length and hopping frequency determine the diffusion coefficient, this allows for a more complete description of surface migration. There is a general agreement now that long jumps occur naturally in the weak friction limit [33,44,56,62,66,67,69]. The increased jump length may even overbalance the effect of the reduced hopping rates and lead to an increase in diffusivity in this regime, which exceeds the values expected from TST. However, for the comparison with experimental results a thorough understanding of the friction at the atomic level is required. Most calculations performed so far concentrate on the friction parameter via the phonon-coupling between adsorbate and substrate (e.g., [56,62,70–72]). This seems to be the most important process for energy dissipation [73–75]. Nevertheless, significant electronic friction (via creation of electron–hole pairs) may exist [72,76–78]. Typically, the friction coefficient in surface migration is a mere fraction of the adsorbate vibrational frequency ($\eta \sim 0.1\omega_0$ [62,72]).

In recent work, a microscopic memory function has been introduced which accounts for the friction parameter [21,69,79–84]. This approach bears the advantage that the memory function can be related to the surface vibrations and on its basis a 'unified picture of the qualitative, universal properties of surface diffusion' was proposed [21].

2.1.3. Computation of hopping migration parameters

Molecular dynamics (MD) simulations of hopping adsorbates are widely employed and have been reviewed in Refs. [20,85]. With such simulations the dynamics are calculated by solving the classical mechanics equations of motion. The temporal and spatial evolution of an adsorbate interacting with vibrating surface atoms are obtained. MD simulations elucidate real systems and provide a means to test the above rate theories. A link between experimental findings and basic theoretical studies can thus be established. MD investigations of the surface migration of single chemisorbed species have been reported in Refs. [44,74,86,87]. MD simulations were similarly employed to address the complex diffusion mechanisms of large adsorbed molecules, where conformational changes of the adsorbate may exist [88–93].

On the other hand, it is possible to perform total energy calculations to elucidate the potential energy surface (PES) relevant in surface migration [94–101]. For this purpose the surface corrugation is mapped by

calculating the energies for different static configurations. The dynamical aspect may be treated in the framework of TST, via calculation of the frustrated translation frequency or other approaches.

It must be noted that the interpretation of both migration barrier and attempt frequency may be complicated by dynamic effects mediated by substrate phonons or lattice distortions. This is discussed in a number of theoretical investigations [21,57,80,81,102–108]. Substantial variations of the migration barrier and attempt frequency with the temperature were proposed in some cases.

It is also possible that the migration barrier calculated for a static substrate–adsorbate configuration may be unequal to that relevant for the migration at finite temperatures. In this case it is convenient to speak of a dynamic migration barrier.

Similarly, care must be taken when the limits of the validity range of the rate theories is approached and the nature of the surface diffusion mechanism is expected to undergo severe changes [21,34,35,109–111].

2.2. Collective processes at finite coverages

From the consideration of isolated adsorbates hopping from site to site on a homogeneous surface basic mechanisms governing surface migration are elucidated. With real systems, however, typically a situation is encountered where the surface is covered by a finite adsorbate concentration Θ.

The tracer diffusion coefficient for an ensemble of interacting adsorbates can be formulated straightforward, analogous to Eq. (2.4), as

$$D^* = \lim_{t\to\infty} \frac{1}{2dnt} \sum_{i=1}^{n} \langle (\Delta \boldsymbol{r}_i)^2 \rangle, \tag{2.22}$$

where n is the total number of particles in the ensemble.

An equivalent expression for D^* can be written in terms of the Green–Kubo velocity–velocity correlation formalism [30,112]

$$D^* = \frac{1}{dn} \sum_{i=1}^{n} \int_0^\infty \langle \boldsymbol{v}_i(0) \cdot \boldsymbol{v}_i(t) \rangle \, \mathrm{d}t. \tag{2.23}$$

Upon considering the stochastic motion in a microscopic picture, it becomes clear that the existence of an adsorbate layer leads to modifications of the atomic environment of an adsorbate under consideration, whose effect must be considered. Provided that $k_B T \ll E_m$, the simplest consequence of a finite coverage is site blocking, i.e., the reduction of the number of accessible sites for a moving adsorbate. When there is exclusively mutual site blocking of adsorbates on a fixed array of bonding sites (the Langmuir lattice gas), the tracer diffusion coefficient varies according to the relation $D^*(Q) = D^*(Q=0)[1-Q]$ [30,113]. In reality the adsorbates are furthermore subject to lateral interactions, which result in the deformation of the PES experienced by an adatom in the vicinity of another one. These adsorbate interactions may lead to correlated motions. Furthermore, surface mass transport via soliton diffusion [114,115] or other complex mechanisms [116–118] are envisioned.

Depending on the nature of the adsorbate–substrate complex the lateral interactions are either repulsive or attractive. This is illustrated in the diagram in Fig. 7, where it is assumed that only the nearest-neighbor ground state is affected. A direct consequence of these deformations is that for interacting adsorbates the migration energy barrier is locally reduced or increased in the case of

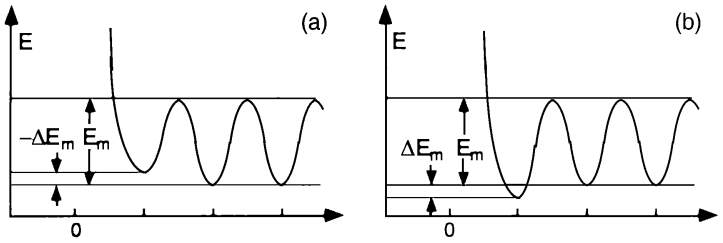

Fig. 7. Schematic potential energy deformation due to (a) repulsive and (b) attractive interactions for an adatom interacting with another adatom at the origin. E_m is the isolated adsorbate migration barrier and $\pm\Delta E_m$ the additional interaction energy.

repulsions or attractions, respectively. When the interactions are small, i.e., $|\Delta E_m| \ll E_m$ the attempt frequency is hardly affected, whereas substantial changes in the respective hopping rate due to a modification of the Boltzmann factor are expected: $\exp[-\beta E_m] \rightarrow \exp[-\beta(E_m \pm \Delta E_m)]$.

2.2.1. Surface diffusion and mass transport

Diffusion at finite coverages is usually described in macroscopic terms via an adsorbate flux density in two dimensions. The *chemical* or *collective diffusion* coefficient $\tilde{D}$ is accordingly defined through Fick's laws [8]. The first of these empirical laws describes the diffusion flux density $\boldsymbol{j}$ across a boarderline, which results from a coverage gradient in a continuum

$$\boldsymbol{j} = -\tilde{D}(\Theta)\nabla_r\Theta(\boldsymbol{r},t) \tag{2.24}$$

upon combination with the continuity equation $-\partial_t\Theta(\boldsymbol{r},t) = \nabla_r\boldsymbol{j}$, Fick's second law is obtained

$$\partial_t\Theta(\boldsymbol{r},t) = \nabla_r \cdot \tilde{D}(\Theta)\nabla_r\Theta(\boldsymbol{r},t). \tag{2.25}$$

The collective diffusion coefficient is thus relevant for the mass transport at surfaces. It generally depends on coverage. Note that these laws disregard the atomic structure of surfaces and are applicable only when the coverage variation is small at the atomic scale [13,30].

The diffusion equation (2.25) is widely employed to determine $\tilde{D}$, since the adsorbate concentration is a measurable quantity. In practice, often the decay of an adjusted coverage gradient is analyzed and (2.25) is solved numerically or analytically for a given geometry. This task is considerably simplified when diffusion coefficients independent of coverage exist or may be assumed and

$$\partial_t\Theta(\boldsymbol{r},t) = \tilde{D}\nabla_r^2\Theta(\boldsymbol{r},t). \tag{2.26}$$

When the temporal decay of a coverage gradient can be spatially resolved, the coverage dependence of $\tilde{D}$ can be determined by the Boltzmann–Matano method [30,119,120]. The corresponding solution of the diffusion equation for an initial step profile with $\Theta(x>0) = \Theta_0$ and $\Theta(x<0) = \Theta_{max}$ provides: $\tilde{D}(\Theta) = (1/2t)\,\mathrm{d}\Theta/\,\mathrm{d}x|_\Theta \int_{\Theta_o}^{\Theta} x\,\mathrm{d}\Theta'$ where t is the elapsed diffusion time, measured from the start of the profile decay.

In most experimental observations collective diffusion can be interpreted in terms of an Arrhenius law. Accordingly, the data are usually analyzed assuming that the energetics and dynamics can be factorized, i.e.

$$\tilde{D}(\Theta) = \tilde{D}_0 \exp[-\beta E_d]. \tag{2.27}$$

The diffusion barrier E_d is then obtained via the relation

$$E_d = -\partial_\beta \ln \tilde{D}. \tag{2.28}$$

It is clear that the migration barrier E_m of isolated adsorbates and E_d are a priori unequal, although they are related and should become identical in the zero coverage limit.

2.2.2. The thermodynamic factor

From a thermodynamics point of view surface mass transport is an irreversible process, i.e., the diffusion equations apply for systems which are not in thermal equilibrium and there is no Fickian diffusion once it is established. For a description from first principles, non-equilibrium thermodynamics are mandatory. In contrast, the thermal aleatoric motion of adsorbates is a natural property for equilibriated systems. They are reflected in the tracer diffusion coefficient, which is defined in the limit $t \to \infty$, thus excluding transport effects. The two coefficients are related. On the one hand the diffusive mass transport is a net flux averaging over a multitude of random displacements, which may be, due to their stochastic nature, directed partly against a chemical potential gradient. On the other hand, the random adsorbate motions of systems in equilibrium give rise to density fluctuations, whose relaxation can be in turn related to collective diffusion (following Onsager's hypothesis that fluctuation relaxation can be described by macroscopic laws [30,121–123]).

A unifying approach is the description of transport diffusion in the framework of irreversible thermodynamics [13,124]. The general diffusion flux at constant temperature is driven by a position dependent chemical potential μ on the surface [18,30,125,126]

$$\boldsymbol{j} = -L\nabla_r \mu, \tag{2.29}$$

where L is a phenomenological transport coefficient. Note that this expression does account for the adsorbate interactions, disregarded by Fick's laws. An expression comparable to Fick's second law is obtained upon reformulating Eq. (2.29) in one dimension

$$j = -L\partial_\Theta \mu \partial_x \Theta, \tag{2.30}$$

which allows for the identification $\tilde{D} = L\partial_\Theta \mu$ in this case. Upon employing specific expressions for the chemical potential, this relation can be used as a starting point to describe collective diffusion [126].

A more rigorous description can be formulated in terms of velocities, where $\boldsymbol{j}$(t) is expressed as

$$\boldsymbol{j}(t) = \sum_{i=1}^{n} \boldsymbol{v}_i(t). \tag{2.31}$$

It is obvious that the diffusion fluxes must change with time when mass transport at the surface occurs and that the diffusivity is a function of this change. In the Green–Kubo formalism this relation is established and can be formulated as [30,112]

$$\tilde{D} = \frac{1}{d\langle(\Delta n)^2\rangle} \int_0^\infty \langle \boldsymbol{j}(0) \cdot \boldsymbol{j}(t)\rangle \, \mathrm{d}t = \frac{1}{d\langle(\Delta n)^2\rangle} \int_0^\infty \left\langle \sum_{i=1}^{n} \boldsymbol{v}_i(0) \cdot \sum_{j=1}^{n} \boldsymbol{v}_j(t) \right\rangle \mathrm{d}t, \tag{2.32}$$

where $\langle(\Delta n)^2\rangle \equiv \langle(n - \langle n\rangle)^2\rangle$ is the corresponding mean square fluctuation of the number of adatoms $n(t)$ in the area element A of the ensemble, which is embedded in an infinite adsorbate layer providing

an ideal reservoir. The thermodynamic mean value of the particle number in A is $\langle n \rangle$. This formulation has the advantage that a correlation between tracer and collective diffusion can be expressed straightforward as [30,127]

$$\tilde{D} = D^* \frac{\langle n \rangle}{d\langle (\Delta n)^2 \rangle} \left[1 + \frac{\int_0^\infty \left\langle \sum_{i \neq j} \boldsymbol{v}_i(0) \cdot \boldsymbol{v}_j(t) \right\rangle \mathrm{d}t}{\int_0^\infty \left\langle \sum_{i=1}^n \boldsymbol{v}_i(0) \cdot \boldsymbol{v}_i(t) \right\rangle \mathrm{d}t} \right]. \tag{2.33}$$

Thus the two diffusion coefficients have in general a complex interdependence. However, in the case where the cross-correlations between the particle velocities are absent or can be neglected, the two coefficients are simply related via the particle number fluctuations

$$\tilde{D} = D^* \frac{\langle n \rangle}{d\langle (\Delta n)^2 \rangle}. \tag{2.34}$$

Now, the mean square number fluctuation is related to μ, β and Θ by the expression [30,126,128]

$$\frac{\langle n \rangle}{\langle (\Delta n)^2 \rangle} = \left. \frac{\partial(\mu\beta)}{\partial \ln \Theta} \right|_T \equiv \Phi, \tag{2.35}$$

whereby the definition of the *thermodynamic factor* Φ is introduced. This allows for the formulation of the so-called Darken equation [129] (originally proposed in the context of volume diffusion in alloys (cf. [13,130])) for the present case [30]

$$\tilde{D}(\Theta) \cong D^*(\Theta) \left. \frac{\partial(\mu\beta)}{\partial \ln \Theta} \right|_T = D^*(\Theta)\Phi. \tag{2.36}$$

For the case of a Langmuir gas, where no adsorbate interactions exist: $\Phi = [1 - \Theta]^{-1}$. Since in this case $D^*(\Theta) = D^*(\Theta = 0)[1 - \Theta]$ (in the absence of memory effects [131]), the chemical diffusion coefficient is independent of coverage, which result nicely illustrates the different nature of the respective coefficients (cf. [18,30]).

When the chemical potential of an adlayer is expressed as the sum of that of a Langmuir gas and the differential heat of adsorption $q(\Theta) = \partial_\Theta \overline{H}_\mathrm{a}(\Theta)$ as interaction term [115,126,132]

$$\mu = \mu_0 + k_\mathrm{B} T \ln \left[\frac{\Theta}{1 - \Theta} \right] - q(\Theta) \tag{2.37}$$

the thermodynamic factor is

$$\Phi = \frac{1}{1 - \Theta} - \beta \partial_\Theta q(\Theta). \tag{2.38}$$

In the limit of $\Theta \to 0$ the interactions between the particles become negligible and it is found that $\Phi = 1$, i.e., for isolated adsorbates the diffusion coefficients become identical. Accordingly, the Gaussian distribution (2.9) is a solution of Fick's second law for an initial δ-function. For the relation of the thermodynamic factor to observable quantities and other approximations for Φ, see Refs. [18,126].

It is well known that in the vicinity of phase transitions both fluctuations and chemical potential exhibit anomalies (e.g., [133]). Surface phase transitions thus strongly affect collective diffusivity in an adsorbate layer [18,21,30,115,134].

2.2.3. Collective diffusion and the hopping model

For a comprehensive description of collective diffusion from a microscopic point of view, the atomistic processes taking place in an ensemble of mobile adsorbates should be considered.

By approximation, collective diffusion can be reconciled with the hopping model by associating a coverage dependent effective jump rate with the motion of individual adsorbates. The ad hoc effective jump rate $\overline{\Gamma}(\Theta)$ accounts for the adsorbate interactions and the site exclusions at finite coverage. Thus collective diffusivity may be expressed as [126]

$$\tilde{D}(\Theta) \cong \frac{a^2}{2d}\overline{\Gamma}(\Theta)\frac{\partial(\mu\beta)}{\partial \ln \Theta}\bigg|_T = \frac{a^2}{2d}\overline{\Gamma}(\Theta)\Phi. \tag{2.39}$$

The leading term on the right-hand side of this expression is designated as the *jump diffusion coefficient* $\overline{D}$

$$\overline{D}(\Theta) = \frac{a^2}{2d}\overline{\Gamma}(\Theta). \tag{2.40}$$

Note the formal similarity of (2.39) with the Darken equation and that of $\overline{D}$ with the tracer diffusion coefficient for an isolated adsorbate (2.4). (cf. [30,135–137] for a more rigorous discussion of the jump diffusion coefficient, see also [123,138,139].) Accordingly, (2.39) is designated as the generalized Darken equation [135,140]. In fact, another formulation for $\overline{D}$ was suggested, which similarly demonstrates its close relation to D^* [127,141]

$$\overline{D} = \lim_{t\to\infty}\frac{1}{2dnt}\left\langle\left[\sum_{i=1}^{n}\Delta \boldsymbol{r}_i\right]^2\right\rangle. \tag{2.41}$$

The subtle difference between $\overline{D}$ and D^* is the averaging procedure. It is easily verified, taking this expression, that $\overline{D}$ and D^* are indeed identical in the absence of correlated motions, since then the average contribution of displacements associated with different adatoms is zero ($\langle \Delta \boldsymbol{r}_i \Delta \boldsymbol{r}_j\rangle = 0$) [127].

Casting $\overline{D}$ in the form (2.40) bears the advantage that a relation to the Kubo–Green equation can be obtained [30,141]

$$\tilde{D} = \frac{\langle n\rangle}{\langle(\Delta n)^2\rangle}\overline{D} = \Phi\overline{D}, \tag{2.42}$$

which reveals that tracer and jump diffusion coefficients are identical when the Darken equation holds.

With diffusivity measurements involving transport frequently a coverage independent $\tilde{D}$ over a concentration interval is assumed. Combining (2.28) and (2.39), the following relation is obtained [30,126]:

$$E_d \cong -\partial_\beta \ln\left[\overline{\Gamma}\Phi\right] = \overline{E} - \Phi^{-1}\frac{\partial^2\mu}{\partial \ln\Theta\partial\beta} = \overline{E} + \Phi^{-1}\frac{\partial \overline{H}_a}{\partial \ln\Theta} = \overline{E} + \Phi^{-1}\Theta q, \tag{2.43}$$

where $\overline{E} \equiv -\partial_\beta \ln\overline{\Gamma}$ is an effective energy barrier for jumps, $\overline{H}_a(\Theta)$ is the heat of adsorption and q the differential heat of adsorption per adatom. From this result it is inferred that the activation energy for collective diffusion depends on both temperature and coverage. This dependence can be associated with the varying adsorbate distribution on a surface, which, due to the lateral interactions, affects the effective hopping rate $\overline{\Gamma}$ and the differential heat of adsorption q. An important consequence is that Arrhenius behavior may not be expected over a wide temperature range for collective hopping diffusion. Note that in

the derivation of (2.43) the dependence of the prefactor on temperature and thermodynamic factor is neglected [126]. From experimental data $\tilde{D}_0$ is obtainable by $T \to \infty$ extrapolation of $\tilde{D}$ and thus necessarily depends on the temperature range under investigation for a temperature-dependent $\tilde{D}$.

2.2.4. Computational methods for collective diffusion

Monte Carlo (MC) simulations (cf. [142–144]) are frequently employed to get insight into the microscopic diffusion scenario and to relate the microscopic processes to experimental observations. The basis for MC simulation of collective surface diffusion are two-dimensional lattice gas models (e.g., [140,145–147]). The motion of adsorbates in the lattice gas description consists of random hops of individual adsorbates between neighboring sites, i.e., it is assumed that adsorbates are localized at specific sites and that collective motion corresponds to a sequence of elementary jumps.

In a simple MC scheme the jump probability ω_{ij} of a randomly selected adatom at an initial site to a randomly selected adjacent final site is calculated. When the final site is occupied, $\omega_{ij} = 0$. When the final site is free, the jump probability is calculated and jumping is allowed when ω_{ij} exceeds a random number r ($0 \leq r \leq 1$). The jump probability thus accounts for the microscopic environment and the temperature. It may be represented by $\omega_{ij} = \kappa^{-1} \exp[-\beta E_{ij}]$, where E_{ij} is the energy barrier for the adsorbate site change and k a scaling factor [148,149]. This choice for the transition rate satisfies the condition of detailed balance (or microscopic reversibility), which ensures evolution of the system towards thermal equilibrium [142–144] $\omega_{ij} P_{\mathrm{i}} = \omega_{ij} P_{\mathrm{f}}$ where P_{i}, P_{f} are the corresponding probability distributions of equilibrium configurations. Detailed balance does not provide a unique condition for the transition probability and several distinct expressions for ω_{ij} are in practice for MC simulations of surface diffusion, notably the Metropolis or the Kawasaki form and the recently introduced transition dynamics algorithm (cf. [21,137,149–151] and references therein). Note that the conversion from simulation time to real time, being of primary interest for the description of the system dynamics, is non-trivial [142–144,150,152]. Frequently it is assumed that the energy of the transition state is constant and that the interactions are reflected exclusively by variations in the depth of the adsorption well. When phase diagrams of the systems under consideration are known, the interaction parameters can be adjusted for their reproduction. In addition to pairwise interactions three or multiple body interactions have been suggested in this context [146,153,154].

MC simulations have been employed to address a variety of questions in collective surface diffusion in an ensemble of adsorbates.

They confirm that $\tilde{D}$ is independent of coverage for a Langmuir gas and demonstrate increased or reduced diffusivity in the presence of next-neighbor repulsions or attractions, respectively [155]. MC simulations were employed to reproduce the decay of density profiles, such as in laser-induced thermal desorption (LITD) experiments (cf. [134,156–160]). Also the Boltzmann–Matano analysis can be checked including the case of interacting adsorbates [155,161,162]. When applied to two-dimensional concentration profile decay, the Boltzmann–Matano method was shown to underestimate the diffusion coefficient [161]. Recent simulations indicate that the chemical diffusion coefficient obtained strongly depends on the chosen time regime [163].

MC simulations provide a means to determine the thermodynamic factor via analysis of the particle number fluctuations in a small area element of the total area employed to model the lattice gas [123,126,137,164,165]. They were performed to systematically investigate interaction effects on particle fluctuations and their relation to the collective, tracer and jump diffusion coefficients [141,166–169]. Local reconstructions and the substrate symmetry effects were investigated (cf. [21,170]). The

effect of adsorbate ordering and phase transitions on collective surface diffusion have been analyzed [134,137,153,164,171–175]. A lattice model and MC simulations were developed to investigate the complex collective diffusion of large molecules such as *n*-alkanes and others [92,93,176]. A combination of MC and an analytical approach was proposed in Ref. [136].

Besides MC methods, other computational means to study collective surface diffusion were employed, such as quasichemical models [126,140], MD simulations [85,122], the real-space renormalization-group approach [177], an analytic kinetic theory within the hard-particle approximation [178], and the stochastic resonance concept [179].

3. Evolution of surface mobility studies

The earliest observations of surface mobility at metals date back some 80 years from now [180,181]. It was noted in particular that the growth speed of small mercury crystallites from a supersaturated vapor proceeding along specific directions was much faster than the rate of condensation from the gas phase [181]. These findings led to the statement that '*adsorbed molecules can migrate on the surface by virtue of thermal motion*' [182]. Soon thereafter it could indirectly be shown that '*two-dimensional mobility also in the case of adsorbed foreign molecules*' exists [182–184].

More direct observations of surface diffusion were accomplished around 1930 by thermionic methods [185–188]. Most of these experiments were performed with adsorbed alkali and alkaline earth metals, but also the first evidence of mobility of adsorbed gas layers was reported for oxygen on tungsten [185,189]. At the same time the significance of surface diffusion for heterogenous catalytic reactions was discussed [185,190–193].

The thermionic observations led to the concept of '*hopping atoms*', i.e., '*atoms whose nuclei describe hopping paths that originate and terminate on the surface*' [187,188] and revealed accordingly '*a definite exponential temperature coefficient indicative of an energy of activation being requisite for the process of lateral diffusion, i.e., in passing from point to point in a non-uniform atomic field*' [191]. These ideas constitute the foundation for the interpretation of surface mobility observations in the following years.

3.1. Field emission microscopy

Modern surface science investigations of surface diffusion employing well-defined and impurity-free surfaces at tungsten and other refractory metal tips under UHV conditions became possible with the development of the field emission microscope (FEM) conceived in the 1930s [194–196]. From now quantitative data about the mobility of chemisorbed gases on metal surfaces could be obtained [197] and many systematic investigations were performed in the following decades [198]. FEM similarly allowed for an elucidation of directed surface diffusion induced by the anisotropy of single crystal substrates [199].

The FEM technique has been reviewed at length [30,127,198,200,201]. In an FEM experiment, electrons emitted from a small area at a metal tip under the influence of a high electric field are magnified on a fluoroscent screen. The instrumental resolution obtainable is $\sim$25 Å. Since the field emisson current depends sensitively on the local work function at the surface, the presence of adsorbates affecting this quantity can be observed. This is the basis of the FEM shadowing method,

where only a fraction of the investigated area is exposed to an adsorbate beam, and the spreading of this adsorbate distribution is monitored.

With the introduction of the fluctuation method the capabilities of FEM were greatly enhanced [30,127,201,202]. This technique allows for the observation of the relaxation of concentration fluctuations in a homogeneous adsorbate layer. The basis of the fluctuation method is the relation between the particle number fluctuations in a small investigated area A (with a typical diameter of 100 Å), which is related to the collective diffusivity (cf. Section 2.2) and is apparent in the measured fluctuations of the field emission current. In practice, the decay of the time autocorrelation function $f_n(t) \equiv \langle \Delta n(0)\Delta n(t)\rangle|_A$ of the fluctuations is determined, where $\Delta n(t) = n(t) - \langle n\rangle$. $f_n(t)$ corresponds to the mean square fluctuation for $t = 0$ and becomes zero in the long time limit. In two dimensions it is related to the collective diffusivity by [30,127]

$$f_n(t) = \frac{\langle (\Delta n)^2 \rangle}{A} \int_A \mathrm{d}^2\boldsymbol{r} \int_A \mathrm{d}^2\boldsymbol{r}' \frac{\exp(-|\boldsymbol{r}-\boldsymbol{r}'|^2/4\tilde{D}t)}{4\pi\tilde{D}t}. \tag{3.1}$$

By integration of this formula, the theoretical decay is calculated. It can be fitted to experimental data, which allows for determination of $\tilde{D}$.

Anisotropic diffusion can be investigated by probing rectangular areas (e.g., [200,203,204]).

Both the FEM shadowing and the FEM fluctuation method were extensively applied to study surface diffusion of adsorbed gas layers, notably H, CO, O. A rich database could be established and many aspects of surface diffusion were elucidated.

Among the disadvantages of FEM are the limited choice of substrate materials (W, Mo, Re, Ta; Pt or Ni with difficulty). In addition the adsorbate systems must induce substantial work function changes and withstand the employed high electric fields without the surface mobility being affected. With the FEM shadowing technique it is also rather difficult to extract the diffusion characteristics for a specific crystallographic orientation at the tip [30].

3.2. Field ion microscopy

The next leap forward in the experimental instrumentarium applicable to surface mobility was the invention of the field ion microscope (FIM) in the 1950s [205,206]. This technique allows to image surfaces with atomic resolution (≈1 Å), and its potential to monitor movements of individual adsorbed atoms was recognized soon after [207] and realized only a few years later [208]. FIM studies contributed a wealth of information on surface migration and other atomic processes, particularly for metal atoms and clusters adsorbed on refractory metal tips [15,16,23,209,210].

In a typical FIM experiment for surface migration of adsorbed atoms, the adsorbate distribution on a metal tip at a low temperature is visualized by an inert imaging gas ionized at the surface by a high electric field. In a subsequent step, the tip is heated to a desired temperature in the absence of the imaging field to induce adsorbate migration. The respective motions are analyzed by imaging after cool-down to the low temperature and determination of the changed particle distribution. From a series of images, the mean square displacement of adatoms is obtained and the tracer diffusion coefficient is calculated using Eqs. (2.7) or (2.8).

FIM was successfully applied to investigate the diffusion of single metal adatoms and clusters strongly bound at metal surfaces. However, studies on the migration of adsorbed non-metals were published only scarcely [211–214]. The main problem with FIM investigation of non-metals is that they

tend to be easily desorbed by the high imaging fields or to be simply invisible in the FIM imaging process [30].

3.3. Laser-induced thermal desorption

With the development of modern UHV technology and surface characterization methods, systematic experiments employing well-defined single crystal metal surfaces became possible.

In the 1980s a versatile technique based on LITD was introduced for the investigation of surface diffusion phenomena [215–218]. LITD is conceptionally straightforward. A specific homogeneous concentration of adsorbates is established on a surface. Subsequently a well-defined area at the surface is depleted from the adsorbate layer by a focused laser pulse. Since thermal equilibrium at the surface is rapidly recovered [219], the bare spot can be refilled only by surface diffusion of adsorbates from the surrounding areas. A second laser impulse is applied to desorb the transported adsorbates after a time interval t from the first pulse. The corresponding amount of material can be quantified by mass spectrometry. For the idealized case of a circular depletion region, with a step-like coverage gradient and a concentration-independent diffusivity, the time-dependent refilling from Fick's first law is [216,220]

$$\frac{S(t)}{S(\infty)} = 1 - 2\int_0^\infty \frac{J_1^2(r/r_0)}{r/r_0} \exp\left(-\frac{\tilde{D}t}{r_0^2}\left(\frac{r}{r_0}\right)^2\right) \mathrm{d}\left(\frac{r}{r_0}\right), \tag{3.2}$$

where $S(t)$ is the measured signal, r_0 the radius of the depleted area and J_1 a Bessel function of order 1, r_0 is typically in the 100 μm range.

Upon measuring the fractional refilling for several time intervals at a given temperature, the diffusivity can be determined from fits using Eq. (3.2) or analogous expressions for other geometries to the experimental data. Experiments performed with different initial coverages provide trends for the coverage dependence of the diffusivity.

The LITD technique has been employed for investigating surface mobility of adsorbed gases (notably H, O, CO, noble gases), physisorbates and large molecules on single crystal surfaces. Among its advantages are its simplicity and the possibility to study virtually all adsorbates, which can be thermally desorbed and detected by a mass spectrometer, and coadsorbate systems. LITD is of course limited to adsorbates which are not too strongly bound and can be desorbed without destructive laser powers. A frequently discussed problem is the possible effect of substrate imperfections in the area under investigation, which may be even created upon irradiation [221,222]. Diffusion over atomic steps is inevitable for the long-range mass transport in the experiments. Another drawback is the lack of spatial information which prevents for the application of the Boltzmann–Matano method (see Ref. [223] for a notable exception). Coverage-independent diffusivities are thus frequently assumed for the data interpretation, and it was pointed out that the concentration variation in the depletion area affects the corresponding results (cf. [134,159,160]). To account for this an iterative data evaluation method has been suggested [224].

3.4. Scanning tunneling microscopy

The advent of the scanning tunneling microscope (STM) [225,226] had a tremendous impact on surface science. STM allows in particular for structure determination and direct observation of

atomistic processes on any conducting surface, which greatly enhances the spectrum of other microscopic techniques such as FIM, FEM, or electron microscopy.

Basic studies on surface diffusion were reported already in the early days of STM [227]. In these measurements characteristic spikes were observed in the tunneling tracks, which were ascribed to highly mobile adsorbates moving much faster than the tunneling tip. This corresponds essentially to a measurement of the fluctuating adsorbate density in the area probed by the STM tip. It was hence suggested that the collective diffusivity can be measured by recording the current fluctuations of the tunnel junction [30,228–230], quite analogous to the FEM fluctuation method. An experiment along this line was performed to study Si adatom diffusion on Si(1 1 1) [231]. Unfortunately the data interpretation is not unambigous as pointed out in two recent studies employing MC simulations to attack this problem [232,233]. Further investigations are required in order to establish STM current fluctuation measurements as a reliable method for surface diffusion [234].

On the other hand, STM measurements can be employed to systematically study tracer diffusion by following adsorbate migration at the atomic level in situ. This was achieved for a variety of systems [235–238], including adsorbed gas atoms and molecules at metal surfaces (cf. Section 4). When metal substrates are employed, the temperature dependence is preferentially investigated by low-temperature [239] or variable-temperature STM [240–242]. In most cases, hopping frequencies were determined from a statistical analysis of series of STM images and Eq. (2.8), whereupon the corresponding activation energies and prefactors can be extracted from Arrhenius plots. In favorable cases, where the mean square displacement of adatoms is determined, data can be analyzed in terms of Eq. (2.7) and the jump mechanims can be elucidated [117,238]. The recently presented 'atom tracking' method allows to follow the migration path of an individual moving adsorbate [236]. When fancy instruments have been developed, surface mobility can be even recorded at video rates and visualized by STM movies [238,243]. The complete analysis and interpretation of such data can only be achieved with the development of adequate computer techniques [238,244,245]. From video data sets, the concentration fluctuations in adsorbate layers can also be obtained, as demonstrated recently [245]. This allows in principle for the characterization of collective diffusion, analogous to FEM.

Care must be taken to exclude the possible effect of tip–surface interactions in STM experiments. Both theoretical and experimental studies indicate the possibility of modified migration energy barriers under the STM tip [246–251]. However, frequently such effects are negligible or can be excluded by working at large tunneling electrode distances.

A further approach to tackle adsorbate tracer diffusion is the analysis of saturation island densities on surfaces as a function of temperature [252–256]. So far, this method has been applied exclusively to metal or semiconductor epitaxial growth, where the lateral interactions between adsorbed atoms are strong and stable islands readily evolve from two-dimensional condensation of mobile adatoms in the course of deposition.

Among the advantages of STM are atomic resolution, its conceptional transparency and versatility, and the appeal of direct visualization. STM can be applied to study anisotropic surface mobility, diffusion on inhomogeneous surfaces, or adsorbate interactions and collective transport effects on a local scale. It is also a technique where a simultaneous characterization of tracer and chemical diffusion on single crystals is feasable.

Limitations of the STM technique are that only rather low diffusivity ranges are accessible, its principal application to small adsorbate concentrations so far and the possible interference of the tunneling tip. Surface mobility studies by STM are currently in plain progress.

3.5. Quasielastic helium atom scattering

About 10 years from now, a promising scattering technique for the analysis of surface diffusion was developed: quasielastic helium atom scattering (QHAS) [108,257–260]. This method provides a mirror image in reciprocal space to the real-space informations of random motions in two dimensions obtained by microscopic measurements. The early development and theory of QHAS have been reviewed in Ref. [258]. QHAS is the surface analogon to quasielastic scattering of neutrons, which was extensively applied to study bulk diffusion phenomena [261]. In a QHAS experiment, an atomic He beam with a sharp energy distribution is directed on a surface. In the presence of a mobile adsorbate layer, diffusively scattered He experience characteristic energy exchanges with the adatoms, which lead to a slight broadening of the energy distribution of the reflected He beam. The width of the so-called quasielastic peak is thus related to the adatom diffusivity. It can be determined by time-of-flight (TOF) measurements of the reflected He beam at different temperatures, which allows for a systematic investigation of the mobility in the adsorbate layer.

The theory for QHAS [258,262] was developed following ideas from neutron scattering [263,264]. It can be summarized as follows [260,265,267]. QHAS measures the Fourier transform of the time-dependent adsorbate pair correlation function $G(\boldsymbol{r}, t)$. In a continuum description, $G(\boldsymbol{r}, t)$ gives the probability that an adatom can be found at position $\boldsymbol{r}$ at time t, under the condition of the presence of an adatom at the origin at $t = 0$. $G(\boldsymbol{r}, t)$ can be viewed as the sum of two contributions [264], the adatom autocorrelation function $G_s(\boldsymbol{r}, t)$, due to the motion of an individual adsorbate, and a second term $G_d(\boldsymbol{r}, t)$, arising from the pair correlation of distinct adsorbates.

The measured signal, i.e., the differential reflection probability, is related to the pair correlation function by

$$\frac{\mathrm{d}^2 r}{\mathrm{d}\Omega\,\mathrm{d}\omega} = \Theta F^2 \int\int G(\boldsymbol{r}, t) \exp[\mathrm{i}(\Delta\boldsymbol{k}\cdot\boldsymbol{r} - \omega t)]\mathrm{d}\boldsymbol{r}\,\mathrm{d}t \equiv \Theta F^2 S(\Delta\boldsymbol{k}, \omega), \tag{3.3}$$

where $\Delta\boldsymbol{k}$ is the parallel wave vector change, $\hbar\omega$ the energy shift and F an atomic form factor accounting for the He–adsorbate interaction. The dynamic structure factor $S(\Delta\boldsymbol{k}, \omega)$ is the Fourier transform of the pair correlation function and contains the information of interest. When the pair correlation between distinct adsorbate motions is appreciable, it is related to the collective diffusivity. However, the data interpretation is difficult in this case [108,258]. Hence, it is advantageous to perform experiments in the low-coverage limit with weakly interacting adsorbates, where island formation can be excluded. Note that the length scale of scattered He atoms probing the dynamics of adatoms is $2\pi/\Delta\boldsymbol{k}$. When the coverage is sufficiently small, correlations can be neglected and $G_d(\mathbf{r}, t)$ is zero. For small correlations, upon application of the Vineyard approximation [264], the dynamical structure factor can be expressed as the product of a static structure factor $S(\Delta\boldsymbol{k})$ and the term $S_s(\Delta\boldsymbol{k}, \omega)$ originating from the autocorrelation function [258]

$$S(\Delta\boldsymbol{k}, \omega) = S(\Delta\boldsymbol{k}) S_s(\Delta\boldsymbol{k}, \omega). \tag{3.4}$$

The system dynamics is thus reflected in $S_s(\Delta\boldsymbol{k}, \omega)$.

For the description of isolated diffusing adsorbates in the continuum limit, the pair correlation function reduces to the Gaussian distribution encountered in Eq. (2.9) and the dynamic structure factor

is calculated as [258]

$$S_s(\Delta\boldsymbol{k},\omega) = \frac{1}{\pi}\frac{(\Delta k)^2}{\omega^2 + (D^*)^2(\Delta k)^4} \tag{3.5}$$

corresponding to a Lorentzian energy profile with a width (FWHM) of

$$\Delta\varepsilon(\Delta\boldsymbol{k}) = 2\hbar D^*(\Delta k)^2. \tag{3.6}$$

For next-neighbor hopping diffusion on a square lattice the Lorentzian energy profile is retained and the peak width is given by [258,266]

$$\Delta\varepsilon(\Delta\boldsymbol{k}) = 4\hbar\sum_{\lambda}\Gamma_s(\lambda)\sin^2\left[\tfrac{1}{2}\Delta\boldsymbol{k}\cdot\lambda\right], \tag{3.7}$$

where $\Gamma_s(\lambda)$ is the hopping rate associated with the jump vector λ (in units of lattice constants). Analogous $\Delta\varepsilon$ expressions can be derived for varying jump lengths and other geometries [258].

In practice, for determination of the diffusivity from a measured signal, the peak broadening due to the adsorbate mobility and the instrument response function must be deconvoluted (cf. [267]). Complementary MD simulations have proven to be very useful [268].

The QHAS technique can be applied over a wide temperature range and to anisotropic diffusion. One of its striking features is that it simultaneously provides additional informations on the dynamics of adsorbed species, such as the energy of the frustrated translation mode. On the other hand, QHAS is limited to the case of high diffusivities exceeding $\approx 5\times10^{-6}\,\mathrm{cm^2\,s^{-1}}$ and requires extensive data interpretation. Recent theoretical studies emphasize the role of additional contributions to the dynamical structure factor from the frustrated translation [82,83,108]. It has been pointed out further that non-diffusive processes may contribute to the peak broadening [269]. QHAS was successfully employed to obtain diffusion characteristics for weakly bound adsorbates at metal surfaces, as summarized in Refs. [260,267,270]. For the case of gases at surfaces, adsorbed CO, H and Xe have been studied so far [34,260,265,271–273].

3.6. Optical methods

The first observations directly monitoring the thermal spreading of a concentration profile on a surface have been performed by spatially resolved photoelectric current measurements [9,274] (cf. Fig. 2). Essentially the same principle, albeit with a magnifying lens providing significantly improved performance and working under UHV conditions, is followed in modern photoemission electron microscopy (PEEM) measurements. Similar to FEM, this method exploits the local work function changes induced by adsorbates. However, by means of PEEM, a complete image of the photoelectron energies from adsorbate layers on single crystal surfaces can be obtained [275–277]. In PEEM experiments for surface diffusion, a coverage gradient is generated on the surface by LITD or deposition through a mask. The subsequent spreading of the adsorbate layer is monitored for various temperatures. Due to the spatial resolution of $\approx$100 nm, a Boltzmann–Matano analysis is usually performable. This has been demonstrated for several systems, including adsorbed CO and O on Pd and Pt surfaces [278,279], and alkali metal surface diffusion [280]. PEEM bridges the gap between atomic resolution microscopies and macroscopic measurements. It is thus an excellent technique to investigate

the possible interference of defects in macroscopic surface diffusion measurements, as demonstrated in a recent study of the CO/Pd(1 1 1) system [222].

Two related, elegant optical diffraction techniques to study collective surface diffusion were introduced around 1990 [281,282]. With these methods, a regular array of one-dimensional concentration profiles on an initially uniform adsorbate layer is created by LITD, using the interference pattern of two laser beams. Typical grating periodicities are in the range $s = 2-5\,\mu m$. The grating amplitude is detected by the diffraction signal from a low-power probe laser. As adsorbate diffusion sets in, a uniform distribution is restored. The corresponding decay of the diffraction signal is a measure of the diffusivity. Initially, the first-order second-harmonic diffraction signal was monitored. This is the second-harmonic diffraction (SHD) technique [281,283–285]. In later sudies, it became clear that it is frequently more advantageous to employ the linear optical diffraction (LOD) method, where the first-order diffraction signal is recorded. It obeys an exponential decay law [282,286,287]

$$S(t) = S(0)\exp\left[-\frac{2\pi^2\tilde{D}}{s^2}t\right], \tag{3.8}$$

where t is the diffusion time and S is the signal strength. This expression holds in favorable cases similarly for the first-order second-harmonic signal [287]. For the derivation of Eq. (3.8) a coverage-independent diffusivity is assumed and the corresponding diffusion equation, Fick's law in the form of Eq. (2.26), is solved. This is often a good approximation as minute concentration modulations ($\approx$0.02 ML) proved to be sufficient for LOD measurements. Hence coverage and temperature-dependent diffusivity can be studied.

Since the gratings are formed by LITD, SHD and LOD have been employed exclusively to adsorbed gas layers, mostly CO [281,283,285,287,288], NH_3 [289], or hydrogen [284,290–295]. A striking feature of LOD is the wide dynamical range recently achieved, which allows for diffusivity measurements from 10^{-15} to $10^{-7}\,cm^2\,s^{-1}$ [295]. Anisotropic surface diffusion can be investigated since the fabricated gratings are one-dimensional. LOD was employed to study the effect of step barriers and coadsorbed impurities in collective surface diffusion [296–298]. Higher-order SHD or LOD peaks have been analyzed to gain insight into adsorbate interactions [299].

Child diseases of the SHD and LOD techniques have been cured over the last years. Some results from the early literature thus have been reinterpretated (concerning diffusion of hydrogen [292–295] and CO [285,287] on Ni surfaces). Both SHD and LOD are techniques averaging a signal from macroscopic areas, which comprises the usual problem of substrate imperfections.

The main features of the currently most important techniques for surface mobility observations of non-metallic adsorbates are compared in Table 1. These methods cover a wide range of diffusivities and length scales. Hence they provide complementary information when similar systems are investigated. Note that the only 'oldtimer' in this collection is the FEM.

3.7. Miscellany

In addition to the aforementioned principal methods, other techniques were sporadically employed to investigate the surface mobility of adsorbed gases.

Spatially resolved work-function measurements were performed with the vibrating capacitor technique to study surface diffusion of oxygen on W(1 1 0); a resolution of $\approx$50 μm could be achieved [125].

Table 1
Principal methods for surface diffusion studies of non-metallic adsorbates on metals

Method	Remarks	Studied adsorbates	Length scale	Range of D ($cm^2\ s^{-1}$)
STM	Tracer diffusion, direct observation, study of interactions	N, O, S, CO, O_2, C_{60}, organic molecules	10 Å	10^{-19}–10^{-16}
QHAS	Tracer diffusion, frustrated translation	CO, S, H, Xe	10 Å	$> 5 \times 10^{-6}$
FEM	Refractory metal tips	H, N, O, CO		
Fluctuation	Collective diffusion		100 Å	10^{-14}–10^{-9}
Shadowing	Collective diffusion, averages over planes		100–1000 Å	10^{-12}–10^{-10}
LOD/SHD	Collective diffusion, coadsorbate systems	H, CO, NH_3	1 μm	10^{-15}–10^{-7}
PEEM	Collective diffusion, study of defects	CO, O	0.1–1000 μm	10^{-9}–10^{-5}
LITD	Collective diffusion, 'macroscopic' coadsorbate systems	H, CO, O, organic molecules	100–1000 μm	10^{-8}–10^{-5}

The diffusion of N on W(1 1 0) was studied by scanning Auger electron spectroscopy (AES) [300]. In a related approach, the coverage-dependent secondary electron emission was employed to investigate oxygen diffusion on a W(1 1 0) surface [301]. Both methods require intense electron beams, which may influence the adsorbate motion or pollute the surface.

Helium atom scattering (HAS) studies have been performed for the observation of macroscopic collective diffusion [302,303]. With these experiments a small gas concentration was adsorbed on a well-defined small spot on a surface. The temperature-dependent decay of the concentration profile was observed and analyzed in terms of Fick's laws.

HAS was initially employed to surface diffusion by exploiting the preferential trapping of adsorbed CO at the steps of a Pt(1 1 1) surface [304]. At low temperatures the mobility is frozen and upon exposure the uniformly distributed CO leads to a substantial intensity decrease of the specular beam intensity. In a subsequent heating step, the migrating CO is trapped at the steps and the onset of diffusion can be determined by the corresponding reincrease in the specular beam intensity. A similar defect-decoration approach was followed by infra-red adsorption spectroscopy (IRAS) for the same system [305,306]. By STM, the inverse phenomenon could be monitored: steps on a Ru(0 0 1) surface were decorated by N atoms (due the preferential dissociation of NO there) and the decay of the created coverage gradient could be directly analyzed [307].

Scanning high-resolution electron energy-loss spectroscopy (HREELS) with a spatial resolution of $\approx$0.3 mm was applied to study CO/Pt(1 1 1). Due to the limited resolution, high temperatures, close to thermal desorption conditions, were required [308].

Nuclear magnetic resonance (NMR) was employed to estimate the surface mobility on metal clusters (notably Pd [309] and Pt [310]) supported on oxide surfaces. With these measurements, the surface mobility related narrowing of the ^{13}C line of adsorbed ^{13}CO is determined as a function of temperature (cf. [311]). Averaging over all cluster facets and their boundaries is of course included.

3.8. Role of defects and impurities

Whenever experiments to study of surface mobility are performed, for the interpretation of the observations possible effects of the ubiquitous imperfections or contaminations must be considered.

These include in particular impurities from the crystal volume or from the residual gas pinned at the surface. Similarly, the presence of atomic steps or other lattice defects such as vacancies may severely affect surface diffusion. Steps may even represent sources for two-dimensional substrate atom evaporation. Both formation and concentration of defects may be temperature dependent.

For instance, adsorbates may preferentially bind to surface steps or other defects which implies reduced surface mobility (e.g., [97,98]). This can be exploited to study the adsorbate diffusion (e.g., [304,306]). More frequently, however, such effects are implicitly contained in the experimental data and it is a challenging task to disentangle their contribution and that of the mobility on the perfect substrate areas.

The effect of substrate steps has been systematically studied by MC simulations. In general, they cause diffusion to be anisotropic as crossing of steps costs an extra activation energy [312–316]. The MC methodology was similarly employed to investigate surface diffusion in the presence of point traps and blocks [317,318].

4. Observations of surface diffusion: non-metals on metals

Surface diffusion is certainly more than an activation energy and a pre-exponential factor, even in the case of isolated adsorbates. Nevertheless, it is customary and useful for practical reasons, to tabulate experimental observations with these parameters. In the following, available data sets will be classified accordingly and briefly discussed (updated tables will be available online at http://ipent.epfl.ch/gr_kern/jv_barth/SD_tables.html). For comparison, the adsorption energies are included, where available. The adsorbates and substrates are arranged according to their position in the periodic system. Related theoretical work will be discussed in the respective context.

4.1. Atoms

4.1.1. Hydrogen

The surface mobility of adsorbed H and its isotopes was investigated by FEM, LITD, LOD and QHAS. In Table 2 a survey on available data is presented.

Hydrogen diffusion is a peculiar case. Due to the small mass of the adsorbate quantum mechanical tunneling through the classical migration barrier is possible. Deviations from the universal Arrhenius behavior are accordingly found at low temperatures. Quantum effects become similarly apparent in the variation of the diffusivity with different hydrogen isotopes. Both phenomena are illustrated by the data reproduced in Fig. 8.

In the high-temperature, semiclassical regime, hydrogen diffusion can be described by an Arrhenius law. The corresponding energy barriers are typically in the range 150–200 meV and amount thus to a small fraction of the respective binding energies ($\sim$5%). The coverage variation of the diffusivity is generally not very pronounced (cf. [223,273,324,328]), indicative of small interactions between the adsorbed H atoms. With the hydrogen on W(1 1 0) system, the application of the FEM fluctuation method to anisotropic diffusion could be demonstrated. However, the effect is weak [203].

The prefactors in LITD, LOD and QHAS measurements are close to the universal $1 \times 10^{-3}\,\mathrm{cm^2\,s^{-1}}$ value, which suggests the validity of a TST-type description for activated diffusion (with the exception of the LITD observations of the ‘pathological’ hydrogen on Pt(1 1 1) system, where trap-limited

Table 2
Hydrogen diffusion on metals (θ is given in terms of the saturation coverage; D_T: tunneling diffusion constant; T_t: transition temperature between high- and low-temperature regime)

System	E_m (meV)	E_d (meV)	D_0 ($cm^2\,s^{-1}$)	θ	T (K)	D_T ($cm^2\,s^{-1}$)	T_t (K)	Method	Reference	E_b (eV)	Reference
^{1}H/W(1 1 0)		177 ± 4	1.7×10^{-7}	0.1	150–180	2×10^{-13}	160	FEM	[319]	3.0	[320]
^{2}H/W(1 1 0)		170 ± 9	3.5×10^{-5}	0.1	100–130	9×10^{-14}	70	FEM	[319]		
^{3}H/W(1 1 0)		208 ± 9	3.3×10^{-3}	0.1	110–120	5×10^{-14}	70	FEM	[319]		
^{1}H/Ru(0 0 0 1)		170 ± 20	6.3×10^{-4}	0.3	260–300	–		LITD	[321,322]	2.9	[323]
^{2}H/Ru(0 0 0 1)		180 ± 20	4.6×10^{-4}	0.3	260–300	–		LITD	[321]		
^{1}H/Rh(1 1 1)		160	1×10^{-3}	0.33	150–250	–		LITD	[324]	2.7	[325]
		140 ± 20	6.5×10^{-3}	0.3	160–210	–		LITD	[223]		
^{2}H/Rh(1 1 1)		190 ± 20	8×10^{-4}	0.33	180–280	–		LITD	[324]		
		140 ± 20	5.7×10^{-4}	0.4	180–220	–		LITD	[223]		
^{1}H/Ni(0 0 1)		170 ± 20	4.5×10^{-3}	0.1	220–280	–		LITD	[216]	2.7	[326]
		150	$2.5 \pm 1 \times 10^{-3}$	1	210–260	–		LITD	[327]		
		140	1×10^{-5}	0.25	100–130	1×10^{-12}	100	FEM	[328]		
		150	1×10^{-6}	0.7	160–200	–	160[a]	LOD	[290,291]		
^{2}H/Ni(0 0 1)		190 ± 20	$8.5 \pm 2 \times 10^{-3}$	1	210–260	–		LITD	[327,329]		
		160	2×10^{-5}	0.15	100–130	1×10^{-12}	100	FEM	[328]		
		220	5×10^{-5}	0.7	170–200	–	170[a]	LOD	[290,291]		
^{1}H/Ni(1 1 1)		130 ± 10	$4 \times 10^{-4\pm1.5}$	0.08	100–120	2×10^{-10}	100	FEM	[328]	2.7	[326]
		196	2.8×10^{-3}	0.3	110–220	–	110[a]	LOD	[295]		
^{2}H/Ni(1 1 1)		140 ± 10	$5 \times 10^{-4\pm1.5}$	0.05	110–120	1×10^{-10}	100	FEM	[328]		
		218	3.4×10^{-3}	0.3	80–150	6×10^{-12}	$\sim$100[a]	LOD	[295]		
^{1}H/Pt(1 1 1)		300 ± 40	1.0	0.24	210–250	–		LITD	[217]	2.5	[330]
	68 ± 5		$1.1 \pm 0.5 \times 10^{-3}$	0.1	140–250	–		QHAS	[273]		
^{2}H/Pt(1 1 1)		300 ± 40	0.5	0.24	190–260	–		LITD	[217]		
	76 ± 7		$1.4 \pm 0.6 \times 10^{-3}$	0.1	140–250	–		QHAS	[273]		

[a]Assuming additive classical hopping and activated tunneling diffusion fitted by an Arrhenius law with activation energies and prefactors for Ni(0 0 1): 50 meV (H, D) and 1.5×10^{-9} (H), $9 \times 10^{-10}\,cm^2\,s^{-1}$(D) [291], Ni(1 1 1): 105 meV (H, D) and 2.4×10^{-7} (H), $1.6 \times 10^{-8}\,cm^2\,s^{-1}$ (D) [295].

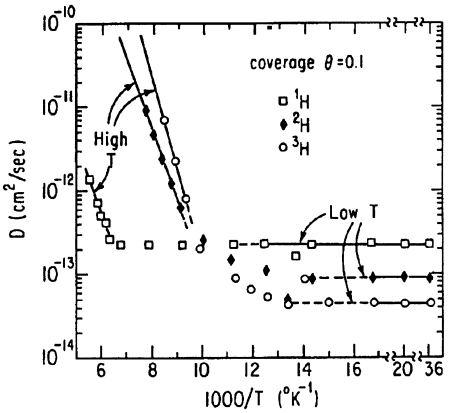

Fig. 8. Diffusivity of hydrogen, deuterium and tritium on W(1 1 0) determined with the FEM fluctuation technique. In the low-temperature regime temperature-independent tunneling diffusion is encountered. From [331].

diffusion seems possible [30]). In contrast, prefactors obtained with the FEM fluctuation method are substantially smaller, in the range 10^{-4}–10^{-5} cm^2 s^{-1}. A strong 'anomalous' isotope effect exists with some systems; i.e., the prefactor increases with the mass of the isotope. This cannot be rationalized in semiclassical models, where the opposite behavior is expected (cf. [331]). Reasons for presence or absence of isotope effects are discussed in Refs. [292,328,331–336]. Static diffusion barriers for H on low-index Pd surfaces were recently determined by LDF calculations to ^{1}H/Pd(0 0 1): 120 meV, ^{1}H/Pd(1 1 0): 100 meV, ^{1}H/Pd(1 1 1): 190 meV [100] and confirm the trend of small E_m/E_b ratios, as the corresponding experimental binding energies are 2.8 [337], 2.8 and 2.7 eV [338], respectively.

Tunneling diffusion effects could be observed by FEM for hydrogen on W(1 1 0) [319,339], W(0 0 1) [340], W(1 1 1) [341] and Ni surfaces [328]; by LOD for hydrogen on Ni(1 1 1) [295] and Ni(0 0 1) [290,291]. The more recent LOD observations on Ni(1 1 1) [295] outdate earlier studies [292–294]. Presently, the transition from the high-temperature to the low-temperature regime is controversely discussed. On the one hand, the FEM observations indicate a sharp transition from activated diffusion, where the hydrogen atoms overcome the barrier, to tunneling diffusion, where quantum mechanical tunneling through the barrier prevails. This interpretation is substantiated by recent theoretical studies of hydrogen and deuterium on Ni(0 0 1) [334–336]. On the other hand, the LOD studies (cf. Fig. 9) indicate a rather smooth transition between two regimes with different thermal activation characteristics: hopping diffusion at high temperatures compatible with TST, and a low-temperature behavior associated with activated small-polaron mediated diffusion [295,331,342]. A smooth transition was similarly obtained in calculations based on the embedded-atom method (EAM) [343,344]. It was further concluded that tunneling diffusion is appreciable well above the transition temperature, which accounts for the small prefactors from FEM measurements [343,344].

While the QHAS and LITD results for hydrogen diffusion on Pt(1 1 1) agree on a weak coverage dependence [217,273], very different activation energies were derived (cf. Table 2). The higher LITD values have been associated with the larger length scale relevant for this technique, where the presence of atomic steps interferes [273]. For comparison, the migration barrier for H/Pt(1 1 1) has been calculated to 120 meV with the EAM [345]. An analysis of QHAS data indicates that the H diffusion is mainly due to single jumps between f.c.c. sites [273].

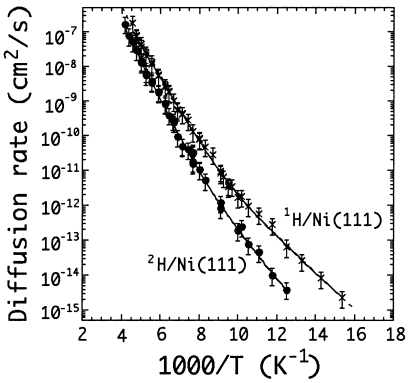

Fig. 9. Diffusion rates for hydrogen and deuterium on Ni(1 1 1) obtained from LOD measurements. The fits of the data were performed assuming additive classical hopping and activated tunneling diffusion. From [295].

Extensive theoretical studies for hydrogen atom diffusion on Cu(0 0 1) have been performed (cf. [346] and references therein).

4.1.2. Group IIIA–VIIA elements (C, Si, N, O, S)

Early investigations dealing with the surface mobility of non-metallic adatoms from the group IIIA–VIIA elements have been performed with the FEM shadowing technique [197,347]. Relatively few systematic studies on single crystal surfaces are currently available, although these adsorbates play an important role in heterogeneous catalysis. The main reasons for this defiancy are the experimental difficulties encountered with the investigation of such systems. The adatoms frequently give a very weak or no contrast in FIM. Due to the typically strong chemical binding at metal surfaces they cannot be studied by LITD or LITD-based techniques. Hence it is not surprising that the majority of the more recent results have been obtained by STM. In Table 3 a survey on the available data is presented.

The only study of C diffusion was performed on Pt(1 1 1) by AES. The decay of a C spot profile was analyzed in terms of Fick's second law and a barrier of $\approx$1.3 eV with a rather high prefactor of $0.2\,\mathrm{cm^2\,s^{-1}}$ were derived [348]. MD calculations employing optimized Lennard–Jones potentials roughly agree with the energy value (providing $E_\mathrm{m} = 1.1\,\mathrm{eV}$) but signal a much lower prefactor of $3.4 \times 10^{-3}\,\mathrm{cm^2\,s^{-1}}$ [86].

The motion of an Si atom on a W(1 1 0) tip was evaluated by FIM in the temperature range 250–280 K, which allowed for an Arrhenius analysis. The migration barrier is high (700 meV) with a prefactor of $3.1 \times 10^{-4}\,\mathrm{cm^2\,s^{-1}}$, close to the universal value [212,213]. Between the Si adatoms oscillatory interactions with an amplitude of $\approx$50 meV were found [211,367].

The surface diffusion of adsorbed N atoms on W(1 1 0) was studied by FEM [347] and AES [300] meaurements. The determined diffusion barrier (900 meV) amounts to $\approx$15% of the binding energy [300]. Recent STM measurements with strongly bound N atoms on Fe(0 0 1) [101] and Ru(0 0 0 1) [307] follow this trend. In all cases the prefactors are close to the TST value.

From an analysis of STM movies resolving N diffusion on Fe(0 0 1) the migration barrier of individual adsorbed atoms could be determined to $E_\mathrm{m} = 920 \pm 40\,\mathrm{meV}$, with an attempt frequency of $4.3 \times 10^{12}\,\mathrm{s^{-1}}$ [101]. The height of the migration barrier was confirmed by DFT calculations, which furthermore indicate that strong lattice distortions accompany the diffusion process [101]. They

Table 3
Non-metal IIIA–VIIA adatom diffusion on metals (θ is given in number of adatoms per substrate atom; estimates for D_0 by original authors in {})

System	E_m (meV)	E_d (meV)	D_0(cm^2 s^{-1})	θ (ML)	T (K)	Method	Reference	E_b (eV)	Reference
C/Pt(1 1 1)		1300 ± 200	0.2	–	860–970	AES	[348]	–	
Si/W(1 1 0)	700 ± 70		$3.1 \times 10^{-4\pm1.3}$	Atom	250–280	FIM	[212,213]	–	
N/W(1 1 0)		900	1.4×10^{-2}	–	800–900	AES	[300]	6.6	[300]
N/Fe(0 0 1)	920 ± 40		8.9×10^{-4}	Atom	299–325	STM	[349]	6.1	[350]
N/Ru(0 0 0 1)	940 ± 150	940 ± 150	$1 \times 10^{-1.7\pm1.5}$	Atom	300–350	STM	[307]	5.7	[351,352]
O/Mo(1 1 0)		740–1130	$1 \times 10^{-1}-10^{-2}$	0.07–0.5	400–600	FEM	[353]	–	
O/W(1 1 0)		1170 ± 90	0.38–0.2	0.4–0.9	1033–1153	CPD[a]	[125]	~5.4	[354]
		610	$2 \times 10^{-7}-1 \times 10^{-4}$	0.15–0.3	500–770	FEM	[355]		
		950	1×10^{-4}	0.56	500–770	FEM	[355]		
		1040	0.2/0.4	0.25/0.5	930–1320	SEE[b]	[301]		
		1050	4.5×10^{-4}	0.6	600–720	FEM[c]	[153]		
O/Pt(1 1 1)		~1200	~2.5	–	400–450	FEM[d]	[356]	3.7	[357,358]
	430 ± 40		$5 \times 10^{-7\pm1}$	Atom	190–205	STM	[242]		
O/Pt(1 0 0)		~1500	~1	–	580–640	FEM[d]	[356]	–	
O/Pt(1 1 0)		$1300 \pm 170\|\|$	$2 \times 10^{3\pm1}$	0–0.2	600–670	PEEM[e]	[279]	–	
O/Ru(0 0 0 1)	700		$\{2 \times 10^{-3}\}$	Atom	300	STM	[243,244]	4.4–5.6	[359–361]
O/Al(1 1 1)	1000		$\{5 \times 10^{-3}\}$	<0.1	440	STM	[362]	7.6	[94]
S/Re(0 0 0 1)		790 ± 10	$\{2 \times 10^{-2}\}$	~0.25	300	STM	[363]	4.3	[364]
S/Ni(1 1 1)	290–300		$\{2.2 \times 10^{-4}\}$	Atom	105–115	FIM	[214]	2.6	[365]
S/Pt(1 1 1)	570 ± 50		4×10^{-5}	Atom	185–200	STM	[245]	–	
S/Cu(1 1 1)	250		$\{1 \times 10^{-4}\}$	<0.16	820	QHAS	[366]	–	

[a] Contact potential difference (work function measurements).
[b] Secondary electron emission.
[c] Along [0 0 1].
[d] Shadowing technique.
[e] $(1 \times 1) \rightarrow (1 \times 2)$- areas, along $[1\,\bar{1}\,0]$.

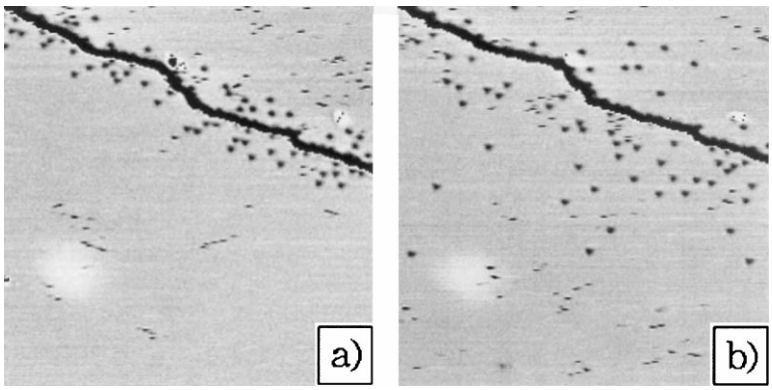

Fig. 10. STM observation of N atom diffusion on Ru(0 0 0 1). In (a) a sharp concentration profile of N at an atomic step was created by dissociative adsorption of NO at 300 K; (b) after 2 h at 300 K the N distribution is smeared out (image sizes $180 \times 200\,\text{Å}^2$). N atoms are imaged as triangular depressions; dashes are due to highly mobile oxygen atoms. From [307].

indicate that the bridge site between adjacent hollow sites is actually a metastable position with an energy of 0.83 eV, whereas the highest energy barrier calculated is 0.91 eV. It could also be shown that the barrier is lowered by -7 meV when the N–N distance is $2a$ due to attractive lateral interactions. Using STM data, these interactions could be quantified from a configuration distribution analysis [349]. In addition to the dominant pair interaction the effect of three-body interactions drives the preferential formation of compact islands [349].

Elegant STM observations with the N/Ru(0 0 0 1) system demonstrate that at low coverage the tracer diffusivity in a uniform N layer is equal to the collective diffusivity, thus directly confirming expectations (cf. Section 2.2; note that the lateral interactions of the N atoms are weak [368]). The collective diffusion was analyzed from the decay of a sharp N concentration profile created at atomic steps by the dissociative adsorption of NO there [369,370]. This is illustrated by the topographs reproduced in Fig. 10 [307].

The mobility of oxygen on W(1 1 0) was investigated by FEM [197,203,355] work-function measurements [125] and secondary electron emission [301]. The early FEM shadowing [197] results are in accordance with later fluctuation data [203,355]. With the latter measurements, a pronounced anisotropy of the diffusion was found for coverages below 0.6 ML [203]. The results have been critically discussed in Refs. [30,371]. In overall agreement the diffusion barrier is $\sim$1 eV at high coverages and substantially reduced at lower coverages, as demonstrated by the FEM data compilation in Fig. 11 [371]. The O/W(1 1 0) system was extensively analyzed by lattice gas models (cf. [21,136,137,140,153,164,174,372]. There is an ongoing debate about the behavior of the collective diffusivity near a continous phase transition in the O layer [137,149,164,174]. The strong changes of the collective diffusivity with the coverage have been associated with polaronic effects [371] and O interactions [137,153].

Investigations of O diffusion on high-index tungsten surfaces are discussed in Refs. [30]. A complex diffusion scenario was recently reported for O/W(0 0 1) on the basis of FEM observations [373].

Oxygen diffusion on Ni(0 0 1) was monitored by STM for an intermediate coverage at 300 K [374]. An activation energy $E_d = 0.99$ eV was estimated using an attempt frequency $\nu_0 = 1 \times 10^{13}\,\text{s}^{-1}$.

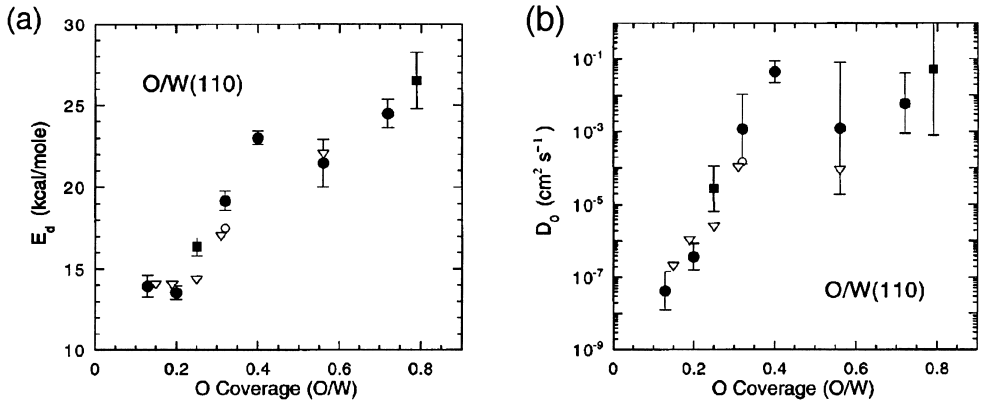

Fig. 11. Activation barrier (a) and prefactor (b) for the diffusion of oxygen on W(1 1 0) as a function of coverage. From FEM observations [371].

Oxygen diffusion on Pt(1 1 1) was studied by FEM shadowing measurements [356]. The high diffusion barrier and prefactor ($\approx$1.2 eV, 2.5 $cm^2\,s^{-1}$) obtained disagree with later estimates ($E_d \approx 0.7$ eV [375]) and MD simulations (0.8 eV, $1.5 \times 10^{-3}\,cm^2\,s^{-1}$) [86,87]. Recent STM observations performed around 200 K indicate even lower parameters for isolated O atoms (0.43 eV, $10^{-6.3\pm1}\,cm^2\,s^{-1}$) [242]. The STM findings stimulated DFT calculations, where these and other experimental data were reinterpreted and $E_m = 0.55$ eV was found with a prefactor of $\approx 10^{-3}\,cm^2\,s^{-1}$, estimated from the frustrated translation frequency [99]. Hence, with the latest values: $E_m/E_b \approx 0.12-0.15$.

Observations of O diffusion on Pt(0 0 1) [356] and Pt(1 1 0) [279] included in Table 3, which were performed with appreciable coverages at higher temperatures and involve long-range oxygen transport, indicate much higher barriers and prefactors. The reasons for these strong discrepancies remain to be clarified. PEEM results for the anisotropic diffusion of oxygen on Pt(1 1 0) are reproduced in Fig. 12.

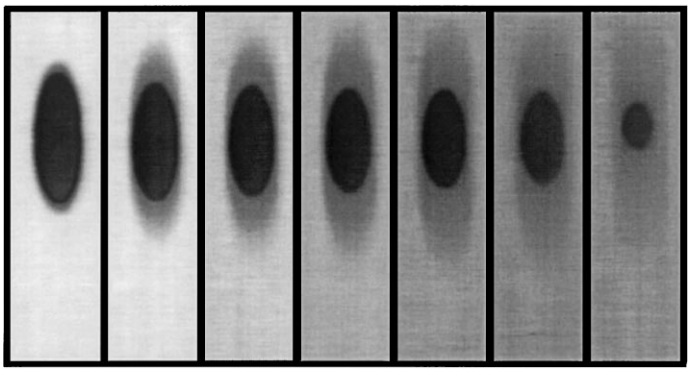

Fig. 12. Sequence of PEEM images (50 μm $\times$ 190 μm) showing anisotropic diffusion of oxygen on Pt(1 1 0) at 606 K. Oxygen is initially concentrated in an elliptical spot, oriented along the $[1\,\bar{1}\,0]$ direction. Time lap between subsequent images: 120 s. From [279].

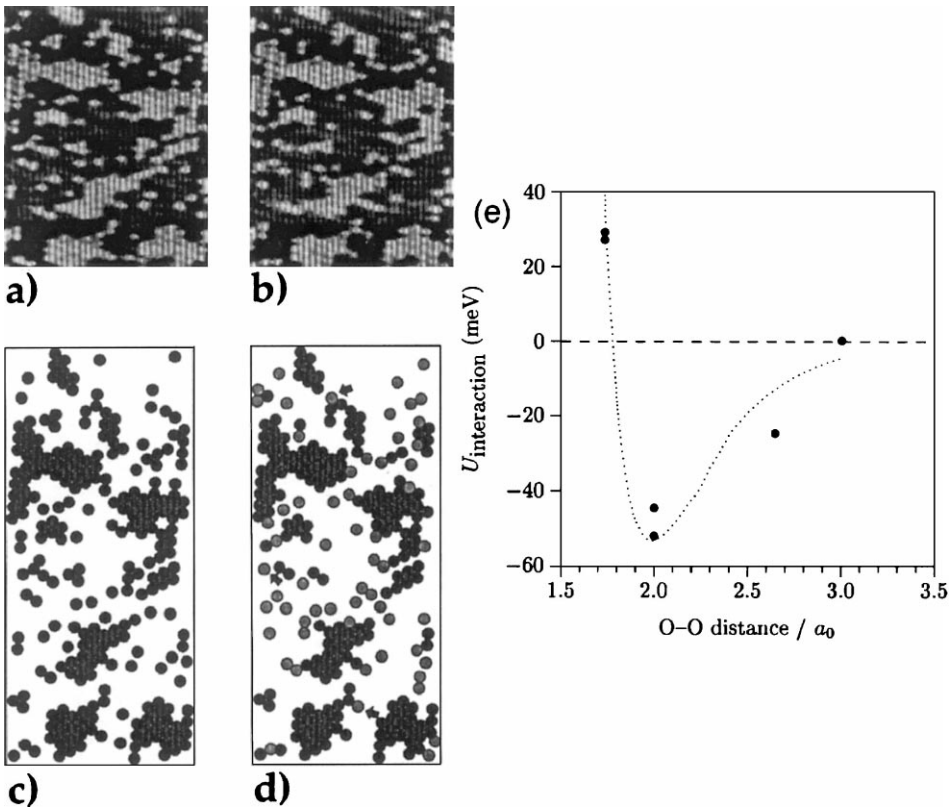

Fig. 13. (a, b) Constant-height STM images monitoring the random motion of isolated O adatoms coexisting with ordered O-islands on a Ru(0 0 0 1) surface for $\theta = 0.09$ ML at 300 K (time lap between subsequent images: 0.17 s; image size 80×190 Å^2). (c, d) Corresponding ball model; the atoms colored lighter in (d) have moved between the measurements. From [243]. (e) O–O pair interaction potential as a function of distance derived from a statistical analysis of O_{ad}-pair hopping events. From [244].

Due to the preparation technique O transport took place from (1×1) to (1×2)-missing-row reconstructed areas [279].

The thermal migration of adsorbed O atoms on Ru(0 0 0 1) was monitored at 300 K by STM [243,244]. Meaurements were performed with isolated adatoms and in the coexistence regime with local (2×2)-patches, as illustrated by the series of STM images reproduced in Fig. 13. Upon assuming a standard attempt frequency of 10^{13} s^{-1}, $E_m \approx 700$ meV is obtained for isolated atoms. Since the binding energy is in the range 4.4–5.6 eV [359–361], the E_m/E_b trend found with O/Pt(1 1 1) is confirmed. From the decay of configurations with interacting adatoms, the O–O interaction energies at the surface could be analyzed. A detailed investigation of the behavior of oxygen atom pairs revealed, in accordance with the preferential arrangement of O atoms in a (2×2) structure, a dominating attractive interaction of $\approx$50 meV for a distance of $2a$ [244]. The complete interaction potential is reproduced in Fig. 13(e).

For high oxygen coverages a $3O(2 \times 2)$ structure is formed on Ru(0 0 0 1) with three O atoms per unit cell. STM observations at 300 K demonstrate the highly directional thermal motion of single vacancies within this layer leading to vacancy self-trapping [376].

Indirect evidence on the mobility of O an Al(1 1 1) was obtained from STM data [362]. Whereas measurements at 300 K indicate immobile O_{ad}, from the island formation at higher temperatures a migration barrier of 1.0–1.1 eV was derived (setting $D_0 \approx 5 \times 10^{-3}\,cm^2\,s^{-1}$). This interpretation is at variance with the O_{ad}-motions at 300 K deduced from more recent STM observations [377]. A large migration barrier is roughly confirmed by DFT calculations, providing $E_m = 0.8$ eV[94]. The binding energy of oxygen atoms was calulated to 7.6 eV [94], thus $E_m/E_b \sim 0.1-0.2$.

The surface diffusion of adsorbed sulphur atoms was investigated under very different conditions: by STM on Re(0 0 0 1) [363] and Pt(1 1 1) [245], on Ni(1 1 1) by FIM [214] and on Cu(1 1 1) by QHAS [366]. With the exception of S/Pt(1 1 1), Arrhenius analysis was not possible. Assuming standard prefactors the diffusion barriers are estimated to 0.8, 0.3 and 0.25 eV, respectively. The corresponding E_m/E_b ratios are in the 0.1–0.2 range.

4.1.3. Noble gases

Noble gases bind to metal surfaces predominantly by weak interactions. As a consequence, the potential variation experienced by the adatoms is generally small and surface mobility investigations require very low substrate temperatures. Early FEM shadowing measurements accordingly indicated small diffusion barriers for adsorbed noble gases on tungsten surfaces [378,379]. It is also important to recognize that the lateral adsorbate interactions may come close to the diffusion barrier.

Systematic surface diffusion studies with noble gases on metals have been performed by FEM, LITD and QHAS. The results are summarized in Table 4.

The FEM fluctuation method was employed for a study of the Xe/W(1 1 0) system [380]. It was found that the diffusion barrier is ≈50 meV at $\theta = 0.3$ and $0.9\theta_s$, and thus amounts to an appreciable fraction of the binding energy, which has been estimated to ≈170 meV [381]. Both repulsive and attractive interactions were invoked to explain the coverage dependence of the mean square fluctuations [30,380]. The pre-exponential factor was very small, $\sim 10^{-8}\,cm^2\,s^{-1}$. This minute value could be rationalized neither by calculations employing the Fokker–Planck formalism [52] nor by MD simulations [122]. The theoretical studies agreed on prefactors of $\sim 10^{-4}\,cm^2\,s^{-1}$, even in the low-coverage limit. The reasons for these discrepancies are unclear. It was speculated on inherently small attempt frequencies for the adsorbed noble gases [52]. For Xe/W(0 0 1) a diffusion barrier of ∼110 meV was deduced from FEM fluctuation measurements [384].

In LITD studies of Xe diffusion on Pt(1 1 1) at low coverages a strong fall-off of the diffusivity was observed, associated with attractive adatom interactions [383]. LITD studies of Kr on Pt(1 1 1) at a constant temperature of 45 K indicate similar trends [382]. At higher Xe coverages between $\theta = 0.25\theta_s$ and θ_s, the diffusion barrier of ≈50 meV did not change and prefactors of $3.4 \times 10^{-4\pm0.5}$ and $1.1 \times 10^{-4\pm0.2}\,cm^2\,s^{-1}$ were determined for $0.25\theta_s$ and θ_s, respectively [383]. In Fig. 14 the LITD results are shown. They were associated with two-dimensional diffusion in a layer of condensed Xe

Table 4
Noble gas diffusion on metals (θ is given in terms of the respective saturation coverage; estimates from original authors in {})

System	E_m (meV)	E_d (meV)	D_0 ($cm^2\,s^{-1}$)	θ	T (K)	Method	Reference	E_b (eV)	Reference
Xe/W(1 1 0)		50 ± 10	7×10^{-8}	0.3	50–70	FEM	[380]	∼0.17	[381]
Kr/Pt(1 1 1)		∼48	$\{1.5 \times 10^{-4}\}$	1	45	LITD	[382]	0.16	[382]
Xe/Pt(1 1 1)		50 ± 10	$3.4 \times 10^{-4\pm0.5}$	0.25	50–80	LITD	[383]	0.29	[383]
	<9.6		–	0.05	105	QHAS	[34]		

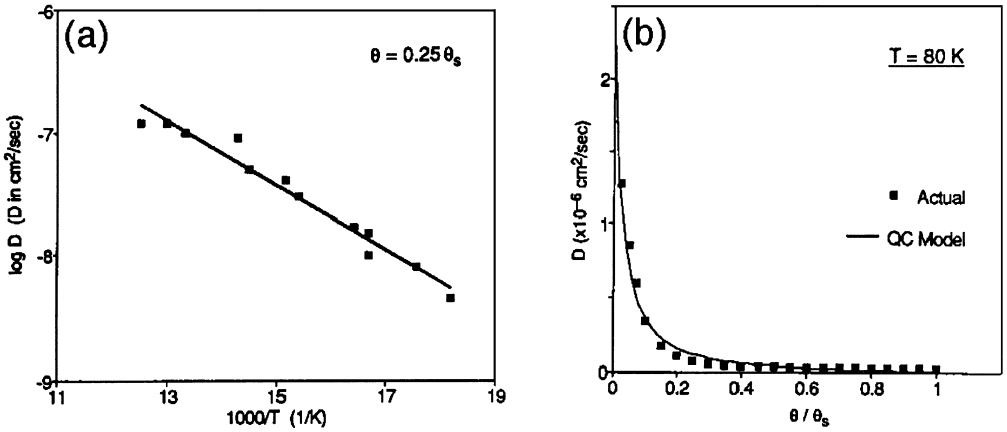

Fig. 14. (a) Arrhenius representation of the surface diffusion coefficient for Xe on Pt(1 1 1) at $\theta = 0.25\theta_s$; (b) Xe surface diffusivity vs coverage at $T = 80$ K. From a LITD analysis [383].

islands coexisting with isolated Xe atoms, evaporated from the edges of the former. The significance of islands reflects the magnitude of the lateral Xe–Xe interactions estimated in earlier studies to ~35 meV [385,386], in qualitative agreement with the recent HAS data based statement that the lateral interactions of adsorbed Xe are similar to that of the gas phase [387].

For comparison, an indirect estimate for the Xe diffusion barrier on Pt(1 1 1) of 30 meV was derived from the energetics of the commensurate–incommensurate phase transition [385], in rough agreement with theoretical predictions [388–390] and an indirect STM estimate from the observation of single Xe migration on Pt(1 1 1) [391]. The STM observations further signal a barrier for two-dimensional evaporation of Xe at Xe-island edges of ≈64 meV [391].

MD simulations indicate long and correlated jumps of diffusing Xe on Pt(1 1 1) due to the small substrate corrugation but agree with the LITD results of 'normal' diffusion [392].

In a recent QHAS study the Xe/Pt(1 1 1) system was investigated for a small coverage at $T = 105$ K. Under these conditions a two-dimensional gas phase should exist [385]. It was found that the corresponding quasielastic peak broadening does not exhibit the Lorentzian shape expected from hopping diffusion mechanisms (cf. Section 3.5). Rather, a Gaussian profile was observed, as illustrated by the plot in Fig. 15. It was associated with a fully mobile two-dimensional gas of adsorbed Xe atoms experiencing a surface corrugation falling below 10 meV [34]. This barrier suggests that $k_B T \approx E_m$ under the conditions where the measurements have been performed, i.e., the surface diffusion is expected to proceed beyond the hopping regime.

An upper limit for the corresponding friction parameter was determined to $\eta \leq 0.25\,\mathrm{ps}^{-1}$ by MD simulations, consistent with recent theoretical estimates for phononic and electronic friction of Xe on silver surfaces [73,76,393].

In marked contrast to the results obtained on Pt(1 1 1), LITD indicates that Xe diffusion on the stepped Pt(11,11,9) surface is coverage independent and proceeds without Xe island formation or trapping at steps [394]. Evidence was obtained for the preferential diffusion of Xe in the direction parallel to the steps, where the data evaluation provided an extraordinarily high prefactor of 50 $\mathrm{cm}^2\,\mathrm{s}^{-1}$ and a barrier of 120 meV [394]. However, in view of recent results (by STM for Xe/Pt(1 1 1) [395] and by HAS for Xe/Pt(9 9 7) [396,397]), demonstrating substantial attractive interaction of noble gas atoms

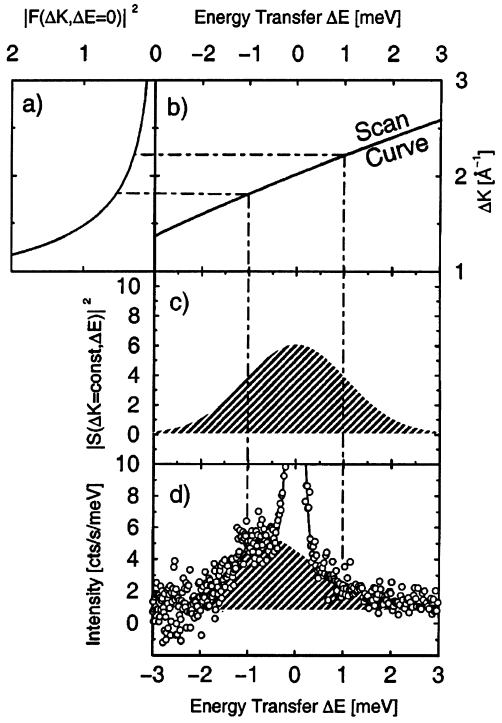

Fig. 15. Gaussian broadening of the QHAS peak observed for $\theta = 0.05\,\theta_{sat}$ Xe on Pt(1 1 1) at $T = 105$ K. The plot shows the origin of the broadening. The observed dependence of the intensity on the momentum transfer in (a) combines with that of the energy transfer (scan curve (b)) to enhance the intensity of the quasielastic peak with Gaussian shape in (c). (d) The resulting peak shape, convoluted with the instrument response function, fits the experimental data (whereby a linear background has been added to (c)). From [34].

with Pt atomic steps, a data reevaluation seems to be appropriate. Presumably both lateral attractive Xe–Xe interactions and the repulsions between Xe located at steps and Xe in terraces suggested from STM observations [395] account for a complex diffusion scenario.

In summary, agreement on the smallness of the barriers for diffusing adsorbed noble gas atoms exists. The pronounced lateral interactions may strongly affect their surface mobility. Further investigations are required to clarify the physical origin of the wide range of the prefactors reported.

4.2. Molecules

With the diffusion of adsorbed molecular species, additional degrees of freedom exist, since molecular rotations, reorientations or conformational changes may correlate with the lateral transport.

4.2.1. Carbon monoxide

The earliest CO surface diffusion studies have been performed with the FEM shadowing method on platinum surfaces [398] and W(1 1 0) [399]. With the latter system, dissociation sets in before diffusion. Over the last years, all modern techniques have been employed. The results are summarized in Table 5.

Table 5
CO diffusion on metals (1 ML corresponds to 1 CO molecule per substrate atom; estimates from original authors in {}; $\|$ is the $[1\,\bar{1}\,0]$ and $\perp$ the [0 0 1] direction on an f.c.c.(1 1 0) substrate)

System	E_m (meV)	E_d (meV)	D_0 (cm^2 s^{-1})	θ (ML)	T (K)	Method	Reference	E_b (eV)	Reference
CO/Mo(1 1 0)		220–560	10^{-3}–10^{4}	0.1–0.8	115–220	FEM	[353]	–	
CO/Ru(0 0 1)		480–270	0.38–0.06	0.27–0.58	290–370	LITD	[400]	1.6	[401]
CO/Rh(1 1 1)		310 ± 20	2×10^{-3}–3×10^{-2}	0.01–0.4	260–400	LITD	[324]	1.3	[402]
CO/Ni(0 0 1)		280–200	0.25–0.03	0.25–0.66	200–300	LITD	[403]	1.2	[404]
	27 ± 3 ⟨1 0 0⟩		$5 \times 10^{-3\pm0.3}$	0.1	–	QHAS	[260]		
	33 ± 3 ⟨1 1 0⟩		$7 \times 10^{-3\pm0.3}$				[270]		
CO/Ni(1 1 0)		170–90$\|$	1.5×10^{-6}–2×10^{-8}	0.1–1	140–220	LOD	[287]	1.3–1.4	[405,406]
		200–120$\perp$	4.5×10^{-6}–2×10^{-8}		180–240				
	$57 \pm 4\|$		1.8×10^{-4}	0.15	200–360	QHAS	[265]		
	$35 \pm 4\perp$		7.3×10^{-5}		240–360				
CO/Ni(1 1 1)		300	1.2×10^{-5}	0.5	219–273	SHD	[281]	1.1	[407]
		290	1×10^{-3}	0.1–0.5	130–220	FEM	[408]		
CO/Pd(1 1 1)		520 ± 30	$1 \times 10^{0\pm2}$	0.1	321–400	PEEM	[278]	1.5	[309]
		175 ± 12	$2.2 \times 10^{-3\pm0.3}$	–	160–260	PEEM	[222]		
CO/Pt(1 1 0)(1 × 2)		$570 \pm 10\|$	$1.5 \times 10^{0\pm1}$	–	320–370	PEEM	[279]	1.9–2.1	[269]
		$480 \pm 30\perp$	$6 \times 10^{-2\pm1}$		320–370	PEEM	[279]		
CO/Pt(1 1 0)′(1 × 1)′		$430 \pm 20\|$	$5 \times 10^{-3\pm1}$	–	320–440	PEEM	[279]		
		$390 \pm 30\perp$	$7 \times 10^{-4\pm1}$		320–440	PEEM	[279]		
CO/Pt(1 1 1)		300	$\{6 \times 10^{-5}\}$	<0.05	150–200	HAS[a]	[304]	1.4	[409]
		170 ± 30	4×10^{-7}	<0.03	90–200	IRAS[a]	[306]		
		260 ± 10	$5.0 \pm 0.1 \times 10^{-7}$	0.01	273–373	HAS	[302]		
		540–550	0.6–1.2	0.1–0.4	320–360	LITD	[410]		
	155 ± 30		–	0.11	37–42	IRAS[b]	[411]		
		540	7.5×10^{2}	–	480–520	HREELS	[308]		
		204 ± 4–	$1.4 \pm 0.4 \times 10^{-6}$–	0.1–0.67	130–320	LOD	[288]		
		130 ± 4	$4.5 \pm 1 \times 10^{-7}$						
	130 ± 20		$\sim 1.4 \times 10^{-4}$	0.05	400	QHAS[c]	[272]		
CO/Cu(0 0 1)	31 ± 10		–	0.06	115–150	QHAS	[271]	0.6	[412]
CO/Cu(1 1 0)	$97 \pm 4\|$		$2.5 \times 10^{-8\pm0.4}$	Monomer	40–55	STM	[413]	0.65	[414,415]
	$103 \pm 5\|$		$3.6 \times 10^{-7\pm0.4}$	Dimer					

[a]Step decoration.
[b]From bridge-to-top site hops.
[c]Estimate from frustrated translation.

The collective diffusion of CO on Mo(1 1 0) was investigated by the FEM fluctuation method at temperatures below 220 K, where dissociation is inhibited [416]. For $\theta < 0.4$ ML the diffusion barrier is ≈220 meV with prefactors in the range 10^{-3}–10^{-4} cm^2 s^{-1}. For higher coverages both prefactor and barrier rise substantially reaching 560 meV and 10^4 cm^2 s^{-1}, respectively, at $\theta = 0.8$ ML. Possibly a coverage dependent change in the CO adsorption geometry is at the origin of this behavior [416].

The collective diffusion of CO on Ru(0 0 1) was investigated by LITD [400]. It was found that the CO diffusivity is almost constant up to $\theta \approx 0.3$ ML and then increases markedly with the coverage: the diffusion barriers fall from 480 to 270 meV and the prefactors from 0.38 to 0.06 cm^2 s^{-1}. Repulsive nearest-neighbor CO interactions (supported by earlier LEED observations [401]) were invoked for the strong coverage dependance. An earlier LITD study of the CO/Rh(1 1 1) system indicated only a weak variation of the diffusivity with coverages up to 0.4 ML, and prefactors in accordance with TST [324]. Ab initio calculations revealing a barrier between top and bridge site have been reported for CO on Rh(0 0 1) [417].

Several reports exist on the mobility of CO on Ni surfaces:

The CO/Ni(0 0 1) system has been studied by both LITD [403] and QHAS [260,270]. While the QHAS data indicate a 'normal' prefactor, from the LITD results rather high values were derived. Contradictory are also the energetics obtained, where the QHAS result signals minute diffusion barriers falling below 50 meV, which is a tiny fraction of the adsorption energy. A modeling of CO/Ni(0 0 1) diffusion taking into account the possibility of top and bridge sites for adsorption is described in Refs. [418]. Diffusion studies of coadsorbed CO and D on Ni(0 0 1) have been performed by LITD [329]. The influence of defects on CO diffusion was investigated by exposing the surface to heavy laser irradiation. As a result reduced diffusivities were observed [221].

Discrepancies exist similarly with the CO/Ni(1 1 0) system, which was investigated by LOD [287] and QHAS [265]. The studies only agree on anisotropic diffusion, reflecting the symmetry of the f.c.c.(1 1 0) substrate lattice. The LOD results indicate a coverage-independent diffusivity for $\theta < 0.7$ ML with a strong decrease of both barriers and prefactors for higher θ (cf. Fig. 16). This behavior correlates with the coverage dependence of the desorption energy [406] and short-range CO–CO interactions were invoked to account for the reduction [287]. For comparision, the low-θ diffusion barriers derived from the QHAS data are substantially smaller and the corresponding prefactors are

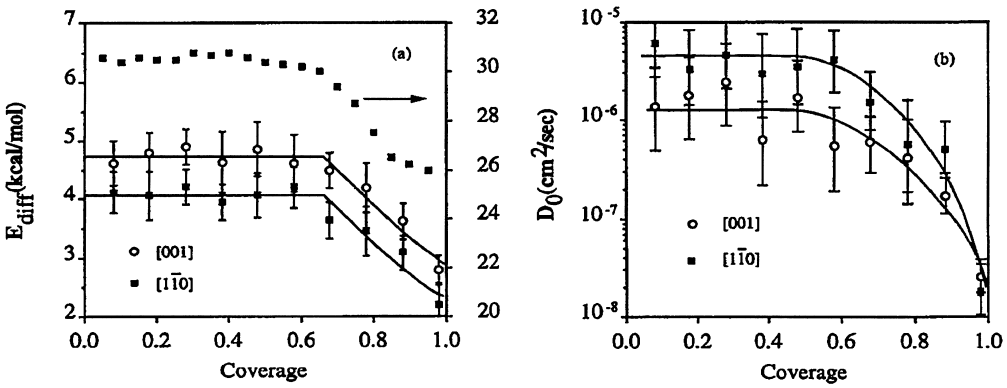

Fig. 16. Coverage dependance of anisotropic CO diffusion on Ni(1 1 0) obtained from LOD observations: (a) diffusion barriers along with the coverage dependence of the desorption energy; (b) corresponding prefactors. From [287].

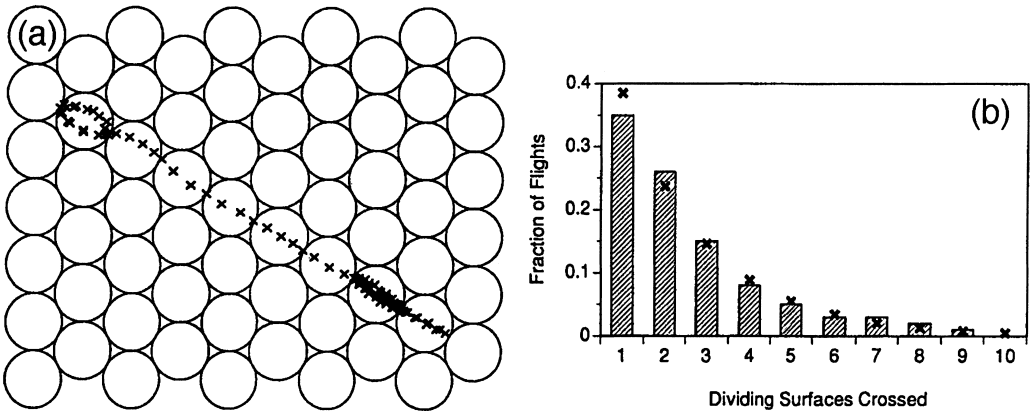

Fig. 17. Molecular dynamics simulation for CO diffusion on a Ni(1 1 1) surface. The representative molecular trajectory at 200 K in (a) shows a long jump with a correlated sequence of transition state crossings (crosses mark the CO position at 0.1 ps intervals, total time: 10 ps). (b) Dividing surfaces crossed per flight for diffusion at 200 K. Crosses mark an exponential fit with a lifetime of $\tau = 3$ ps. From [44].

higher (cf. Table 5). Effects of impurities such as S, O and K on CO diffusion on Ni(1 1 0) were investigated by LOD [296,297].

The diffusion of CO on Ni(1 1 1) was observed by SHD [281] and the FEM fluctuation technique [408]. The FEM results indicate coverage-independent parameters in the range investigated (0.1–0.5 ML). Both studies agree on a diffusion barrier of ≈300 meV.

An extensive theoretical investigation of single CO diffusion on Ni(1 1 1) was performed by MD [44]. It was found that Arrhenius behavior is obeyed in the temperature range 175–1000 K (with $E_m = 95$ meV and $D_0 = 8.4 \times 10^{-3}$ cm^2 s^{-1}). A representative trajectory at 200 K is reproduced in Fig. 17a demonstrating that molecules acquiring sufficient energy to overcome the migration barrier usually remain excited and cross another transition state. The corresponding jump length distribution is reproduced in Fig. 17b. It can be fitted by an expression suggested for one-dimensional diffusion [16] with the jump probability over n sites given by $P_n = c\exp[-na/\overline{v}\tau]$, where τ is a lifetime for the relaxation of the lateral translational motion, $\overline{v} = \sqrt{2k_BT/\pi m}$ the average velocity through the initial dividing surface for an equilibrium ensemble of particles of mass m; c a normalization constant.

Ab initio calculations have been performed to gain insight into the diffusion of CO on Pd(1 1 0) [96]. An adsorption heat of -1.43 eV and migration barriers of 300 and 600 meV along [0 0 1] and $[1\,\overline{1}\,0]$ were calculated, respectively. Furthermore a coupling between the translational and the rotational motion of the molecule was found, which is possibly equally applicable for the CO/Ni(1 1 0) system [96].

For the CO/Pd(1 1 1) system PEEM results have been obtained [222,278]. With the first study the refilling of a ∼200 μm bare spot created by LITD on the CO covered surface was analyzed [278], whereupon a migration barrier of 520 meV and a prefactor of 1 cm^2 s^{-1} were derived from a Boltzmann–Matano analysis. The second study [222] indicates a substantially smaller barrier of 175 meV and a 'normal' prefactor from a detailed analysis on a more local scale of the spreading of a 100 μm wide CO strip created via adsorption through a mask, as shown in Fig. 18 [222]. In particular, it was pointed out that unresolved defect features sensitively influence the adsorbate diffusion even on a

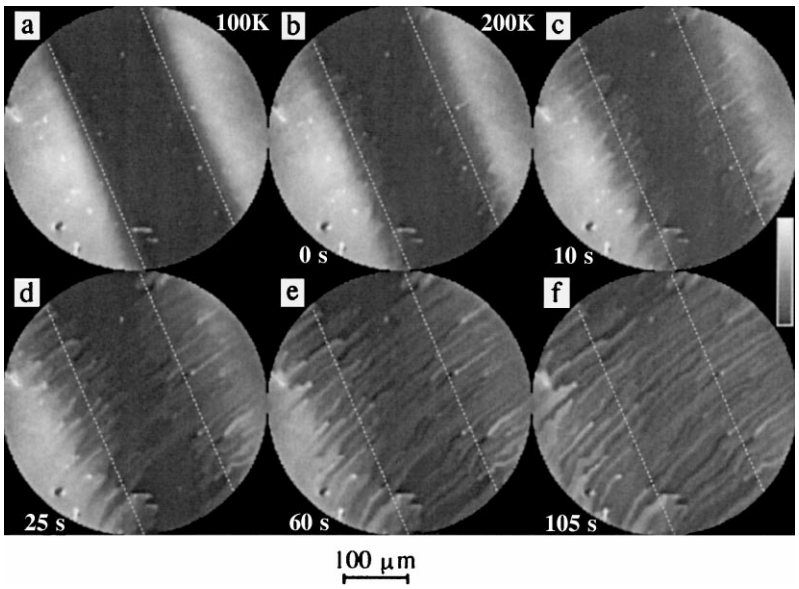

Fig. 18. PEEM observation of a CO strip with a coverage of 0.33 ML adsorbed through a mask on Pd(1 1 1). (a) as prepared at 100 K; (b) temporal evolution after heating to 200 K. The adsorbate mobility is guided by morphological features at the surface leading to quasi-one-dimensional diffusion of CO-'streamers'. From [222].

well-prepared surface and that results comparable with those of the first study could be obtained on a mildly sputtered surface [222].

PEEM studies have been performed for the CO/Pt(1 1 0) system where the refilling of a desorption spot created by LITD was monitored [279]. The clean Pt(1 1 0) surface exhibits a (1×2) reconstruction, whereas upon CO adsorption the bulk (1×1) termination is restored. The experiments demonstrated that the structural transformation of the Pt surface strongly affects the CO diffusion. Diffusion experiments performed at $T < 380$ K exhibit two different diffusivities depending on the state of the surface. Since only the initial state of the (1×1) phase is well known and structural changes may occur in the diffusion region, it is designated as '(1×1)'. Ab initio calculations of the surface diffusion PESs for CO on (1×1) and (1×2) Pt(1 1 0) were reported recently [269]. It was found that the diffusion saddle points are 0.4 Å away from the bridge site with barrier heights 0.13 and 0.17 eV, respectively.

The diffusion of CO on Pt(1 1 1) was studied by a variety of techniques, including notably defect-decoration methods [304,306], HAS [302], LITD [410], scanning HREELS [308], LOD [288] and QHAS [272] (cf. Table 5). Recent LOD data are compared with earlier results in Fig. 19 [288]. The obtained diffusion parameters scatter strongly and it seems clear that either different processes have been actually observed or some data interpretations are erroneous. It was argued that the substantial deviations in the data sets are due to the employment of different techniques investigating different length scales and the presence of substrate defects, particularly atomic steps [288]. This idea relies on LOD data taken on a sample with a high density of steps, where markedly increased diffusion barriers and prefactors were observed as compared to a substrate with a lower step density investigated with the same apparatus (cf. Fig. 19).

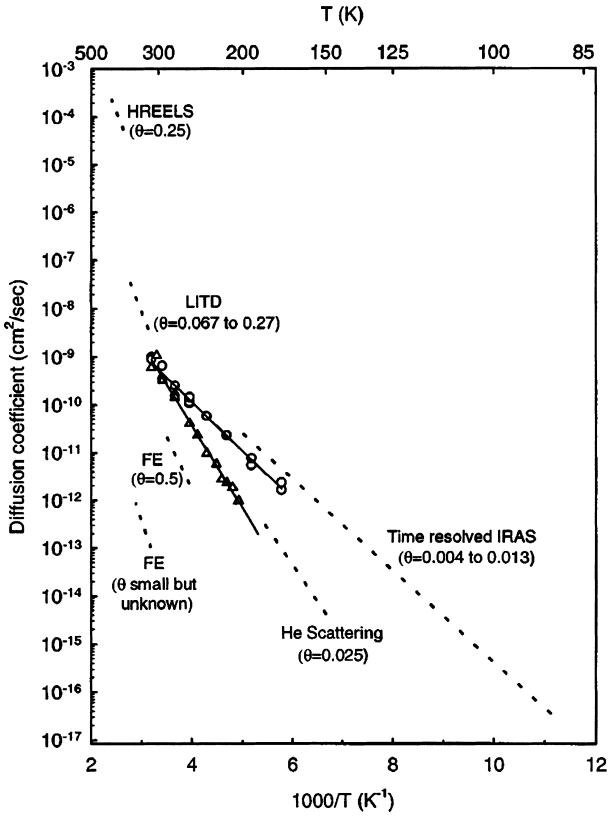

Fig. 19. Arrhenius plot comprising different CO/Pt(1 1 1) surface diffusion data sets. The dashed lines symbolize results from IRAS [306], HAS [304], FEM [398], LITD [410], and HREELS [308] studies. LOD results obtained on <0.1° (2°) miscut surface at a coverage of ~0.1 ML (0.3 ML) are represented by circles (triangles). From [288].

The LOD observations on a small-miscut crystal are in line with the time-resolved IRAS results, where step decoration was analyzed [306], and HAS data [302], indicating a diffusion barrier in the vicinity of 200 meV and low prefactors in the range 10^{-6}–10^{-7} $cm^2\,s^{-1}$. In recent MD simulations a somewhat larger barrier of 252 meV and a prefactor of 3.3×10^{-4} $cm^2\,s^{-1}$ were obtained [419]. Even smaller barriers of 130 and 155 meV were estimated from the frustrated translation energy by QHAS [272] and from IRAS measurements (where hopping rates from the bridge to the top sites could be determined [411]), respectively. The CO diffusivity is weakly growing with increasing coverages, which reflects the operation of repulsive CO–CO interactions, in agreement with recent theoretical results [420]. Effects of steps and P-contaminations on the CO diffusion were systematically studied recently [421–423].

The CO/Cu(0 0 1) system was studied by LITD [215]. Data taken at $T = 140\,K$ indicate $E_d \sim 100\,meV$, assuming a prefactor of 0.1–0.01 $cm^2\,s^{-1}$. In a recent HAS/IRAS study the lateral PES experienced by the CO molecules was addressed [271]. Based on a simple model analysis it was concluded that subtle molecular reorientations occur in the diffusion process, substantiating the CO/Pd(1 1 0) ab initio calculations [96]. A schematic contour plot is depicted in Fig. 20b (note, however, that related recent theoretical work with CO/Pt(1 1 0) revealed a more complex potential [269]).

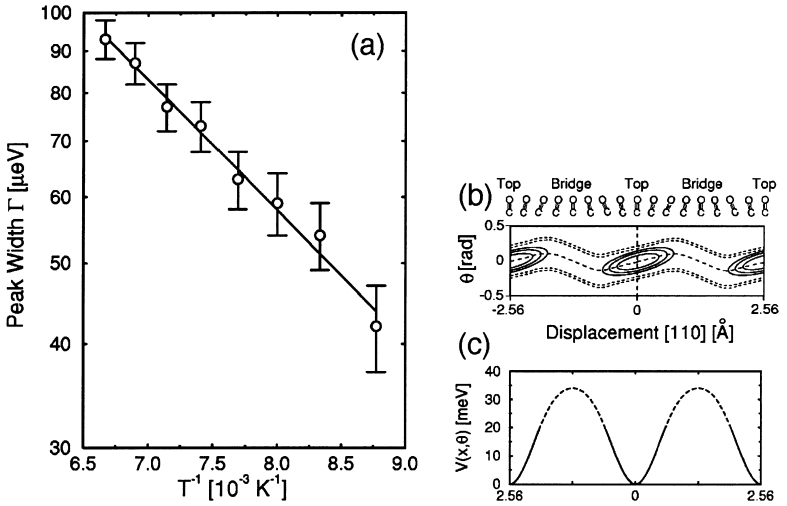

Fig. 20. (a) Arrhenius plot of the temperature dependence of the quasielastic peak width for 0.059 ML CO on a Cu(0 0 1) surface. The solid line fit yields an activation energy of 31 ± 10 meV. (b) Two-dimensional cut in the (x, θ) plane for CO/Cu(0 0 1) along [1 1 0] with transient CO configurations indicated. x and θ are the lateral displacement and the tilt angle with respect to the surface normal, respectively. Equipotential lines have a spacing of 10 meV. (c) Potential energy along the reaction coordinate in [1 1 0] with the barrier at the bridge site derived from (a). From [271].

Corresponding QHAS data indicate a dynamic migration barrier of 31 ± 10 meV [271] (cf. Fig. 20). Recent MD simulations of equilibrated CO on Cu(0 0 1) demonstrate that the friction they experience is mainly of phononic origin. For the diffusion an Arrhenius law was confirmed over a wide temperature range (~200–400 K) with $E_m = 132 \pm 6$ meV and $D_0 \approx 2.4 \pm 0.4 \times 10^{-3}\,cm^2\,s^{-1}$ [74].

Low-temperature STM observations have been reported for CO on Cu(1 1 0) [413]. The diffusion is anisotropic along $[1\,\bar{1}\,0]$. For single molecules an activation energy of 97 ± 4 meV along with a rather small prefactor of $2.5 \times 10^{-8\pm0.37}\,cm^2\,s^{-1}$ was found. Attractive lateral interactions between the CO exist leading to the formation of CO-strings in [0 0 1] (cf. Fig. 21a). Surprisingly it turned out that the molecular diffusion is enhanced by the CO interactions and that the dimers move more rapidly than the monomers, as shown in Fig. 21b. This enhancement is predominantly driven by a substantial increase of the dimer diffusion prefactor by a factor $1.44 \times 10^{1\pm0.55}$ with respect to the monomers', which result was associated with entropy effects [413].

Summarizing, it turns out that many results concerning CO diffusion are contradictory although strong efforts have been undertaken and considerable insight has been gained. There is a conspicuous overall trend that the diffusion characteristics correlate with the length scale of the methods employed, i.e., larger diffusion barriers and prefactors from macroscopic observations of surface diffusion (LITD, etc.) contrast results where surface diffusion is probed on a local scale (QHAS, STM) indicating smaller values. Recent studies furthermore signal extraordinarily small prefactors, for which a theoretical explanation is currently lacking.

4.2.2. Other anorganic molecules

A small number of studies on surface mobility of anorganic molecules other than CO at metal surfaces exists, which is presented in Table 6.

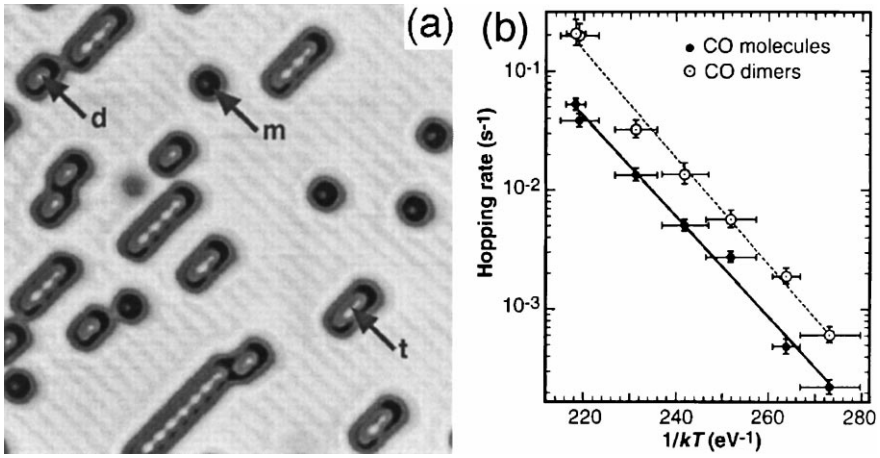

Fig. 21. (a) The STM topograph of CO adsorbed on Cu(1 1 0) recorded at 9 K reveals the coexistence of CO monomers and oligomers oriented in the [0 0 1] direction. Monomers, dimers and trimers are marked by m, d and t, respectively. (b) Arrhenius plot of the diffusion of CO molecules (filled circles) and CO dimers (open circles) in $[1\,\bar{1}\,0]$. The hopping frequencies were extracted from STM observations at $T = 42-53$ K. From [413].

The diffusion of ammonia on Re(0 0 1) was studied by SHD [289]. For coverages below ≈0.12 ML the diffusion barrier is 150 ± 30 meV. With higher coverages repulsive lateral NH_3-interactions influence the diffusion process and lead to an increased mobility [424]. The magnitude of these interactions was analyzed in detail by MC simulations [429] and ab initio calculations [420], which agree on a repulsive energy of ≈90 meV for an intermolecular spacing of $2a$.

The operation of repulsive interactions was similarly deduced for NO adsorbed on Pt(1 1 1), a system studied by HAS [303]. From the analysis of the decay of a NO covered spot at the surface, a diffusion barrier of 510 ± 50 meV and a prefactor of 2.4×10^{-3} cm^2 s^{-1} were derived [303].

The lateral PES of the NO/Pt(1 1 0)(1 × 2) system was explored by a combined IRAS and density functional theory investigation [430]. Distinct potential energy minima could be identified by the calculations and hopping barriers of metastable NO species could be estimated by IRAS from the disappearance of the corresponding vibrational modes at specific threshold temperatures.

In recent MC simulations the role of surface diffusion for the ordering of NO on Rh(1 1 1) was addressed. The results demonstrate that the increasing saturation coverage and lateral ordering at higher temperatures are due to the enhanced molecular surface mobility [431]. The diffusion parameters were

Table 6
Diffusion of anorganic molecules on metal surfaces (θ is given in number of admolecules per substrate atom; estimates by original authors in {}; $\parallel$ is the $[1\,\bar{1}\,0]$ and $\perp$ the [0 0 1] direction on an f.c.c.(1 1 0) substrate)

System	E_m (meV)	E_d (meV)	D_0 (cm^2 s^{-1})	θ (ML)	T (K)	Method	Reference	E_b (eV)	Reference
NH_3/Re(0 0 1)		150 ± 30	2.8×10^{-3}	0.12	110–140	SHD	[289]	0.9	[424]
NO/Pt(1 1 1)		510 ± 50	2.4×10^{-3}	∼0.1	310–360	HAS	[303]	1.3	[303]
O_2/Ag(1 1 0)	$220 \pm 50\parallel$ ∼300$\perp$		$4 \times 10^{-3\pm3}$ $\{4 \times 10^{-3}\}$	Monomer	60–100	STM	[425]	0.4–0.8	[426–428]

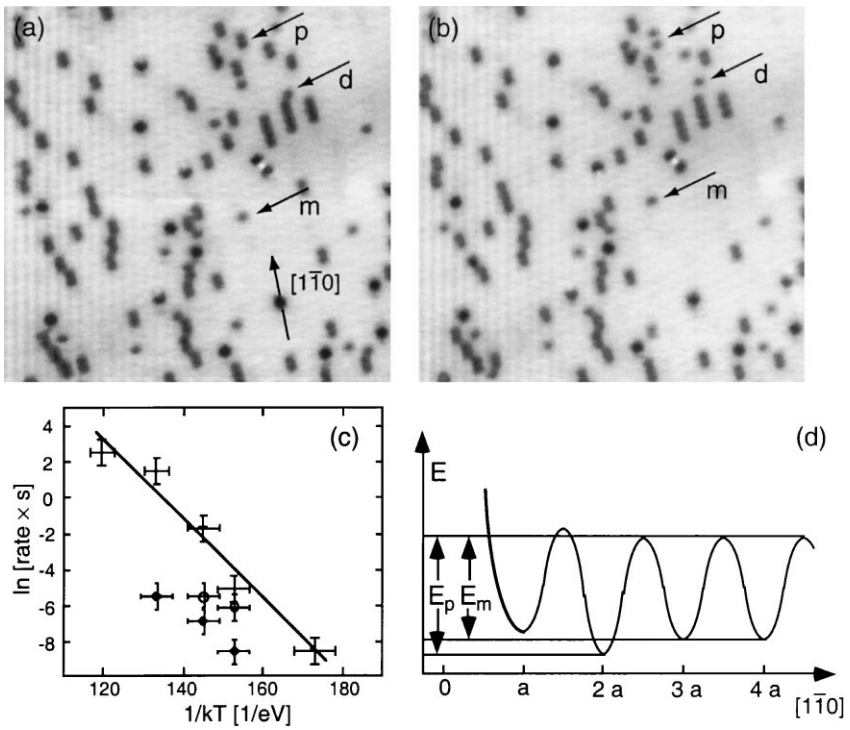

Fig. 22. (a, b) STM topographs of molecular oxygen adsorbed on Ag(1 1 0) recorded at 76 K with a time lap of 200 s. The migration of single oxygen molecules and the decay of O_2-pairs and diagonal arrangements are marked by arrows m, p and d, respectively. (c) Arrhenius representation of the respective rates (plus signs: monomer migration, open circle: decay of diagonal couple and filled diamonds: pairs). (d) Schematic potential diagram in $[1\,\bar{1}\,0]$ for an O_2-molecule interacting with another molecule located at the origin; E_m (E_p) corresponds to the barrier for monomer migration (pair decay). From [425].

optimized to fit LEED results: for $T \leq 200\,\mathrm{K}$ a barrier of 560 meV and an attempt frequency of $3 \times 10^{13}\,\mathrm{s}^{-1}$ was found.

Direct observations of both molecular migration and interactions could be achieved for oxygen molecules on Ag(1 1 0) by STM [425]. The data reproduced in Fig. 22 demonstrate that already at very low coverages the O_2-distribution at the surface is strongly influenced by the lateral attractive intermolecular interactions, which induce the formation of O_2-strings in the Ag $[1\,\bar{1}\,0]$ troughs and a diagonal coupling of molecules in neighboring troughs, both with equilibrium distances of $2a$ along $[1\,\bar{1}\,0]$. Since the interactions are weak, the thermal decay of such aggregates could be monitored simultaneously with the monomer diffusion, which is exclusively directed along $[1\,\bar{1}\,0]$ for $T < 100\,\mathrm{K}$. From the determination of the rates for the respective processes, the monomer migration barrier was determined to 220 ± 50 meV, the next nearest-neighbor attractive energy in $[1\,\bar{1}\,0]$ to 40 ± 10 meV, and the coupling energy for molecules in adjacent troughs to 20 ± 10 meV [425]. The measured migration barrier is in agreement with the calculated difference in energy of 180 meV for O_2 in fourfold hollow sites and long bridge sites [432]. An analysis of the jump length distribution furthermore indicated that an appreciable fraction of the molecules performs long jumps [433].

A theoretical investigation of the diffusion mechanisms of a rigid homonuclear dimer employing a Lennard–Jones potential revealed a variety of diffusion mechanisms which were associated with the

molecular degrees of freedom [434]. Note that rotation of single oxygen molecules adsorbed flat on Pt(1 1 1) could be indeed induced and viewed by STM at 8 K [435].

4.2.3. Organic adsorbates

A fair number of studies on the surface mobility of adsorbed organic molecules can be found in the literature. A survey of the reported results is given in Table 7. The techniques applied so far are LITD and STM. The investigated adsorbates cover the range from small molecules with simple adsorption configurations to large organic molecules which exceed by far the dimensions of the respective surface unit cells. In any case additional degrees of freedom need to be considered. These include rotational motions or the occupation of different adsorption sites. With large and flexible species also conformational changes may be of importance in the molecular mobility.

Systematic observations on the mobility of *n*-alkanes (propane, *n*-butane, *n*-pentane and *n*-hexane with the chemical formula C_nH_{2n+2}) on Ru(0 0 1) were performed with the LITD technique [436]. It was found that Arrhenius behavior is obeyed in all cases and that the diffusion barrier increases linearly with the alkane chain length from 130 ± 10 to 210 ± 10 meV, whereas only small variations in the prefactors ($\sim 0.15\ cm^2\ s^{-1}$) exist [436] (cf. Fig. 23). The observed diffusion coefficients are quite independent of coverage, indicating small lateral interactions. It was suggested that the *n*-alkanes move in a rigid configuration on the surface [436]. In related investigations employing pentane isomers it was found that the diffusion barriers scale inversely with the degree of branching of the isomers [437]. Upon fluorination of *n*-butane both the diffusion barrier and the prefactor were found to be lowered [438]. Recent HAS observations with octane on Ru(0 0 1) indicate that electron–hole pair creation is involved in the damping of the molecular motion [78].

The observations of the *n*-alkane diffusion triggered extensive theoretical investigations, mostly employing MC and MD simulations [88–92,176,447]. From systematic simulations of a series of

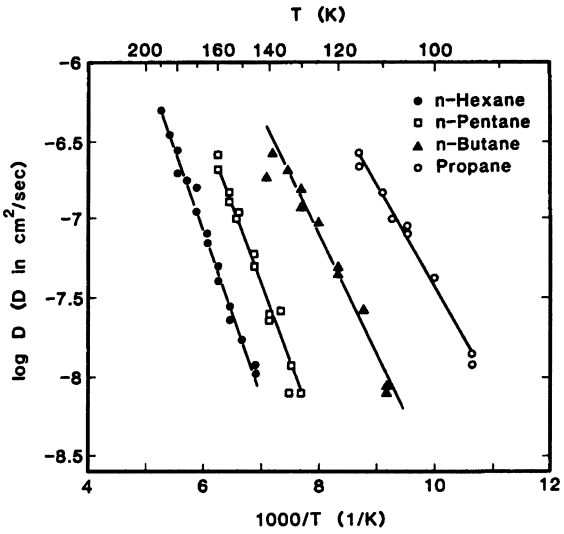

Fig. 23. Arrhenius plots of the surface diffusion coefficients for a series of *n*-alkanes adsorbed on Ru(0 0 1) at $\theta = 0.2\,\theta_{sat}$. From a LITD investigation [436].

Table 7
Diffusion of organic molecules on metals (θ is given in terms of the respective saturation coverage; estimates by original authors in {}; $\|$ is the $[1\,\bar{1}\,0]$ and $\perp$ the [0 0 1] direction on an f.c.c.(1 1 0) substrate)

System	E_m (meV)	E_d (meV)	D_0 (cm^2 s^{-1})	θ (ML)	T (K)	Method	Reference	E_b (eV)	Reference
C_3H_8/Ru(0 0 0 1)		130 ± 10	0.11	0.2	95–115	LITD	[436]	0.48	[436]
n-C_4H_{10}/Ru(0 0 0 1)		150 ± 10	0.11	0.2	110–140	LITD	[436]	0.52	[436]
n-C_5H_{12}/Ru(0 0 0 1)		200 ± 10	0.30	0.2	130–160	LITD	[436,437]	0.60	[436]
n-C_6H_{14}/Ru(0 0 0 1)		210 ± 10	0.16	0.2	140–190	LITD	[436]	0.65	[436]
Isopentane/Ru(0 0 0 1)		180 ± 10	$5.5 \times 10^{-2\pm0.1}$	0.1	130–160	LITD	[437]	0.59	[437]
Cyclo-pentane/Ru(0 0 0 1)		140 ± 10	$6.0 \times 10^{-4\pm0.1}$	0.1	130–160	LITD	[437]	0.52	[437]
Neopentane/Ru(0 0 0 1)		130 ± 10	$4.0 \times 10^{-2\pm0.1}$	0.1	130–160	LITD	[437]	0.46	[437]
Perfluoro-n-pentane/Ru(0 0 0 1)		130 ± 10	$5.9 \times 10^{-2\pm0.2}$	<0.1	95–120	LITD	[438]	0.56	[438]
Tetramethyl-silane/Ru(0 0 0 1)		140 ± 5	$5.9 \times 10^{-2\pm0.1}$	0.4	100–130	LITD	[439]	0.53	[439]
C_2H_2/Pd(1 1 0)	$\sim$570		$\{8 \times 10^{-4}\}$	Monomer	250–260	STM	[440]	–	
C_2H_2/Pd(1 1 1)	$\sim$180		$\{2 \times 10^{-3}\}$	Monomer	65–70	STM	[441]	0.36	[441]
C_6H_6/Pd(1 1 0)	$\sim$570$\perp$		$\{8 \times 10^{-4}\}$	Monomer	210–230	STM	[442]	1.1$\pm$0.2	[443]
PVBA/Pd(1 1 0)	$830 \pm 30\|$		$7.6 \times 10^{-6\pm0.4}$	Monomer	330–370	STM	[444]	–	
C_{60}/Pd(1 1 0)	$\sim$1500		–	Monomer	440–480	STM	[445,458]	–	
C_2H_2/Cu(0 0 1)	530 ± 10		$1.6 \times 10^{-2.4\pm0.2}$	Monomer	180–210	STM	[446]	–	
CH_4/Pt(1 1 1)		$\sim$23	$\{3.3 \times 10^{-4}\}$	Low	45	LITD	[382]	0.16	[382]

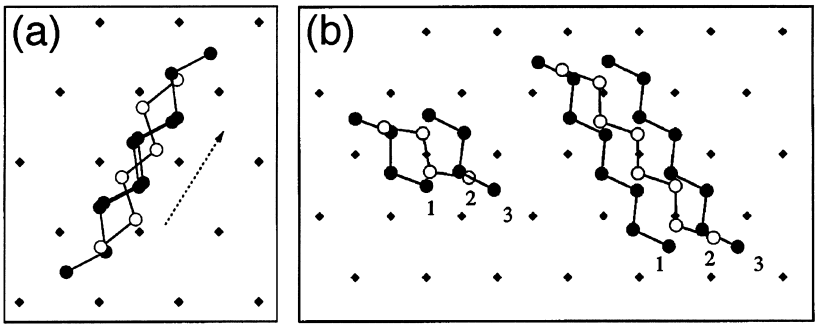

Fig. 24. Selected molecular configurations involved in (a) *n*-hexane and (b) *n*-butane and *n*-octane hopping on Pt(1 1 1) along easy migration paths. The molecular motion follows the sequence 1–2–3 in (b). Filled (open) circles indicate the carbon backbone position of the molecule at the binding site (transition state), diamonds correspond to Pt surface atoms. From [92].

n-alkanes (*n*-C_3H_8, *n*-C_6H_{14}, *n*-$C_{10}H_{22}$ and *n*-$C_{20}H_{42}$) on W(0 0 1) the trends observed experimentally on Ru(0 0 1) were confirmed in the 300–1000 K range (i.e., Arrhenius behavior, increase of E_m with the chain length), albeit with significantly smaller prefactors close to $1 \times 10^{-3}\,cm^2\,s^{-1}$ [88]. In a recent detailed TST study of *n*-alkane (*n*-butane–*n*-decane) diffusion on Pt(1 1 1) the respective mechanisms were addressed in detail [92]. It was found in particular that the hopping between nearest-neighbor sites is not strictly obeyed and directional anisotropy can be induced by the molecular orientation [92]. In addition, the motion of larger molecules involves transient occupation of local minima. Some typical diffusion paths are illustrated by the model in Fig. 24 [92]. Again, the theoretical prefactors were found to be close to the universal value.

In related theoretical studies the diffusion and spreading of chain-like molecules on solid surfaces was considered [93,448]. Chains were modeled as connected segments occupying sites on a square lattice, whereby the chain flexibility and attractive interactions can be varied [93]. The coverage and interaction dependence of tracer and collective diffusion coefficient calculated from MC simulations are displayed in the diagrams in Fig. 25. Further aspects are considered in Refs. [449–451]. Note that

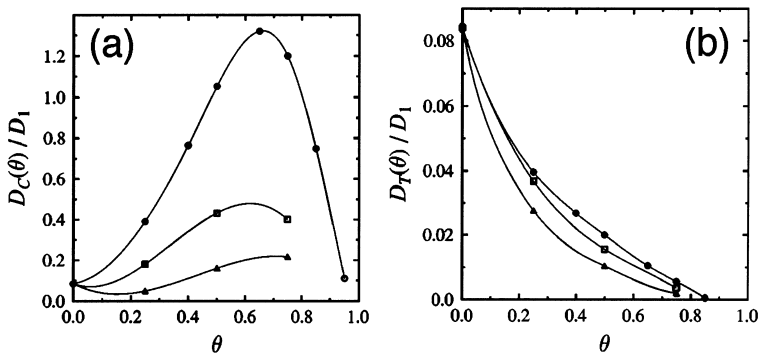

Fig. 25. Surface diffusion of flexible chain-like molecules consisting of six segments on a square substrate as a function of coverage. The collective diffusion coefficient and the tracer diffusion coefficient are shown in (a) and (b), respectively. Circles symbolize the case of non-interacting molecules; with increasing interactions the diffusivity is lowered (squares and triangles). Both curves are normalized by the single monomer diffusion coefficient D_1. From Ref. [93].

the conformational adaption of a large and flexible molecular species (Cu–tetra (3,5,di-*tert*-butyl-phenyl) porphyrin) upon adsorption on different metal substrates (Cu(0 0 1) and Ag(1 1 0)) was recently observed [452].

The mobility of various organic adsorbates on low-index Pd surfaces has been observed by STM. With adsorbed ethylene and benzene on Pd(1 1 0) only rough estimates were possible. Using standard attempt frequencies, the same barrier of 570 meV for motion of benzene in [0 0 1] perpendicular to the Pd atomic rows [442] and for the diffusion of C_2H_2 [440] was obtained. For comparision, adsorbed benzene on Cu(1 1 1) is highly mobile already at $T = 77$ K [453].

On Pd(1 1 1) both rotational and translational motions of adsorbed acetylene could be monitored [441]. The molecules rotate among three equivalent orientations at the same threefold site at the timescale of seconds for $T = 44$ K. Using a prefactor of 10^{13} s^{-1}, an activation barrier for rotation of $\approx$113 meV was estimated. Molecular migration became observable only at higher temperatures. From the rates determined at 65 and 70 K a migration barrier of $\approx$180 meV was calculated using the same prefactor [441].

A systematic study was reported for the thermal migration of PVBA (4-*trans*-2-(pyrid-4-yl-vinyl) benzoic acid) on Pd(1 1 0) [444]. This rigid and large organic molecule interacts strongly with the Pd substrate and binds diagonally to two neighboring Pd troughs (cf. Fig. 26). No changes in the adsorption geometry exist at different coverages [454]. The diffusion of single molecules is strictly one-dimensional in $[1\,\bar{1}\,0]$, i.e., along the Pd surface atom rows, whereby the molecular orientation is strictly retained, as demonstrated by the data reproduced in Fig. 26. It obeys an Arrhenius law with a migration

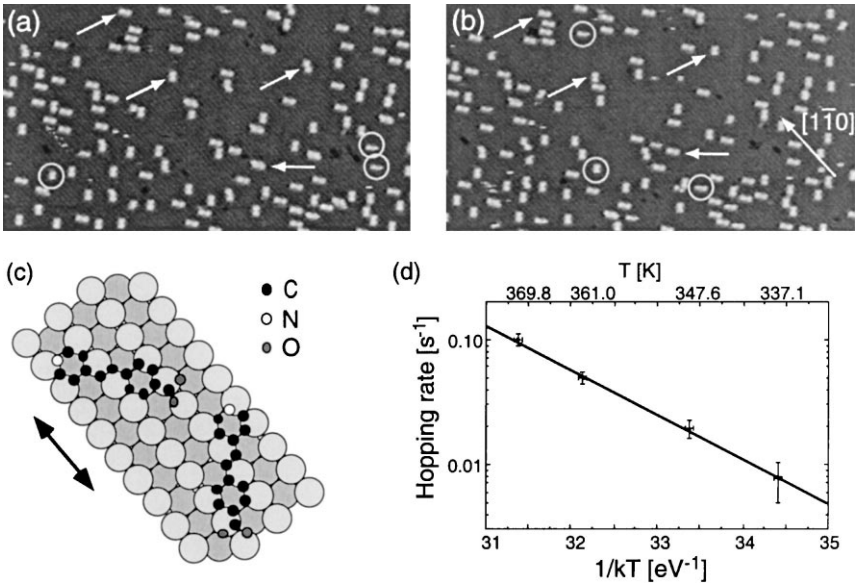

Fig. 26. Surface diffusion of the rigid rodlike molecule 4-*trans*-2-(pyrid-4-yl-vinyl) benzoic acid on Pd(1 1 0). In (a) and (b) two consecutive STM images taken at 361 K are shown which demonstrate the one-dimensional motion. Arrows indicate molecules whose position changed; circles mark fractionally imaged molecules moving under the STM tip in the course of the measurement. (c) Model for the flat adsorption geometry explaining the two observed molecular orientations in the STM data. The length of the molecule is 12.5 Å. (d) Arrhenius plot of single molecule hopping rates. From [444].

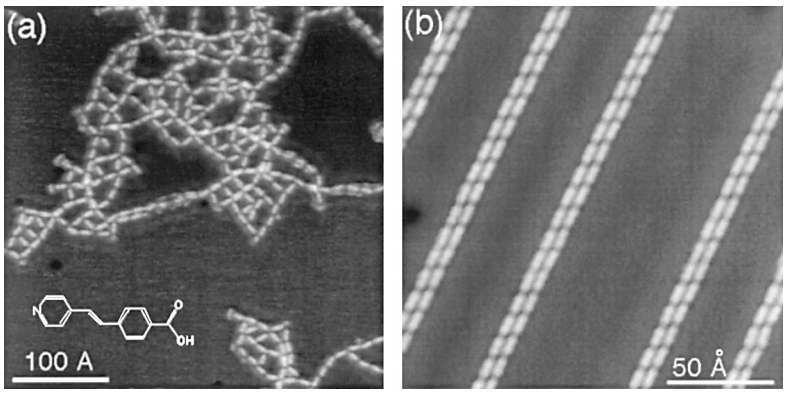

Fig. 27. (a) Complex diffusion limited aggregation of 4-*trans*-2-(pyrid-4-yl-vinyl) benzoic acid lying flat on Ag(1 1 1). The hydrogen bonding between the molecular endgroups stabilizes a molecular network upon adsorption at $T = 125$ K. (b) For the H-bond mediated self-assembly of molecular twin chains at 300 K both rotational and translational molecular mobility is required. Measured at 77 K. From [455,458].

barrier of 830 ± 30 meV and a prefactor of $7.6 \times 10^{-6\pm0.4}$ cm^2 s $-$ 1 [444]. In related investigations of the C_{60}/Pd(1 1 0) system, it was found that the migration of the adsorbed C_{60} depends sensitively on the state of the STM tip and the tunneling conditions. As a consequence, the diffusion barrier could merely be estimated to $\sim$1500 meV [445].

A complex diffusion limited aggregation scenario was observed in the PVBA/Ag(1 1 1) system at low temperatures. The operation of anisotropic hydrogen bonding between the molecular endgroups in conjunction with the smoothness of the substrate leads to the formation of molecular networks, as demonstrated by the STM data in Fig. 27. At higher temperatures, the molecules self-assemble at the surface to extended molecular chains, which are again stabilized by hydrogen bonding. The formation of this structure provides indirect evidence of both rotational and translational molecular rearrangements [455], similar with other systems [456,457].

LITD observations demonstrate a coverage independent mobility of methane on a Pt(1 1 1) surface, indicating weak lateral interactions. At a temperature of 45 K a diffusion coefficient of 1×10^{-6} cm^2 s^{-1} was found [382].

In a recent STM study of C_2H_2 on Cu(0 0 1) molecular rotation and diffusion could be monitored [446]. Both processes were found to obey an Arrhenius law. The activation energy for diffusion (rotation) is 530 ± 10 meV (169 ± 3 meV) with a prefactor of $10^{13.6\pm0.2}$ s^{-1} ($10^{11.8\pm0.2}$ s^{-1}). At lower temperatures, rotations induced by the tunneling current could be monitored (cf. Fig. 28). It was proposed that they are mediated by the coupling of vibrational excitations to the rotational motion [459]. The continous rotation of a single large organic molecule laterally confined in a small surface area has been observed by STM at room temperature [460].

5. Conception of transient mobility at surfaces

Transient mobility stands for the lateral motion of molecules (or atoms) being in metastable states or in the process of thermalization at a surface, i.e., it is surface mobility prior to the accomodation in the

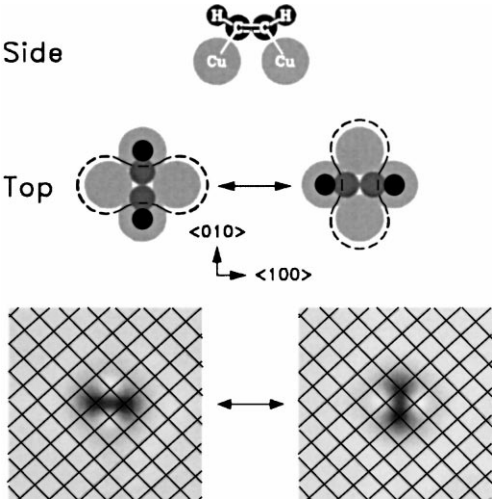

Fig. 28. Frustrated rotational motion of C_2H_2 on a Cu(0 0 1) surface induced by tunneling electrons at 8 K. The model shows top and side views of the molecular adsorption site and angular orientations. In the corresponding STM data the configurations of a specific C_2H_2 molecule at the same adsorption site with respect to the Cu substrate (indicated as a square lattice) are illustrated. From [459]. At higher temperatures thermal rotation occurs [446].

thermodynamic equilibrium state. The adsorption dynamics and the shape of the PES experienced by the adsorbing species need to be considered for an understanding of this phenomenon.

5.1. Precursors and 'hot' species

Any molecule is subject to attractive van der Waals forces in the vicinity of a metal surface. In the case of *physisorption*, the molecules are bound to the surface by such weak interactions. The adsorption energy gain is increased upon *chemisorption*, where chemical bonds between the molecule and the surface atoms are formed. A further energy gain is feasible in exothermic *dissociative chemisorption*, where intermolecular bonds are disrupted and reinforced bonding of the dissociation products to the surface occurs.

In many cases surface chemical bond formation or dissociative adsorption at a surface can be supressed by a reduction of the substrate temperature. Physisorbed or molecularly chemisorbed species can thus be stabilized. Translated into a one-dimensional energy diagram, this behavior suggests energy barriers between physisorbed and chemisorbed state viz. between molecular and dissociative chemisorption, as illustrated in Fig. 29. With the existence of such energy barriers, it seems clear that even at high temperatures molecules can be briefly trapped in the physisorbed state prior to chemisorption viz. molecularly chemisorbed prior to dissociation. Such transiently physisorbed or chemisorbed molecules are called *precursors*. Much insight on their nature has been obtained by molecular beam studies [461–465]. Kinetic models incorporating mobile precursor states have been put forward in several studies [466–471] to explain the temperature or coverage dependence of the sticking of molecules on metal surfaces.

Now consider the time evolution of adsorption per se. It implies the dissipation of the released binding energy within the substrate. The energy dissipation in physisorption and molecular

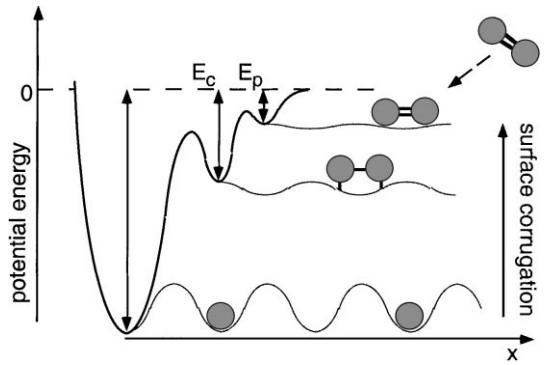

Fig. 29. One-dimensional energy diagram for precursor-mediated dissociative chemisorption of a diatomic molecule with physisorbed, chemisorbed molecular and chemisorbed atomic state. The corresponding lateral surface corrugation is expected to vary with the potential energy of the respective states as indicated.

chemisorption is mediated mainly by the coupling to the substrate phonon bath (e.g., [74,473–475]). With large chemisorption energies electron–hole pair formation may additionally contribute [476]. In extreme situations even chemisorptive particle emission was observed [477]. In any case, the equilibration of the adsorbate will take place on a finite timescale. It is thus expected that an adsorbing molecule climbing down the energy ladder has hyperthermal energies prior to the stabilization in an energy minimum. The corresponding time-dependent variation of the vertical position of an adsorbing molecule at a surface is schematically illustrated in Fig. 30 [472]. Similarly, an efficient lateral transport of the hyperthermal molecule at the surface can be envisioned [478]. In order to make a distinction to the precursor states introduced above, the hyperthermal species are designated as *hot precursors* (following [479]). They may be relevant both in the case of a single potential energy

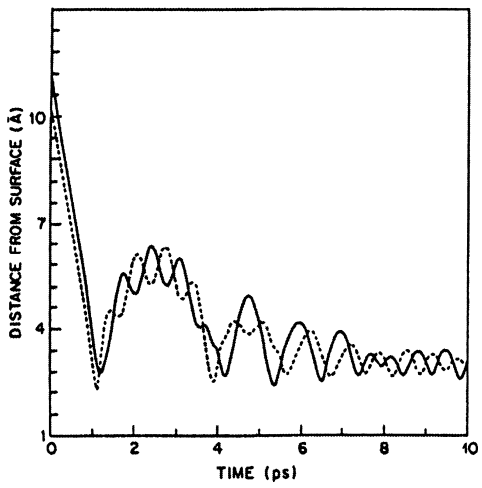

Fig. 30. Evolution of the vertical distance from the surface in typical trapping events for N_2 at an Ag(1 1 1) surface. From [472].

minimum in the PES of an adsorbate (e.g., the case of noble gas atoms which are exclusively physisorbed on metals) and in the access of a local minimum in the PES.

Note that the reasoning based on the one-dimensional precursor picture may be inadequate [480]. Particularly with molecular adsorption, due to the molecular degrees of freedom, a multi-dimensional PES must be considered for a complete description of the system dynamics [481–483]. The respective physisorbed or chemisorbed states are not always unique, since different configurations (binding sites, molecular orientations) may be possible for the same adsorbate.

Transient species can similarly evolve in the exothermic bond scission of a molecular species at a surface. Consider for simplicity a diatomic chemisorbed precursor that has come to equilibrium with the substrate at a low temperature. The precursor is subsequently dissociated by increasing the temperature. The released chemisorption energy gain may be transferred as kinetic energy to the evolving atoms. These hyperthermal '*hot adatoms*' may transport efficiently at the surface in the dissipation of the excess energy. When the dissociation occurs in the chemisorption process from the gas phase, the total energy gain is even higher. The corresponding hot-diffusion scenario may be rather complex.

The following terminology will be employed here:

1. a *precursor* is a molecule in a metastable state at a local minimum of the PES,
2. a *hot precursor* is a hyperthermal adsorbing molecule (or atom) in the process of thermalization with the substrate lattice,
3. a *hot adatom* is a hyperthermal dissociation product in the process of thermalization, which evolved in exothermic bond scission of a molecule at a surface.

Transient mobility comprises the lateral motion of any of such species at a surface. Note that with the present definition exclusively transport on the pristine surface is addressed. The precursor species introduced above include both 'intrinsic precursors' and 'trapped molecules' in the common sense [17,464,470,484,485], but exclude the 'extrinsic precursors' invoked for the lateral diffusive transport of molecules on top of already adsorbed particles in the formation of an adsorbed layer [17,186,188,464,470,484–486].

Some interesting consequences for surface chemical reactions arise from transient mobility. Traditionally, it was believed that '*the reaction which takes place at the surface of a catalyst may occur by interaction between molecules or atoms adsorbed in adjacent spaces on the surface, . . . or it may take place directly as a result of a collision between a gas molecule and an adsorbed molecule or atom on the surface*' [487], which distinctions were termed later: (i) the Langmuir–Hinshelwood mechanism involving adsorbed reactants in thermal equilibrium with the surface, and (ii) the Eley–Rideal mechanism, where a reaction occurs directly at the point of impact between an incident particle from the gas phase and an adsorbate. Precursors and hot adatoms are believed to open new channels for surface chemical reactions [479,488–490] (note that the corresponding semantics are unfortunately not unique [479,485,490]). In particular, transient mobility may allow adsorbing species to attain reaction sites or reaction partners on a surface, not accessible for the equilibrated state by thermal migration. With the operation of hot adatom or (hot) precursor mechanisms, energy barriers may be overcome or reaction pathways can be envisioned which are out of scope for equilibrated species with thermal energies [479,490]. They may be effective either in the course of (dissociative) adsorption or with the induced dissociation of an adsorbed molecule and the subsequent interaction of the formed hot adatoms with a coadsorbed species at the surface.

Speculations on transient mobility, put forward in metal-on-metal epitaxial growth [491] could not be confirmed by recent investigations (cf. [256,492,493]).

5.2. Theoretical aspects

Most theoretical studies for transient mobility phenomena employed MD simulations. There is an overall agreement that the typical timescale for thermalization is in the picosecond range.

Early MD investigations on the dynamics of the interaction of noble gases with the Pt(1 1 1) surface led to the suggestion that in adsorption the 'atoms may glide across the surface for several hundreds of ångströms before equilibration of tangential momentum' [478,494], i.e., the noble gas atoms remain 'laterally hot' due to the small surface corrugation [478].

The dynamics of H-atom adsorption on Cu(1 1 1) were investigated by MD [495] and quasiclassical calculations [496,497]. It turned out that the hydrogen equilibration with a 2.4 eV energy gain requires a large number of collisions with the surface, which is related to the small H-to-Cu mass ratio. Exemplaric trajectories of hot hydrogen are shown in Fig. 31. In addition to the lateral movement the atoms were found to oscillate vertically at a height of 1–3 Å above the surface. Considering phononic energy transfer only, a dissipation timescale of $\sim$4 ps was estimated at 300 K [497]. All studies agree on the formation of hot precursors which are relevant for surface chemistry.

For the case of strong chemisorption of atomic species only MD calculations for the deposition of metals on a metal surface exist, which indicate no transient mobility due to efficient dissipation of the adsorption energy [493].

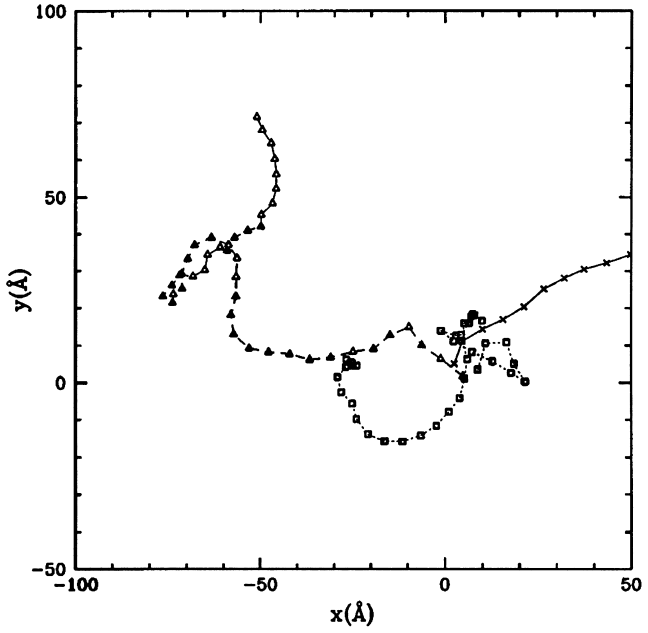

Fig. 31. Simulated trajectories of three hot hydrogen atoms in the plane of a 300 K Cu(1 1 1) surface with initial points of impact near the origin. H-atoms started 7 Å above the surface with 70 meV translational energy. The symbols indicate successive collisions with the surface (the atom marked by $\times$'s travels $\approx$ 200 Å beyond the plotted area). From [497].

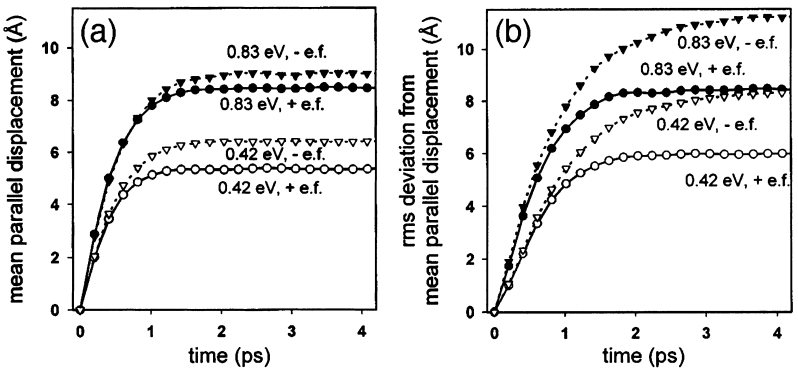

Fig. 32. (a) Ballistic motion of nascent CO adsorbates, impinging with indicated energies at 45° on Cu(0 0 1) held at 100 K along the [1 1 0] azimuth. The first contact with the surface appears at $t = 0$. The mean molecular displacement along the surface projection of the incident velocity is plotted for the case of phononic friction only (circles) and with the additional effect of electronic friction via creation of electron–hole pairs (triangles). (b) Hot diffusion under the same conditions. The r.m.s. deviation from the mean of the displacement along the surface projection of the incident velocity is shown. From [74].

The adsorption of CO on Ni(1 1 1) was simulated by MD for model PESs with different precursor states [481]. It was concluded that transient mobility of hot precursors exists on the picosecond timescale. The transport characteristics depend on the detailed shape of the PES employed. They were found to be different for molecules being temporarily trapped in the precursor well and those which are accelerated into the chemisorption well. On a simulation timescale of 10 ps equilibrium was not reached [481].

In a recent study the accomodation of CO on a Cu(0 0 1) surface was investigated by MD simulations, in particular with regard to the contribution of electron–hole pairs [74]. With this system the molecules equilibrate with the surface within ~6 ps without passing through an intermediate precursor state. The adsorption energy gain is 0.59 eV. A distinction could be made between ballistic transport in adsorption (where the original adsorbate momentum is maintained) and 'hot diffusion' (where the memory of the original momentum is lost but excess kinetic energy is retained). The results reproduced in Fig. 32 demonstrate transient mobility of nascent adsorbates over distances of 5–10 Å within 2 ps following initial surface contact. The energy dissipation is mediated predominantly by phononic friction. Electronic friction results in stronger damping of hot diffusion and a reduction of ~1 Å of the ballistic mean displacement at the surface [74].

The transient mobility of hot adatoms at a surface was modeled for the case of dissociative chemisorption of oxygen on Al(1 1 1) [498,499]. The O atoms were placed in the chemisorption potential with a corrugation of ~0.4 eV. Based on realistic estimates and calculations, an initial excess energy of 3.5 eV per oxygen atom was chosen, corresponding to a start velocity of 65 Å ps^{-1}. Results of MD simulations with this initial condition indicate that the transient motion in the surface plane is terminated within 0.2–0.3 ps, whereby an average lateral displacement of 6–8 Å is reached. The representative trajectories reproduced in Fig. 33 demonstrate that the initial momentum is rapidly randomized and ballistic motion prevails only in the very initial stage of the hot oxygen transport [498]. These conclusions were substantiated by further dynamical simulations employing ab initio results. An upper transient mobility limit of 10–15 Å on the chemisorption potential surface was found with the maximum initial energy possible [499].

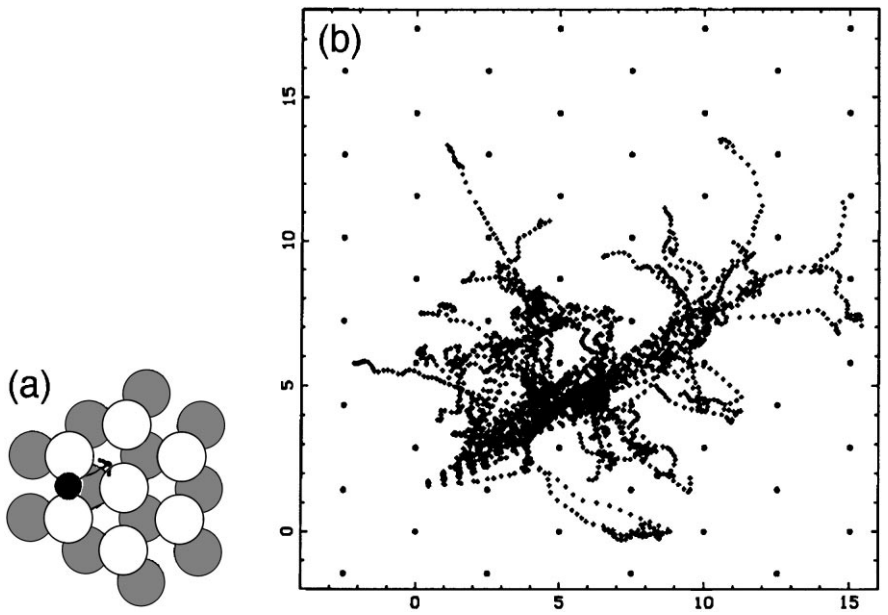

Fig. 33. Molecular dynamics simulation for trajectories of hot oxygen atoms on an Al(1 1 1) surface. (a) Ball model for the starting configuration. (b) Time evolution of the lateral oxygen position from 64 simulations (total time is 0.45 ps, positions are indicated in 9 fs steps). The equilibrium positions of the substrate atoms are marked by dots (units of axes are in Å). From [498].

6. Observations of transient mobility phenomena

Experimental indications pointing to the existence of mobile precursor species came rather late. They were firstly deduced from the nitrogen atom distribution formed in dissociative N_2 adsorption on stepped W(1 1 0) surfaces [500]. During the last few years a fair number of studies employing indirect observation tools were performed, where the existence of hot atoms or hot precursors needed to be invoked for the understanding of reaction pathways at surfaces. Examples include oxidation of coadsorbed CO via thermal or UV dissociation of chemisorbed O_2 at Pt surfaces [501–504], surface chemical reactions involving hot precursors with hydrogen on metals (e.g., [490,505–510]), and hot adatom mediated desorption of coadsorbed species [511–513].

However, to date, STM is the only technique allowing for the elucidation of transient mobility phenomena at the atomic level. This is usually achieved by an a posteriori analysis of the local adsorbate distribution on a surface evolving in (dissociative) adsorption or upon dissociation of a precursor. The experiment must be performed under conditions where the effect of thermal diffusion of the final products can be neglected or distinguished from transient mobility contributions. Accordingly, the adsorption mechanism and the diffusion characteristics of the equilibriated species must be known or determined.

6.1. Precursors and hot precursors

The conceptionally simplest case where transient mobility can occur and was theoretically suggested [478,494] is the physisorption of a noble gas atom on a metal surface, where a PES with a single

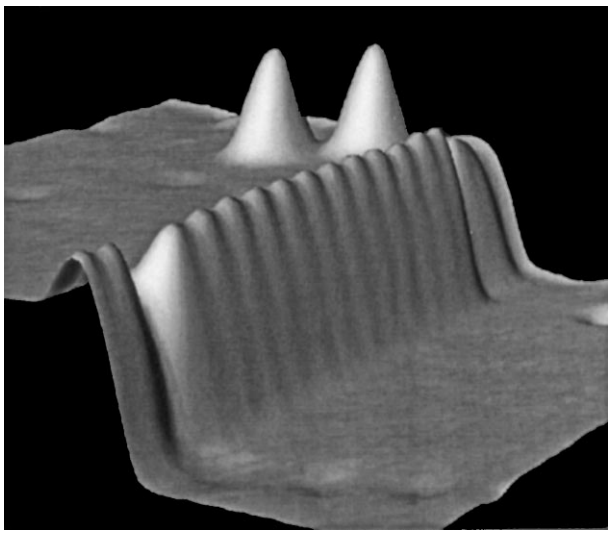

Fig. 34. STM topograph revealing the decoration of an atomic step upon adsorption of a small amount of Xe on a Pt(1 1 1) surface at 4 K. Since the temperature was too low to allow for appreciable thermal diffusion of Ar atoms and the sticking coefficient is close to unity, this arrangement must be associated with transient mobility (image size 100×100 Å^2; from [514]).

minimum exists. Since the migration barrier with such systems is expected to be small (cf. Section 4.3), the experiments must be performed at very low temperatures. STM observations on the adsorption of Xe on Pt(1 1 1) at 4 K indeed revealed that the noble gas atoms travel over hundreds of ångströms before they reach their final adsorption site [514]. This was inferred from the decoration of Pt atomic steps and surface defects at dilute Xe coverages. A typical result is reproduced in Fig. 34. Since the Xe sticking coefficient is high and the upper limit of the hopping rate falls below 0.1 s^{-1} under the employed conditions, these findings are a clear indication of transient mobility of a hot precursor [514,515]. The preferential step decoration is associated with the increased binding energy at the step sites [391,397]. In contrast, no indications of transient mobility were found in earlier STM observations of the Xe/Ni(1 1 0) system, where a higher surface corrugation and stronger bonding is expected [239,514]. Step decoration due to transient motions was observed for benzene adsorption on Ni(1 1 0) at 4 K, but attributed to a modified corrugation potential in the step vicinity [516].

The possible operation of hot precursor mechanisms in noble gas adsorption was confirmed by HAS investigations of Ar, Kr and Xe adsorption on Cu(1 1 0) [517]. Transient mobility was inferred from an analysis of the initial increase of the sticking coefficient with the coverage, which is mediated by the formation of two-dimensional noble-gas islands. The trapping efficiency of such islands exceeds that expected from geometric considerations. It could be rationalized with a highly mobile hot precursor [517].

With the adsorption of molecular oxygen on the Ag(1 1 0) surface molecular beam experiments [518,519] and ab initio calculations [95,428] suggest that the chemisorption well is reached directly, i.e., without passing through an intermediate precursor (the earlier reported physisorption state [520] seems to interfere only with appreciable oxygen coverages [521]). The molecular distribution at the surface upon O_2-exposure could be resolved by STM measurements at temperatures around 65 K, where thermal diffusion is minute on the timescale of the experiments [522]. The data revealed that

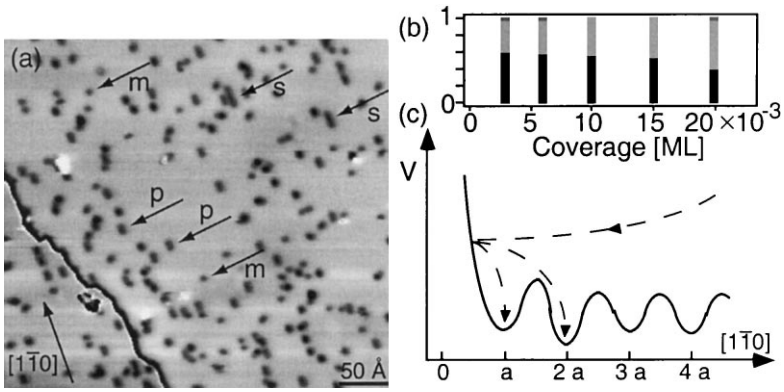

Fig. 35. (a) The one-dimensional agglomeration of molecular oxygen upon adsorption of 0.02 ML molecular oxygen on an Ag(1 1 0) surface at 65 K is associated with transient mobility of a hot precursor species. Molecular oxygen monomers, pairs and strings are marked by m, p and s, respectively. (b) Proportions of single (black), pairs (light gray) and strings (dark gray) of O_2 vs. coverage from STM observations at $T = 60-67$ K. (c) Schematic potential of two O_2 molecules along $[1\,\bar{1}\,0]$ and trajectory for pair formation with a hot precursor molecule dissipating its excess energy by collision with a second molecule accomodated at $x = 0$. From [522].

O_2-pairs and strings, which are oriented along the substrate $[1\,\bar{1}\,0]$ troughs, evolve from the lowest coverages, as illustrated by the image reproduced in Fig. 35a [522]. These distributions could be attributed neither to statistical adsorption, where the molecules rest at the surface at the point of initial impact (since the fraction of the molecules found in aggregates is too high) nor to a local increase of the small initial sticking coefficient in the vicinity of already adsorbed molecules (since the sticking probability decreases strongly with increasing coverage). Hence a hot precursor state in which the molecules are skating across the surface must exist. The one-dimensional oxygen agglomeration was associated with the efficient energy release by impact of hot precursors onto the equilibrated species [522], as sketched in Fig. 35c. This interpretation is in line with molecular beam studies of the O_2/Ag(1 1 1) system, where transient trapping–desorption without complete thermalization of the molecules was observed [523].

The existence of a mobile molecular oxygen precursor could be similarly demonstrated by STM observations of O_2-adsorption on Cu(1 1 0) at 4 K [524]. The observed adsorption scenario is rather complex since dissociative and molecular chemisorption coproceed. It could not be conclusively elucidated. However, the formation of adsorbate clusters and the immobility of the equilibrated species provide clear evidence for long-range transient mobility of a (possibly hot) precursor [524].

The significance of transient mobility for surface chemical reactions could be demonstrated with the adsorption of oxygen on Pt(1 1 1). With this system a precursor-mediated adsorption scenario, following the physisorption–chemisorption–dissociation route is widely accepted [483,525–527] (cf. Fig. 29). STM observations in the temperature range 95–160 K, where surface diffusion of chemisorbed atoms is suppressed, demonstrate the formation of atomic oxygen clusters [528]. This indicates the existence of a mobile O_2-precursor state, which preferrably is dissociated and comes to rest in the vicinity of atomic oxygen. For similar oxygen exposures increased clustering evolves with reduced substrate temperature, as demonstrated by the data shown in Fig. 36. The corresponding strong temperature dependence of the sticking (which had been noticed earlier [529]) was associated with the competition between the thermal desorption of precursors and their surface mobility, which allows

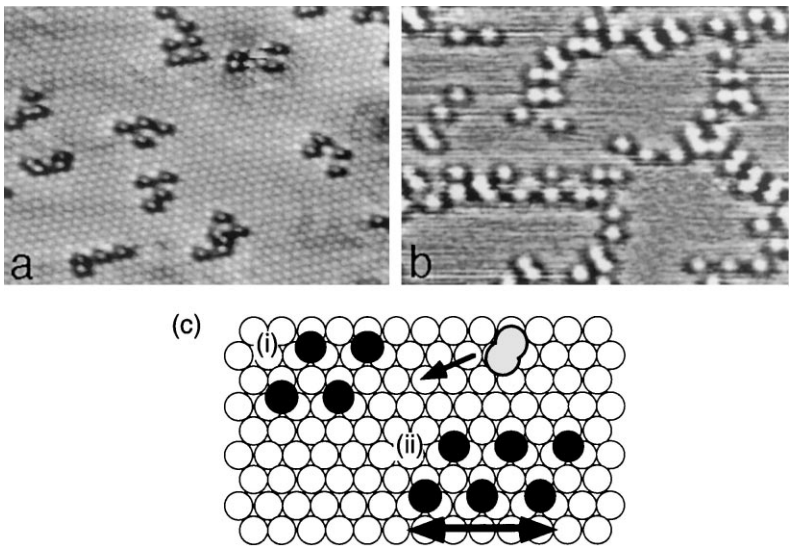

Fig. 36. Precursor-mediated aggregation of atomic oxygen in low-temperature adsorption of O_2 on Pt(1 1 1). (a) At $T = 140$ K groups consisting of 4–6 O_{ad}-atoms have formed from dissociation of 2–3 molecules (3 L dose, image 100×60 Å^2 with the Pt atomic lattice resolved). (b) The one-dimensional islands from strings of O-pairs in $[1\,\bar{1}\,0]$ at $T = 105$ K reflect an increased precursor lifetime at the surface and anisotropic precursor–atom interactions (1 L dose, image 70×40 Å^2). (c) Schematic illustration of the one-dimensional growth of O_{ad}-chains. In (i) an oxygen precursor molecule (shaded) approaches an atom island; (ii) on its dissociation a chain string evolves. From [528].

them to attain the preferred dissociation sites. Increased precursor surface lifetimes at lower temperatures are expected to go along with growing mean lateral transport. This signals that the precursor thermalizes with the substrate to some extent. The fact that with temperatures falling below 90 K islands from molecular oxygen are formed [528,530] and molecular surface diffusion could be excluded for $T < 70$ K [530] indicates that the diffusion of the chemisorbed species is not relevant. Accordingly, the suggested island growth via competition between lateral precursor mobility and its thermal desorption can be qualitatively rationalized using the depth of the physisorption potential ($\sim$100 meV [531]) and assuming thermal diffusion with an estimated barrier being $\sim$1/5 of the physisorption energy. The corresponding mean free path $\langle\lambda\rangle = 2\sqrt{D^*\tau} \sim a\exp[\frac{1}{2}\beta(E_b - E_m)]$ at the surface matches the requirements for the aggregates found ($\tau = \nu_0^{-1}\exp[\beta E_b]$ is the surface lifetime). By shadowing the exposed surface area with the STM tip, the precursor mobility could be estimated to $\sim$1000 Å at $T = 51$ K [530].

The mobility of a molecular precursor is similarly decisive in the dissociative adsorption of NO on a Ru(0 0 1) surface [369]. This could be deduced from the decoration of atomic steps at the crystal surface with atomic N (cf. Fig. 10) [369], which result from the preferential precursor dissociation at these 'active sites' [532].

6.2. Hot adatom mechanisms

The earliest indications for a hot adatom mechanism were reported for the O_2/Al(1 1 1) system. Oxygen adsorbs dissociatively on Al(1 1 1) down to 20 K [533], whereby no molecular precursor states

exist [534]. This is confirmed by recent ab initio calculations for O_2 on Al(1 1 1), indicating direct dissociation [535–537]. STM observations at 300 K were interpreted in terms of the formation of isolated, immobile O_{ad}-atoms evolving upon exposing the surface to small doses of molecular oxygen [538,539], i.e., it was suggested that there is no indication for the expected pairs of oxygen adatoms, which could be associated with the two oxygen atoms necessarily formed in the disruption of the intermolecular bond at the surface. In order to rationalize these findings, a mobile hot adatom species was proposed which draws its hyperthermal energy from an internal energy transfer in the dissociative adsorption and traverses the surface ballistically with a mean free path of ~40 Å per atom. However, more recent STM observations, performed both at room and low temperature, indicate short-range transient motions with the formation of oxygen atom pairs [377]. A preferential O–O distance of $\sqrt{3}a$ was found at low temperature. It was suggested that the complex imaging characteristics of neighboring O had led to a misinterpretation in the earlier work [377]. Accordingly, the theoretical results and simulations discussed in Section 5.2 demonstrate short-range transport of hot O adatoms on the corrugated chemisorption PES [498,499]. With regard to the initial STM findings, it was pointed out that the abstraction channel (i.e., chemisorptive oxygen atom emission [540,541]) is energetically open since the sum of the O_{ad} binding energy exceeds the molecular bond by 2–3 eV [499]. In addition were discussed: the effect of lateral transport of weakly bound oxygen species as well as motions via ballistic 'canonball' trajectories resulting from dissociation of molecules with their axis perpendicular to the surface [499].

A clear-cut demonstration for the formation of hot adatoms moving laterally on a surface was achieved for the dissociative adsorption of O_2 on Pt(1 1 1). The energy gain with this system is 1.1 eV/atom, when equipartition between the dissociation products is assumed [242]. The STM image reproduced in Fig. 37a demonstrates a random distribution of individual pairs of adsorbed oxygen atoms, each of which originated from the breaking of the intermolecular bond at the surface [242]. In contrast to the clustering observed at lower temperatures (cf. Section 6.1), these pairs are the exclusive low-coverage species formed at $T \approx 160$ K. Since the O_{ad}-atoms are immobile on the timescale of the experiment, they reflect the situation right after the dissociation event. Thus it can be inferred that hot oxygen adatoms have formed which travel only over short distances from the point of dissociation

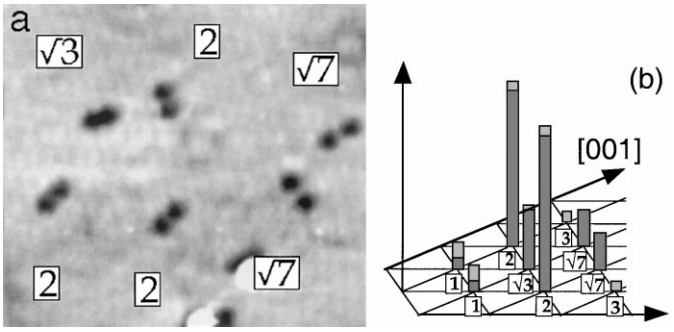

Fig. 37. (a) STM image of oxygen atom pairs on a Pt(1 1 1) surface resulting from the dissociative adsorption at $T = 154$ K (1.2 L dose, image 110 × 92 Å^2); the distance between the O atoms in the pairs are indicated in multiples of a. (b) Histogram of the lateral intrapair separation from 55 events. The average frequencies of $1a$, $\sqrt{3}a$, $2a$, $\sqrt{7}a$ and $3a$ were 7.3, 21.8, 56.4, 12.7 and 1.8%. Gray tops of the bars indicate variations between two data sets at 160 and 163 K. From [242].

[242]. From a statistical analysis of a large number of atom pairs, it could be deduced that the interatomic distance scatters between $1a$ and $3a$ (cf. Fig. 37b), whereby all O atoms occupy f.c.c. substrate sites. The preferred O_{ad}–O_{ad}-spacing is $2a$, similar with that of the thermodynamic equilibrium $p(2 \times 2)$ structure on Pt(1 1 1) at higher coverages. The observed distributions agree well with the simulations performed for transient mobility in dissociative adsorption of oxygen on Al(1 1 1) [498,499] (cf. Section 6.1). This suggests that the atoms formed in the dissociation event indeed transport on the chemisorption PES (with a corrugation of $\sim$0.5 eV, cf. [242] and Section 4.2). Note that short-range repulsive interactions between the oxygen atoms are expected to cause a deformation of the surface corrugation potential (cf. Section 2.2) with a lowered barrier for migration in O_{ad}–O_{ad} configurations where interatomic distance fall below $2a$. Their effect in the transient motion could not be conclusively disentangled so far.

Further STM investigations of the O_2/Pt(1 1 1) system were performed with molecular oxygen in equilibrium with the surface, which is known to bind in a flat configuration [527]. It could be demonstrated that principally the same transient mobility occurs when their dissociation is induced by thermal heating or UV radiation [530,542]. Furthermore, inelastic tunneling electrons were employed to dissociate the molecular species using the STM tip as a chemistry tool [542]. In any case the product atoms were found close to the site of the original molecule and their preferential distance was $2a$ [530], albeit in the non-thermal dissociation processes also the population of h.c.p. sites was observed.

In related STM experiments, the tunneling current was employed to excite and laterally displace single CO atoms on a Cu(1 1 1) surface at 15 K [543]. Most of the molecules perform next-neighbor

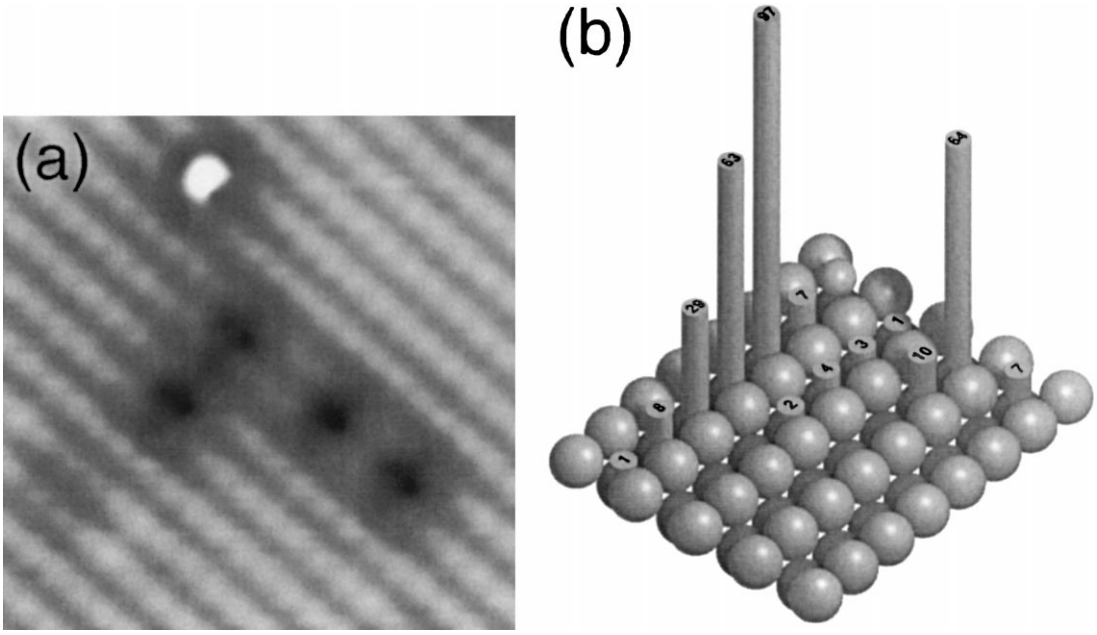

Fig. 38. (a) STM image of atomic (depressions) and molecular oxygen (protrusion) on Cu(1 1 0) upon adsorption at 4 K (image 37×37 Å^2). The orientation of the atom pairs formed in the dissociation with respect to the Cu atom rows is clearly visible. (b) The histogram of the lateral intrapair separation from 296 dissociation events signals that the hot atoms moved principally along the two high-symmetry directions at the surface. From [524].

jumps, but also long jumps over $2a$–$3a$ directed preferentially along the high-symmetry lattice directions were found. The latter were associated with hot diffusion. However, since long jumps with similar characteristics were suggested for the thermal diffusion of adsorbed CO on Ni(1 1 1) [44], this interpretation seems to be not unique.

Recent STM experiments with the O_2/Ag(0 0 1) system indicate transient mobility in dissociative adsorption at $T = 140$ K with the preferential separation of the O_{ad}-atoms being either $7a$ or $14a$. It was speculated that two distinct dissociation mechanisms exist [544].

The role of substrate anisotropy in hot adatom mechanisms could be demonstrated by STM observations of oxygen adsorption on Cu(1 1 0) [524]. Even at 4 K molecular and dissociative adsorption coproceed. Again the hot atoms travel only over short distances, as demonstrated by the STM image in Fig. 38a. The corresponding statistics of the intrapair separation in Fig. 38b reveals that they are preferentially oriented either along the $[1\,\bar{1}\,0]$-direction of the substrate atomic rows, or perpendicularly to it in [0 0 1]. Based on these observations it was suggested that flat-lying molecules with their axis oriented along either $[1\,\bar{1}\,0]$ or [0 0 1] have an enhanced dissociation probability. In agreement, ab initio calculations for the O_2/Ag(1 1 0) system indicate that these orientations are energetically favorable for molecular chemisorption [95].

7. Resume

The comprehensive analysis of surface mobility is a challenging issue from both the experimental and theoretical point of view. During the last years powerful new methods have been developed and applied to investigate the characteristics of surface diffusion and the transport of transient species at metal surfaces.

In particular, it became possible to elucidate tracer diffusion at the nanometer scale for many atomic and molecular adsorbates at well-defined single crystal surfaces. Furthermore, methods are at hand which allow for the characterization of collective diffusion phenomena in great detail. The combined study of surface diffusion and adsorbate interactions with both direct and indirect methods is necessary for complete system description. Complementary state of the art theoretical investigations can lead to an in-depth insight into the nature of the underlying physics and chemistry. There are still awesome obstacles on this avenue, as obvious from the frequent contradictions when results obtained with different techniques or approaches are jointly discussed.

Transient motions of precursors and hot species in the adsorption of gases at metals have been suggested on indirect findings and rationalized on theoretical grounds. Today they can be evidenced by STM observations. Depending on the respective adsorption or dissociation scenario, the resulting transport can be restricted to a few surface lattice constants or amount to distances of thousands of ångströms. Transient mobility studies are at an early stage and further insight into this intriguing phenomenon can be expected in the near future.

Acknowledgements

The fruitful cooperation with T. Zambelli, J. Weckesser, J. Wintterlin, G. Ertl and K. Kern is gratefully acknowledged. Their dedication, enthusiasm, critical reflections, discussions, suggestions

and benevolent support stimulated this paper. Special thanks go to T. Ala-Nissila, F. Besenbacher, H. Brune, H. Conrad, D. Eigler, R. Ferrando, K. Fichthorn, S.M. George, R. Gomer, A.P. Graham, T. Hjelt, W. Ho, B. Jackson, S. Renisch, H.H. Rotermund, H.-P. Rust, M. Schmid, W.-D. Schneider, R. Schuster, D.V. Shalashilin, Y.R. Shen, M.C. Tringides, J. Trost, T.T. Tsong, J. Tully, G. Wahnström, X. Xiao and X.D. Zhu for kindly providing illustrations, inspiring comments and communication of unpublished work.

References

[1] J. Ingenhousz (cf. Encyclopedia Britannica).
[2] R. Brown, Phil. Mag. N.S. 4 (1828) 161.
[3] R. Brown, Phil. Mag. N.S. 6 (1829) 161.
[4] S. Chandrasekhar, Rev. Mod. Phys. 15 (1943) 1.
[5] N. Wax (Ed.), Selected Papers on Noise and Stochastic Processes, Dover, New York, 1954.
[6] W. Coffey, Adv. Chem. Phys. 63 (1985) 69.
[7] J. Perrin, Les Atomes, Alcan, Paris, 1936.
[8] A. Fick, Ann. Phys. 170 (1855) 59.
[9] R.C.L. Bosworth, Proc. R. Soc. A 150 (1935) 58.
[10] Y. Adda, J. Philibert, La Diffusion dans les Solides, Presses Universitaires de France, Paris, 1966.
[11] J.R. Manning, Diffusion Kinetics for Atoms in Crystals, Van Nostrand, Princeton, 1968.
[12] C.P. Flynn, Point Defects and Diffusion, Clarendon Press, Oxford, 1972.
[13] J. Philibert, Diffusion et transport de matière dans les solides, Les éditions de Physique, Paris, 1985, English Edition, Atom Movements: Diffusion and Mass Transport in Solids, 1991.
[14] J.E. Lennard-Jones, Trans. Faraday Soc. 28 (1932) 333.
[15] G. Ehrlich, K. Stolt, Ann. Rev. Phys. Chem. 31 (1980) 603.
[16] T.T. Tsong, Prog. Surf. Sci. 10 (1980) 165.
[17] M.A. Morris, M. Bowker, D.A. King, in: C.H. Bamford, C.F.H. Tipper, R.G. Compton (Eds.), Simple Processes at the Gas–Solid Interface, Elsevier, Amsterdam, 1984, p. 1.
[18] A.G. Naumovets, Y.S. Vedula, Surf. Sci. Rep. 4 (1985) 365.
[19] A. Kapoor, R.T. Yang, C. Wong, Catal. Rev.-Sci. Eng. 31 (1989) 129.
[20] S.J. Lombardo, A.T. Bell, Surf. Sci. Rep. 13 (1991) 1.
[21] T. Ala-Nissila, S.C. Ying, Prog. Surf. Sci. 39 (1992) 227.
[22] H.P. Bonzel, in: O. Madelung (Ed.), Landolt–Börnstein III/26: Diffusion in Solid Metals and Alloys, Springer, Berlin, 1993.
[23] G.L. Kellogg, Surf. Sci. Rep. 21 (1994) 1.
[24] E.G. Seebauer, C.E. Allen, Prog. Surf. Sci. 49 (1995) 265.
[25] V.P. Zhdanov, Elementary Physicochemical Processes on Solid Surfaces, Plenum Press, New York, 1991.
[26] R.C. Baetzold, in: E. Shustorovich (Ed.), Metal–Surface Reaction Energetics: Theory and Applications to Heterogeneous Catalysis, Chemisorption and Surface Diffusion, VCH, Weinheim, 1991, p. 109.
[27] V.T. Binh (Ed.), Surface Mobilities on Solid Materials, Plenum Press, New York, 1981.
[28] M. Grunze, J.J. Weimer, H.J. Kreuzer (Eds.), Diffusion at Interfaces: Microscopic Concepts, Springer Series in Surface Science, Springer, Berlin, 1988.
[29] M.C. Tringides (Ed.), Surface Diffusion: Atomistic and Collective Processes, Plenum Press, New York, 1997.
[30] R. Gomer, Rep. Prog. Phys. 53 (1990) 917.
[31] A. Einstein, Ann. Phys. 17 (1905) 549.
[32] A. Einstein, in: R. Fürth (Ed.), Investigations on the Theory of Brownian Movement, Dover, New York, 1956.
[33] R. Ferrando, R. Spadacini, G.E. Tommei, Phys. Rev. E 48 (1993) 2437.
[34] J. Ellis, A.P. Graham, J.P. Toennies, Phys. Rev. Lett. 82 (1999) 5072.
[35] J.V. Barth, H. Brune, B. Fischer, J. Weckesser, K. Kern, Phys. Rev. Lett. 84 (2000) 1732.

[36] V.P. Zhdanov, Surf. Sci. Rep. 12 (1991) 183.
[37] G. Ehrlich, F.G. Hudda, J. Chem. Phys. 44 (1966) 1050.
[38] M. Abramowitz, I.A. Stegun, Handbook of Mathematical Functions, Dover, New York, 1973.
[39] S.C. Wang, J.D. Wrigley, G. Ehrlich, J. Chem. Phys. 91 (1989) 5087.
[40] J.D. Wrigley, M.E. Twigg, G. Ehrlich, J. Chem. Phys. 93 (1990) 2885.
[41] S. Glasstone, K.J. Laidler, H. Eyring, The Theory of Rate Processes, McGraw-Hill, New York, 1941.
[42] P. Hänggi, P. Talkner, M. Borkovec, Rev. Mod. Phys. 62 (1990) 251.
[43] R. Gomer, in: V.T. Binh (Ed.), Surface Mobilities on Solid Materials, Plenum Press, New York, 1981, p. 15.
[44] K.D. Dobbs, D.J. Doren, J. Chem. Phys. 97 (1992) 3722.
[45] P. Langevin, Comptes Rendus 146 (1908) 530.
[46] O. Klein, Arkiv Mat. Astr. Fys. 16 (1922) 5.
[47] H.A. Kramers, Physica (Utrecht) 7 (1940) 284.
[48] H. Risken, The Fokker–Planck Equation, Springer, Berlin, 1989.
[49] N.G. van Kampen, Stochastic Processes in Physics and Chemistry, North-Holland, Amsterdam, 1981.
[50] V.I. Mel'nikov, Phys. Rep. 209 (1991) 1.
[51] P. Talkner, P. Hänggi (Eds.), New Trends in Kramers' Rate Theory, Kluwer Academic Publishers, Dordrecht, 1995.
[52] J.R. Banavar, M.H. Cohen, R. Gomer, Surf. Sci. 107 (1981) 113.
[53] W.G. Kleppmann, R. Zayher, Phys. Rev. B 22 (1985) 6044.
[54] G. Wahnström, Surf. Sci. 159 (1985) 311.
[55] G. Wahnström, Surf. Sci. 164 (1985) 449.
[56] G. Wahnström, Phys. Rev. B 33 (1986) 1020.
[57] G. Wahnström, J. Chem. Phys. 84 (1986) 5931.
[58] V.P. Zhdanov, Surf. Sci. 214 (1989) 289.
[59] R. Ferrando, R. Spadacini, G.E. Tommei, Surf. Sci. 265 (1992) 273.
[60] R. Ferrando, E. Scalas, M. Torri, Surf. Sci. 311 (1994) 411.
[61] Y. Georgievskii, E. Pollak, Phys. Rev. E 49 (1994) 5098.
[62] Y. Georgievskii, M.A. Kozhushner, E. Pollak, J. Chem. Phys. 102 (1995) 6908.
[63] G. Caratti, R. Ferrando, R. Spadacini, G.E. Tommei, Phys. Rev. E 54 (1996) 4708.
[64] Y. Georgievskii, E. Pollak, Surf. Sci. 355 (1996) L366.
[65] S.Y. Krylov, A.V. Prosyanov, J.J.M. Beenakker, J. Chem. Phys. 107 (1997) 6970.
[66] J.J.M. Beenakker, S.Y. Krylov, Surf. Sci. 411 (1998) L816.
[67] M. Azzouz, H.J. Kreuzer, M.R.A. Shegelski, Phys. Rev. Lett. 80 (1998) 1477.
[68] L.Y. Chen, S.C. Ying, Phys. Rev. B 60 (1999) 16965.
[69] L.Y. Chen, M.R. Baldan, S.C. Ying, Phys. Rev. B 54 (1996) 8856.
[70] C. Caroli, B. Roulet, D. Saint-James, Phys. Rev. B 18 (1978) 545.
[71] B.N.J. Persson, R. Ryberg, Phys. Rev. B 32 (1985) 3586.
[72] B.N.J. Persson, Sliding Friction, Springer, Berlin, 1998.
[73] M.S. Tomassone, J.B. Sokoloff, A. Widom, J. Krim, Phys. Rev. Lett. 79 (1997) 4798.
[74] J.T. Kindt, J.C. Tully, M. Head-Gordon, M.A. Gomez, J. Chem. Phys. 109 (1998) 3629.
[75] D. Fuhrmann, C. Wöll, New J. Phys. 1 (1998) 1.
[76] B.N.J. Persson, A. Nitzan, Surf. Sci. 367 (1996) 261.
[77] A.I. Volokitin, O.M. Braun, V.M. Yakovlev, Surf. Sci. 172 (1986) 31.
[78] G. Witte, K. Weiss, P. Jakob, J. Braun, K.L. Kostov, C. Wöll, Phys. Rev. Lett. 80 (1998) 121.
[79] S.C. Ying, Phys. Rev. B 41 (1990) 7068.
[80] T. Ala-Nissila, S.C. Ying, Phys. Rev. Lett. 65 (1990) 879.
[81] T. Ala-Nissila, S.C. Ying, Phys. Rev. B 42 (1990) 10264.
[82] L.Y. Chen, S.C. Ying, Phys. Rev. Lett. 71 (1993) 4361.
[83] L.Y. Chen, S.C. Ying, Phys. Rev. B 49 (1994) 13838.
[84] T. Hjelt, I. Vattulainen, T. Ala-Nissila, S.C. Ying, Surf. Sci. 449 (2000) L255.
[85] J.D. Doll, A.F. Voter, Ann. Rev. Phys. Chem. 38 (1987) 413.
[86] J.D. Doll, D.L. Freeman, Surf. Sci. 134 (1983) 769.
[87] S.M. Levine, S.H. Garofalini, Surf. Sci. 167 (1986) 198.

[88] D. Cohen, Y. Zeiri, J. Chem. Phys. 97 (1992) 1531.
[89] M. Silverberg, J. Chem. Phys. 99 (1993) 9255.
[90] D. Huang, Y. Chen, K.A. Fichthorn, J. Chem. Phys. 101 (1994) 11021.
[91] K.A. Fichthorn, J.S. Raut, in: M. Tringides (Ed.), Surface Diffusion: Atomistic and Collective Processes, Plenum Press, New York, 1997, p. 409.
[92] J.S. Raut, K.A. Fichthorn, J. Chem. Phys. 108 (1998) 1626.
[93] T. Hjelt, S. Herminghaus, T. Ala-Nissila, S.C. Ying, Phys. Rev. E 57 (1998) 1864.
[94] J. Jacobsen, B. Hammer, K.W. Jacobsen, J.K. Nørskov, Phys. Rev. B 52 (1995) 14954.
[95] P.A. Gravil, D.M. Bird, J.A. White, Phys. Rev. Lett. 77 (1996) 3933.
[96] P. Hu, D.A. King, S. Crampin, M.-H. Lee, M.C. Payne, J. Chem. Phys. 107 (1997) 8103.
[97] P.J. Feibelman, in: M.C. Tringides (Ed.), Surface Diffusion: Atomistic and Collective Processes, Plenum Press, New York, 1997, p. 510.
[98] P.J. Feibelman, E. Stefanie, T. Michely, Phys. Rev. Lett. 77 (1997) 2257.
[99] A. Bogicevic, J. Strömquist, B.I. Lundqvist, Phys. Rev. B 57 (1998) 4289.
[100] W. Dong, V. Ledentu, P. Sautet, A. Eichler, J. Hafner, Surf. Sci. 411 (1998) 123.
[101] M.Ø. Pedersen, L. Österlund, J.J. Mortensen, M. Mavrikakis, L.B. Hansen, I. Stensgaard, E. Lægsgaard, J.K. Nørskov, F.M. Besenbacher, Phys. Rev. Lett., in press.
[102] T. Ala-Nissila, W.K. Han, S.C. Ying, Phys. Rev. Lett. 68 (1992) 1866.
[103] D.E. Sanders, A.E. DePristo, Surf. Sci. 264 (1992) L169.
[104] G. Boisvert, L.J. Lewis, A. Yelon, Phys. Rev. Lett. 75 (1995) 469.
[105] A. Cucchetti, S.C. Ying, Phys. Rev. B 54 (1996) 3300.
[106] G.C. Kallinteris, G.A. Evangelakis, N.I. Papanicolaou, Surf. Sci. 369 (1996) 185.
[107] U. Kürpick, A. Kara, T.S. Rahman, Phys. Rev. Lett. 78 (1997) 1086.
[108] A.P. Graham, F. Hofmann, J.P. Toennies, L.Y. Chen, S.Y. Ying, Phys. Rev. B 56 (1997) 10567.
[109] R. Ferrando, G. Treglia, Phys. Rev. B 50 (1994) 12104.
[110] R. Ferrando, G. Treglia, Phys. Rev. Lett. 76 (1996) 2109.
[111] F. Montalenti, R. Ferrando, Phys. Rev. B 59 (1999) 5881.
[112] G.F. Mazenko, in: V.T. Binh (Ed.), Surface Mobilities on Solid Materials, Plenum Press, New York, 1981, p. 27.
[113] R. Kutner, Phys. Lett. 81 (1981) 239.
[114] I.F. Lyuksyutov, V.L. Pokrovsky, JETP Lett. 33 (1981) 326.
[115] A.T. Loburets, A.G. Naumovets, Y.S. Vedula, in: M.C. Tringides (Ed.), Surface Diffusion: Atomistic and Collective Processes, Plenum Press, New York, 1997, p. 509.
[116] S.C. Wang, U. Kürpick, G. Ehrlich, Phys. Rev. Lett. 81 (1998) 4923.
[117] T.R. Linderoth, S. Horch, L. Petersen, S. Helveg, E. Lægsgaard, I. Stensgaard, F. Besenbacher, Phys. Rev. Lett. 82 (1999) 1494.
[118] F. Montalenti, R. Ferrando, Phys. Rev. Lett. 82 (1999) 1498.
[119] L. Boltzmann, Ann. Phys. 53 (1894) 959.
[120] C. Matano, Jpn. J. Phys. 8 (1933) 109.
[121] L. Onsager, Phys. Rev. 37 (1931) 405.
[122] S.M. Valone, J.D. Doll, Surf. Sci. 139 (1984) 478.
[123] D.A. Reed, G. Ehrlich, Surf. Sci. 105 (1981) 603.
[124] I. Prigogine, Introduction to Thermodynamics of Irreversible Processes, Wiley, New York, 1961.
[125] R. Butz, H. Wagner, Surf. Sci. 63 (1977) 448.
[126] D.A. Reed, G. Ehrlich, Surf. Sci. 102 (1981) 588.
[127] R. Gomer, in: M.C. Tringides (Ed.), Surface Diffusion: Atomistic and Collective Processes, Plenum Press, New York, 1997, p. 510.
[128] L.D. Landau, E.M. Lifshitz, Statistical Physics, Pergamon Press, Oxford, 1979.
[129] L.S. Darken, Trans. Am. Inst. Mineral. Met. Eng. 175 (1948) 184.
[130] G.E. Murch, R.J. Thorn, Phil. Mag. A 40 (1979) 477.
[131] R. Ferrando, E. Scalas, Surf. Sci. 281 (1993) 178.
[132] A.W. Adamson, Physical Chemistry of Surfaces, Wiley, New York, 1976.
[133] H.E. Stanley, Introduction to Phase Transitions and Critical Phenomena, Clarendon Press, Oxford, 1971.

[134] X.-P. Jiang, H. Metiu, J. Chem. Phys. 88 (1988) 1891.
[135] R. Ferrando, E. Scalas, M. Torri, Phys. Lett. A 186 (1994) 415.
[136] T. Hjelt, I. Vattulainen, J. Merikoski, T. Ala-Nissila, S.C. Ying, Surf. Sci. 380 (1997) L501.
[137] I. Vattulainen, J. Merikoski, T. Ala-Nissila, S.C. Ying, Phys. Rev. B 57 (1998) 1896.
[138] V.P. Zhdanov, Surf. Sci. 149 (1985) L13.
[139] Z. Chvoj, H. Conrad, V. Chab, Surf. Sci. 352–354 (1996) 983.
[140] A. Danani, R. Ferrando, E. Scalas, M. Torri, Int. J. Mod. Phys. B 11 (1997) 2217.
[141] C. Uebing, R. Gomer, J. Chem. Phys. 100 (1994) 7759.
[142] K. Binder (Ed.), Monte Carlo Methods in Statistical Physics, Springer, Berlin, 1979.
[143] K. Binder (Ed.), Applications of the Monte Carlo Methods in Statistical Physics, Springer, Berlin, 1984.
[144] K. Binder (Ed.), The Monte Carlo Methods in Condensed Matter Physics, Springer, Berlin, 1992.
[145] K. Kehr, K. Binder, in: K. Binder (Ed.), Monte Carlo Method in Statistical Physics, Springer, Berlin, 1987, p. 181.
[146] D. Sahu, S.C. Ying, J.M. Kosterlitz, in: J.F. van der Veen, M.A. van Hove (Eds.), The Structure of Surfaces II, Springer, Berlin, 1988.
[147] C. Uebing, in: M.C. Tringides (Ed.), Surface Diffusion: Atomistic and Collective Processes, Plenum Press, New York, 1997, p. 443.
[148] M. Tringides, R. Gomer, Surf. Sci. 166 (1986) 419.
[149] C. Uebing, R. Gomer, Surf. Sci. 381 (1997) 33.
[150] H.C. Kang, W.H. Weinberg, J. Chem. Phys. 90 (1989) 2824.
[151] T. Ala-Nissila, J. Kjoll, S.C. Ying, Phys. Rev. B 46 (1992) 846.
[152] Y.K. Tovbin, Prog. Surf. Sci. 34 (1990) 1.
[153] M. Tringides, R. Gomer, Surf. Sci. 145 (1984) 121.
[154] B.N.J. Persson, Surf. Sci. Rep. 15 (1992) 1.
[155] M. Bowker, D.A. King, Surf. Sci. 71 (1978) 583.
[156] M. Tringides, Surf. Sci. 204 (1988) 345.
[157] M. Tringides, J. Chem. Phys. 92 (1990) 2077.
[158] L.A. Ray, R.C. Baetzold, J. Chem. Phys. 93 (1990) 2871.
[159] L.A. Ray, R.C. Baetzold, J. Simon, Surf. Sci. 235 (1990) 47.
[160] M. Tringides, R. Gomer, Surf. Sci. 265 (1992) 283.
[161] J. Sanchez, D.P. Quinn, M.C. Tringides, Surf. Sci. 391 (1997) 101.
[162] Q. Li, M. Tringides, Surf. Sci. 365 (1996) 495.
[163] P. Nikunen, I. Vattulainen, T. Ala-Nissila, Surf. Sci. 447 (2000) L162.
[164] C. Uebing, V.P. Zhdanov, J. Chem. Phys. 109 (1998) 3197.
[165] J.A. Goldstein, G. Ehrlich, Surf. Sci. 420 (1999) 1.
[166] C. Uebing, R. Gomer, J. Chem. Phys. 95 (1991) 7626.
[167] C. Uebing, R. Gomer, J. Chem. Phys. 95 (1991) 7636.
[168] C. Uebing, R. Gomer, J. Chem. Phys. 95 (1991) 7641.
[169] C. Uebing, R. Gomer, J. Chem. Phys. 95 (1991) 7648.
[170] F. Nieto, C. Uebing, V. Pereyra, Surf. Sci. 416 (1998) 152.
[171] A. Sadiq, K. Binder, Surf. Sci. 128 (1983) 350.
[172] A.V. Myshlyavtsev, A.A. Stepanov, C. Uebing, V.P. Zhdanov, Phys. Rev. B 52 (1995) 5977.
[173] C. Uebing, R. Gomer, Surf. Sci. 331–333 (1985) 930.
[174] I. Vattulainen, J. Merikoski, T. Ala-Nissila, S.C. Ying, Phys. Rev. Lett. 79 (1997) 257.
[175] F. Nieto, A.A. Tarasenko, C. Uebing, V. Pereyra, Europhys. Lett. 43 (1998) 558.
[176] J.S. Raut, K.A. Fichthorn, J. Chem. Phys. 110 (1999) 587.
[177] A.A. Tarasenko, L. Jastrabik, C. Uebing, Phys. Rev. B 57 (1998) 10166.
[178] S.Y. Krylov, J.J.M. Beenakker, M.C. Tringides, Surf. Sci. 420 (1999) 233.
[179] J. Kallunki, M. Dubé, T. Ala-Nissila, J. Phys.: Condens. Matter. 11 (1999) 9841.
[180] L. Hamburger, Kolloid Z. 23 (1918) 12.
[181] M. Volmer, I. Estermann, Z. Phys. 7 (1921) 13.
[182] M. Volmer, Trans. Faraday Soc. 28 (1932) 359.
[183] M. Volmer, G. Adhikari, Z. Phys. 35 (1925) 170.

[184] F. Moll, Z. Phys. Chem. 136 (1928) 183.
[185] J.A. Becker, Trans. Am. Electrochem. Soc. 55 (1929) 153.
[186] I. Langmuir, Chem. Rev. 6 (1929) 451.
[187] I. Langmuir, J.B. Taylor, Phys. Rev. 40 (1932) 463.
[188] J.B. Taylor, I. Langmuir, Phys. Rev. 44 (1933) 423.
[189] J.A. Becker, Trans. Faraday Soc. 28 (1933) 148.
[190] H. Cassel, Naturwiss. 14 (1926) 103.
[191] E.K. Rideal, Trans. Faraday Soc. 28 (1932) 139.
[192] I. Langmuir, Chem. Rev. 13 (1933) 147.
[193] G.M. Schwab (Ed.), Handbuch der Katalyse, Springer, Wien, 1943.
[194] E.W. Müller, Z. Phys. 108 (1938) 668.
[195] E.W. Müller, Z. Phys. 126 (1949) 642.
[196] E.W. Müller, Z. Elektrochem. 59 (1955) 372.
[197] R. Gomer, J.K. Hulm, J. Chem. Phys. 27 (1957) 1363.
[198] R. Gomer, Field Emission and Field Ionization, Harvard University Press, Cambridge, 1961.
[199] M. Drechsler, Z. Elektrochem. 58 (1954) 334.
[200] R. Gomer, in: V.T. Binh (Ed.), Surface Mobilities on Solid Materials, Plenum Press, New York, 1981, p. 127.
[201] R. Gomer, Surf. Sci. 299/300 (1994) 129.
[202] R. Gomer, Surf. Sci. 38 (1973) 373.
[203] M. Tringides, R. Gomer, Surf. Sci. 155 (1985) 254.
[204] M. Tringides, R. Gomer, J. Chem. Phys. 84 (1986) 4049.
[205] E.W. Müller, Z. Phys. 131 (1951) 136.
[206] E.W. Müller, T.T. Tsong, Field Ion Microscopy, Principles and Applications, Elsevier, New York, 1969.
[207] E.W. Müller, Z. Elektrochem. 61 (1957) 43.
[208] G. Ehrlich, F.G. Hudda, J. Chem. Phys. 44 (1966) 1039.
[209] D.W. Bassett, in: V.T. Binh (Ed.), Surface Mobilities on Solid Materials, Plenum Press, New York, 1983, p. 63.
[210] G. Ehrlich, Surf. Sci. 299/300 (1994) 628.
[211] T.T. Tsong, R. Casanova, Phys. Rev. Lett. 47 (1981) 113.
[212] R. Casanova, T.T. Tsong, Surf. Sci. 109 (1981) L497.
[213] T.T. Tsong, in: V.T. Binh (Ed.), Surface Mobilities on Solid Materials, Plenum Press, New York, 1983, p. 109.
[214] G.L. Kellogg, J. Chem. Phys. 83 (1985) 852.
[215] R. Viswanathan, D.R. Burgess, P.C. Stair, E. Weitz, J. Vac. Sci. Technol. 20 (1982) 605.
[216] S.M. George, A.M. deSantolo, R.B. Hall, Surf. Sci. 159 (1985) L425.
[217] E.G. Seebauer, L.D. Schmidt, Chem. Phys. Lett. 123 (1986) 129.
[218] S.M. George, in: M. Grunze, J.J. Weimer, H.J. Kreuzer (Eds.), Diffusion at Interfaces: Microscopic Concepts, Springer, Berlin, 1988, p. 2.
[219] J.L. Brand, S.M. George, Surf. Sci. 167 (1986) 341.
[220] J. Crank, The Mathematics of Diffusion, Oxford University Press, Oxford, 1975.
[221] J.N. Russell, R.B. Hall, Surf. Sci. 203 (1988) L642.
[222] M. Snabl, O. Borusik, V. Chab, M. Ondrejcek, W. Stenzel, H. Conrad, A.M. Bradshaw, Surf. Sci. 385 (1997) L1016.
[223] S.S. Mann, T. Seto, C.J. Barnes, D.A. King, Surf. Sci. 261 (1992) 155.
[224] M.V. Arena, E.D. Westre, S.M. George, Surf. Sci. 261 (1992) 129.
[225] G. Binnig, H. Rohrer, Helv. Phys. Acta 55 (1982) 726.
[226] G. Binnig, H. Rohrer, C. Gerber, E. Weibel, Phys. Rev. Lett. 49 (1982) 57.
[227] G. Binnig, H. Fuchs, E. Stoll, Surf. Sci. 169 (1986) L295.
[228] R. Gomer, Appl. Phys. A 39 (1986) 1.
[229] M. Sumetskii, A.A. Kornyshev, Phys. Rev. B 48 (1993) 17493.
[230] M. Sumetskii, A.A. Kornyshev, U. Stimming, Surf. Sci. 307–309 (1994) 23.
[231] M. Lozano, M. Tringides, Europhys. Lett. 30 (1995) 537.
[232] X. Wang, Q. Li, M.C. Tringides, Phys. Rev. B 57 (1998) 7275.
[233] A. Wander, J. Harrison, D.A. King, Surf. Sci. 397 (1998) 406.

[234] M.C. Tringides, M. Gupalo, Q. Li, X. Wang, in: A. Pekalski, K. Sznajd-Weron (Eds.), Anomalous Diffusion. From Basis to Applications, Springer, Berlin, 1999, p. 389.
[235] E. Ganz, S.K. Theiss, I.-S. Hwang, J. Golovchenko, Phys. Rev. Lett. 68 (1992) 1567.
[236] B.S. Swartzentruber, Phys. Rev. Lett. 76 (1996) 549.
[237] J.M. Gómez-Rodríguez, J.J. Sáenz, A.M. Baró, J.-Y. Veuillen, R.C. Cinti, Phys. Rev. Lett. 76 (1996) 799.
[238] T.R. Linderoth, S. Horch, E. Lægsgaard, I. Stensgaard, F. Besenbacher, Phys. Rev. Lett. 78 (1997) 4978.
[239] D.M. Eigler, E.K. Schweizer, Nature 344 (1990) 524.
[240] M. Bott, T. Michely, G. Comsa, Surf. Sci. 272 (1992) 161.
[241] H. Röder, H. Brune, J.P. Bucher, K. Kern, Surf. Sci. 298 (1993) 121.
[242] J. Wintterlin, R. Schuster, G. Ertl, Phys. Rev. Lett. 77 (1996) 123.
[243] J. Wintterlin, J. Trost, S. Renisch, R. Schuster, T. Zambelli, G. Ertl, Surf. Sci. 394 (1997) 159.
[244] S. Renisch, R. Schuster, J. Wintterlin, G. Ertl, Phys. Rev. Lett. 82 (1999) 3839.
[245] S. Renisch, Ph.D. Thesis, FU Berlin, 1999.
[246] P. Ebert, M.G. Lagally, K. Urban, Phys. Rev. Lett. 70 (1993) 1437.
[247] Y.W. Mo, Phys. Rev. Lett. 71 (1993) 2923.
[248] M. Bott, M. Hohage, M. Morgenstern, T. Michely, G. Comsa, Phys. Rev. Lett. 76 (1996) 1304.
[249] M.R. Sorensen, K.W. Jacobsen, H. Jonsson, Phys. Rev. Lett. 77 (1996) 5067.
[250] J. Li, R. Berndt, W.-D. Schneider, Phys. Rev. Lett. 76 (1996) 1888.
[251] J.M. Carpinelli, B.S. Swartzentruber, Phys. Rev. B 58 (1998) 13423.
[252] Y.W. Mo, J. Kleiner, M.B. Webb, M.G. Lagally, Phys. Rev. Lett. 66 (1991) 1998.
[253] J.A. Stroscio, D.T. Pierce, R.A. Dragoset, Phys. Rev. Lett. 70 (1993) 3615.
[254] H. Brune, H. Röder, C. Boragno, K. Kern, Phys. Rev. Lett. 73 (1994) 1955.
[255] H. Brune, Surf. Sci. Rep. 31 (1998) 121.
[256] H. Brune, G.S. Bales, J. Jacobsen, C. Boragno, K. Kern, Phys. Rev. B 60 (1999) 5991.
[257] J.W.M. Frenken, J.P. Toennies, C. Wöll, Phys. Rev. Lett. 60 (1988) 1727.
[258] J.W.M. Frenken, B.J. Hinch, in: E. Hulpke (Ed.), Helium Atom Scattering from Surfaces, Springer, Berlin, 1992, p. 287.
[259] J. Ellis, J.P. Toennies, Phys. Rev. Lett. 70 (1993) 2118.
[260] F. Hofmann, W. Schöllkopf, J.P. Toennies, in: Chemical Dynamics of Transient Species, Proceedings of the 38th Welch Foundation Symposium, 1994, p. 197.
[261] M. Bée, Quasielastic Neutron Scattering, Hilger, London, 1988.
[262] A.C. Levi, R. Spadacini, G.E. Tommei, Surf. Sci. 121 (1982) 504.
[263] L. Van Hove, Phys. Rev. 95 (1954) 249.
[264] G.H. Vineyard, Phys. Rev. 110 (1958) 999.
[265] M.F. Bertino, F. Hofmann, W. Steinhögl, J.P. Toennies, J. Chem. Phys. 105 (1996) 11297.
[266] C.T. Chudley, R.J. Elliott, Proc. Phys. Soc. 767 (1961) 353.
[267] A.P. Graham, W. Silvestri, J.P. Toennies, in: M.C. Tringides (Ed.), Surface Diffusion: Atomistic and Collective Processes, Plenum Press, New York, 1997, p. 565.
[268] J. Ellis, A.P. Graham, Surf. Sci. 377 (1997) 833.
[269] Q. Ge, D.A. King, J. Chem. Phys. 111 (1999) 9461.
[270] F. Hofmann, W. Schöllkopf, J.P. Toennies, Chem. Rev. 96 (1996) 1307.
[271] A.P. Graham, F. Hofmann, J.P. Toennies, G.P. Williams, C.J. Hirschmugl, J. Ellis, J. Chem. Phys. 108 (1998) 7825.
[272] A.P. Graham, J.P. Toennies, Europhys. Lett. 42 (1998) 449.
[273] A.P. Graham, A. Menzel, J.P. Toennies, J. Chem. Phys. 111 (1999) 1676.
[274] R.C.L. Bosworth, Proc. R. Soc. A 154 (1936) 112.
[275] W. Engel, M.E. Kordesch, H.H. Rotermund, S. Kubala, A. von Oertzen, Ultramicroscopy 36 (1991) 148.
[276] E. Bauer, Surf. Sci. 299/300 (1994) 102.
[277] H.H. Rotermund, Surf. Sci. Rep. 29 (1997) 265.
[278] A. von Oertzen, H.H. Rotermund, S. Nettesheim, Chem. Phys. Lett. 199 (1992) 131.
[279] A. von Oertzen, H.H. Rotermund, S. Nettesheim, Surf. Sci. Lett. 311 (1994) 322.
[280] M. Snabl, M. Ondrejcek, V. Chab, Z. Chvoj, W. Stenzel, H. Conrad, A.M. Bradshaw, J. Chem. Phys. 108 (1997) 4212.
[281] X.D. Zhu, T. Rasing, Y.R. Shen, Phys. Rev. Lett. 61 (1988) 2883.
[282] X.-D. Xiao, Y. Xie, Y.R. Shen, Surf. Sci. 271 (1992) 295.

[283] X.-D. Xiao, X.D. Zhu, W. Daum, Y.R. Shen, Phys. Rev. Lett. 66 (1991) 2352.
[284] G.A. Reider, U. Höfer, T.F. Heinz, Phys. Rev. Lett. 66 (1991) 1994.
[285] X.-D. Xiao, X.D. Zhu, W. Daum, Y.R. Shen, Phys. Rev. B 46 (1992) 9732.
[286] X.D. Zhu, Mod. Phys. Lett. B 6 (1992) 1217.
[287] X.-D. Xiao, Y. Xie, Y.R. Shen, Phys. Rev. B 48 (1993) 17452.
[288] J. Ma, X. Xiao, N.J. DiNardo, M.M.T. Loy, Phys. Rev. B 58 (1998) 4977.
[289] Z. Rosenzweig, I. Farbman, M. Asscher, J. Chem. Phys. 98 (1993) 8277.
[290] X.D. Zhu, A. Lee, A. Wong, U. Linke, Phys. Rev. Lett. 68 (1992) 1862.
[291] A. Lee, X.D. Zhu, L. Deng, U. Linke, Phys. Rev. B 46 (1992) 15472.
[292] A. Lee, X.D. Zhu, A. Wong, L. Deng, U. Linke, Phys. Rev. B 48 (1993) 11256.
[293] A. Wong, A. Lee, X.D. Zhu, Phys. Rev. B 51 (1995) 4418.
[294] X.D. Zhu, G.X. Gao, in: M.C. Tringides (Ed.), Surface Diffusion: Atomistic and Collective Processes, Plenum Press, New York, 1997, p. 607.
[295] G.X. Gao, E. Nabighian, X.D. Zhu, Phys. Rev. Lett. 79 (1997) 3696.
[296] X.-D. Xiao, Y. Xie, C. Jakobsen, H. Galloway, M. Salmeron, Y.R. Shen, Phys. Rev. Lett. 74 (1995) 3860.
[297] X.-D. Xiao, Y. Xie, C. Jakobsen, Y.R. Shen, Phys. Rev. B 56 (1997) 12529.
[298] E. Nabighian, X.D. Zhu, Phys. Rev. B 58 (1998) 7552.
[299] R.W. Verhoef, M. Asscher, Surf. Sci. 376 (1997) 395.
[300] A. Polak, G. Ehrlich, J. Vac. Sci. Technol. A 14 (1977) 407.
[301] M. Bowker, D.A. King, Surf. Sci. 94 (1980) 564.
[302] M. Croci, C. Félix, G. Vandoni, W. Harbich, R. Monot, Surf. Sci. 290 (1992) L667.
[303] M. Croci, C. Félix, G. Vandoni, W. Harbich, R. Monot, Surf. Sci. 307–309 (1994) 460.
[304] B. Poelsema, L.K. Verheij, G. Comsa, Phys. Rev. Lett. 49 (1982) 1731.
[305] J.E. Reutt-Robey, D.J. Doren, Y.J. Chabal, S.B. Christmann, Phys. Rev. Lett. 61 (1988) 2778.
[306] J.E. Reutt-Robey, D.J. Doren, Y.J. Chabal, S.B. Christmann, J. Chem. Phys. 93 (1990) 9113.
[307] T. Zambelli, J. Trost, J. Wintterlin, G. Ertl, Phys. Rev. Lett. 76 (1996) 795.
[308] H. Froitzheim, M. Schulze, Surf. Sci. 320 (1994) 85.
[309] S.E. Shore, J.P. Ansermet, C.P. Slichter, J.H. Sinfelt, Phys. Rev. Lett. 58 (1987) 953.
[310] L.R. Becerra, C.A. Klug, C.P. Slichter, J.H. Sinfelt, J. Phys. Chem. 97 (1993) 12014.
[311] J.P. Ansermet, C.P. Slichter, J.H. Sinfelt, Prog. NMR Spectrosc. 22 (1990) 401.
[312] C. Uebing, R. Gomer, Surf. Sci. 306 (1994) 419.
[313] C. Uebing, R. Gomer, Surf. Sci. 306 (1994) 427.
[314] C. Uebing, R. Gomer, Surf. Sci. 317 (1994) 165.
[315] C. Uebing, Phys. Rev. B 49 (1994) 13913.
[316] E.C. Viljoen, C. Uebing, Surf. Sci. 352–354 (1996) 1007.
[317] C.H. Mak, H.C. Andersen, S.M. George, J. Chem. Phys. 88 (1988) 4052.
[318] F. Nieto, C. Uebing, Ber. Bunsenges. Phys. Chem. 102 (1998) 156.
[319] S.C. Wang, R. Gomer, J. Chem. Phys. 83 (1985) 4193.
[320] P.W. Tamm, L.D. Schmidt, J. Chem. Phys. 54 (1971) 4775.
[321] C.H. Mak, J.L. Brand, B.G. Koehler, S.M. George, Surf. Sci. 188 (1987) 312.
[322] C.H. Mak, J.L. Brand, A.A. Deckert, S.M. George, J. Chem. Phys. 85 (1986) 1676.
[323] P. Feulner, D. Menzel, Surf. Sci. 154 (1985) 465.
[324] E.G. Seebauer, A.C.F. Kong, L.D. Schmidt, J. Chem. Phys. 88 (1988) 6597.
[325] T.W. Root, L.D. Schmidt, G.B. Fisher, Surf. Sci. 150 (1985) 173.
[326] K. Christmann, O. Schober, G. Ertl, M. Neumann, J. Chem. Phys. 60 (1974) 4528.
[327] D.R. Mullins, B. Roop, S.A. Costello, J.M. White, Surf. Sci. 186 (1987) 67.
[328] T.S. Lin, R. Gomer, Surf. Sci. 255 (1991) 41.
[329] D.R. Mullins, B. Roop, J.M. White, Chem. Phys. Lett. 129 (1986) 511.
[330] K. Christmann, G. Ertl, T. Pignet, Surf. Sci. 54 (1976) 365.
[331] A. Auerbach, K.F. Freed, R. Gomer, J. Chem. Phys. 86 (1987) 2356.
[332] S.M. Valone, A.F. Voter, J.D. Doll, Surf. Sci. 155 (1985) 687.
[333] J.G. Lauderdale, D.G. Truhlar, J. Chem. Phys. 84 (1986) 1843.

[334] T.R. Mattson, U. Engberg, G. Wahnström, Phys. Rev. Lett. 71 (1993) 2615.
[335] T.R. Mattson, G. Wahnström, Phys. Rev. B 51 (1994) 1885.
[336] T.R. Mattson, G. Wahnström, Phys. Rev. B 56 (1997) 14944.
[337] R.J. Behm, K.J. Christmann, G. Ertl, Surf. Sci. 99 (1980) 320.
[338] H. Conrad, G. Ertl, E.E. Latta, Surf. Sci. 41 (1974) 435.
[339] R. DiFoggio, R. Gomer, Phys. Rev. B 25 (1982) 2490.
[340] E.A. Daniels, R. Gomer, Surf. Sci. 336 (1995) 245.
[341] C. Dharmadhikari, R. Gomer, Surf. Sci. 143 (1984) 223.
[342] C.P. Flynn, A.M. Stoneham, Phys. Rev. B 1 (1970) 3966.
[343] S.E. Wonchoba, W.-P. Hu, D.G. Truhlar, Phys. Rev. B 51 (1995) 9985.
[344] S.E. Wonchoba, D.G. Truhlar, Phys. Rev. B 53 (1996) 11222.
[345] P. Blandin, P. Ballone, Surf. Sci. 331–333 (1995) 891.
[346] D.H. Zhang, J.C. Light, S.-Y. Lee, J. Chem. Phys. 111 (1999) 5741.
[347] G. Ehrlich, F.G. Hudda, J. Chem. Phys. 35 (1961) 1421.
[348] M.T. Martin, J.B. Hudson, J. Vac. Sci. Technol. 15 (1978) 474.
[349] L. Österlund, M.Ø. Pedersen, I. Stensgaard, E. Lægsgaard, F.M. Besenbacher, Phys. Rev. Lett. 83 (1999) 4812.
[350] J.J. Mortensen, M.V. Ganduglia-Pirovano, L.B. Hansen, B. Hammer, P. Stoltze, J.K. Nørskov, Surf. Sci. 422 (1999) 8.
[351] T. Matsushima, Surf. Sci. 197 (1988) L287.
[352] H. Shi, K. Jacobi, G. Ertl, J. Chem. Phys. 99 (1993) 9248.
[353] Y. Song, R. Gomer, Surf. Sci. 290 (1993) 1.
[354] C. Kohrt, R. Gomer, J. Chem. Phys. 52 (1970) 3283.
[355] J.-R. Chen, R. Gomer, Surf. Sci. 79 (1979) 413.
[356] R. Lewis, R. Gomer, Surf. Sci. 12 (1968) 157.
[357] C.T. Campbell, G. Ertl, H. Kuipers, J. Segner, Surf. Sci. 107 (1981) 220.
[358] D.H. Parker, M.E. Bartram, B.E. Koel, Surf. Sci. 217 (1989) 489.
[359] T.E. Madey, H.A. Engelhardt, D. Menzel, Surf. Sci. 48 (1975) 304.
[360] L. Surnev, G. Rangelov, G. Bliznakov, Surf. Sci. 159 (1985) 299.
[361] C. Stampfl, M. Scheffler, Phys. Rev. B 54 (1996) 2868.
[362] J. Trost, H. Brune, J. Wintterlin, R.J. Behm, G. Ertl, J. Chem. Phys. 108 (1998) 1740.
[363] J.C. Dunphy, P. Sautet, D.F. Ogletree, O. Dabbousi, M.B. Salmeron, Phys. Rev. B 47 (1993) 2320.
[364] D.G. Kelly, A.J. Gellmann, M. Salmeron, G.A. Somorjai, V. Maurice, H. Huber, J. Oudar, Surf. Sci. 204 (1988) 1.
[365] J.G. McCarty, H. Wise, J. Chem. Phys. 72 (1980) 6332.
[366] B.J. Hinch, J.W.M. Frenken, G. Zhang, J.P. Toennies, Surf. Sci. 259 (1991) 288.
[367] T.T. Tsong, in: V.T. Binh (Ed.), Surface Mobilities on Solid Materials, Plenum Press, New York, 1983, p. 247.
[368] J. Trost, T. Zambelli, J. Wintterlin, G. Ertl, Phys. Rev. B 54 (1996) 17850.
[369] T. Zambelli, J. Wintterlin, J. Trost, G. Ertl, Science 273 (1996) 1688.
[370] B. Hammer, Phys. Rev. Lett. 83 (1999) 3681.
[371] T.-U. Nahm, R. Gomer, J. Chem. Phys. 106 (1997) 10349.
[372] S.C. Ying, I. Vattulainen, J. Merikoski, T. Hjelt, T. Ala-Nissila, Phys. Rev. B 58 (1998) 2170.
[373] E.A. Daniels, R. Gomer, Surf. Sci. 397 (1998) 209.
[374] E. Kopatzki, R.J. Behm, Surf. Sci. 245 (1991) 255.
[375] R.E. Palmer, J. Vac. Sci. Technol. 12 (1975) 1403.
[376] P. Jakob, M. Gsell, D. Menzel, Phys. Rev. B 59 (1999) 13285.
[377] M. Schmid, G. Leonardelli, P. Varga, unpublished.
[378] R. Gomer, J. Phys. Chem. 63 (1959) 468.
[379] G. Ehrlich, F.G. Hudda, J. Chem. Phys. 30 (1959) 493.
[380] J.-R. Chen, R. Gomer, Surf. Sci. 94 (1980) 456.
[381] R. Opila, R. Gomer, Surf. Sci. 112 (1981) 1.
[382] D.L. Meixner, S.M. George, Surf. Sci 297 (1993) 27.
[383] D.L. Meixner, S.M. George, J. Chem. Phys. 98 (1993) 9115.
[384] T. Okano, Jpn. J. Appl. Phys. 22 (1983) 1496.
[385] K. Kern, R. David, P. Zeppenfeld, G. Comsa, Surf. Sci. 195 (1988) 353.

[386] H.R. Siddiqui, P.J. Chen, X. Guo, J.T. Yates, J. Chem. Phys. 92 (1990) 7690.
[387] L.W. Bruch, A.P. Graham, J.P. Toennies, Mol. Phys. 95 (1998) 579.
[388] D.S. Bethune, J.A. Barker, C.T. Rettner, J. Chem. Phys. 92 (1990) 6847.
[389] J.E. Müller, Phys. Rev. Lett. 65 (1990) 3021.
[390] P.A. Rejto, H.C. Anderson, J. Chem. Phys. 98 (1993) 7636.
[391] S. Horch, P. Zeppenfeld, G. Comsa, Surf. Sci. Lett. 331–333 (1995) 908.
[392] D.S. Sholl, R.T. Skodje, Physica D 71 (1994) 273.
[393] A. Liebsch, S. Gonçalves, M. Kiwi, Phys. Rev. B 60 (1999) 5034.
[394] O. Sneh, S.M. George, J. Chem. Phys. 101 (1994) 3287.
[395] P. Zeppenfeld, S. Horch, G. Comsa, Phys. Rev. Lett. 73 (1994) 1259.
[396] V. Marsico, M. Blanc, K. Kuhnke, K. Kern, Phys. Rev. Lett. 78 (1997) 94.
[397] V. Pouthier, C. Ramseyer, C. Girardet, K. Kuhnke, V. Marsico, M. Blanc, R. Schuster, K. Kern, Phys. Rev. B 56 (1997) 4211.
[398] R. Lewis, R. Gomer, Nuovo Cimento 5 (Suppl. I) (1967) 506.
[399] J.-R. Chen, R. Gomer, Surf. Sci. 81 (1979) 589.
[400] A.A. Deckert, J.L. Brand, M.V. Arena, S.M. George, Surf. Sci. 208 (1989) 441.
[401] H. Pfnür, P. Feulner, D. Menzel, J. Chem. Phys. 79 (1983) 4613.
[402] T.W. Root, L.D. Schmidt, G.B. Fisher, Surf. Sci. 150 (1985) 173.
[403] B. Roop, S.A. Costello, D.R. Mullins, J.M. White, J. Chem. Phys. 86 (1987) 3003.
[404] M. Kiskinova, D.W. Goodman, Surf. Sci. 108 (1981) 64.
[405] J. Bauhofer, M. Hock, J. Küppers, Surf. Sci. 191 (1987) 395.
[406] C.S. Feigerle, S.R. Desai, S.H. Overbury, J. Chem. Phys. 93 (1990) 787.
[407] K. Christmann, O. Schober, G. Ertl, J. Chem. Phys. 60 (1974) 4719.
[408] T.S. Lin, H.J. Lu, R. Gomer, Surf. Sci. 234 (1990) 251.
[409] E.G. Seebauer, A.C.F. Kong, L.D. Schmidt, Surf. Sci. 176 (1986) 134.
[410] V.J. Kwasniewski, L.D. Schmidt, Surf. Sci. 274 (1992) 329.
[411] J.V. Nekrylova, I. Harrison, J. Chem. Phys. 101 (1994) 1730.
[412] J.C. Tracy, J. Chem. Phys. 56 (1972) 2748.
[413] B. Briner, M. Doering, H.-P. Rust, A.M. Bradshaw, Science 278 (1997) 257.
[414] K. Horn, M. Hussain, J. Pritchard, Surf. Sci. 63 (1976) 244.
[415] J. Ahner, D. Mocuta, R.D. Ramsier, J.T. Yates, J. Chem. Phys. 105 (1996) 6553.
[416] Y. Song, R. Gomer, Surf. Sci. 295 (1993) 174.
[417] A. Eichler, J. Hafner, J. Chem. Phys. 109 (1998) 5585.
[418] V.P. Zhdanov, P.R. Norton, Surf. Sci. 350 (1996) 271.
[419] L. Wang, Q. Fe, G.D. Billing, Surf. Sci. 304 (1994) L413.
[420] D.R. Jennison, P.A. Schultz, M.P. Sears, Phys. Rev. Lett. 77 (1996) 4828.
[421] J. Ma, X. Xiao, M.M.T. Loy, Surf. Sci. 423 (1999) 85.
[422] J. Ma, L. Cai, X. Xiao, M.M.T. Loy, Surf. Sci. 425 (1999) 131.
[423] M. Torri, J.A.W. Elliott, J. Chem. Phys. 111 (1999) 1686.
[424] I. Farbman, Z. Rosenzweig, M. Asscher, Surf. Sci. 225 (1990) 249.
[425] J.V. Barth, T. Zambelli, J. Wintterlin, R. Schuster, G. Ertl, Phys. Rev. B 55 (1997) 12902.
[426] C.T. Campbell, Surf. Sci. 157 (1985) 43.
[427] N. Nakatsuji, K. Nakai, J. Chem. Phys. 98 (1993) 2423.
[428] P.A. Gravil, J.A. White, D.M. Bird, Surf. Sci. 352–354 (1996) 248.
[429] I. Farbman, M. Asscher, A. Ben-Saul, J. Chem. Phys. 104 (1996) 5674.
[430] W.A. Brown, Q. Ge, R.K. Sharma, D.A. King, Chem. Phys. Lett. 299 (1999) 253.
[431] R.M. van Hardeveld, M.J.P. Hopstaken, J.J. Lukkien, P.A.J. Hilbers, A.P.J. Hansen, R.A. van Santen, J.W. Niemandsverdriet, Chem. Phys. Lett. 302 (1999) 98.
[432] D.M. Bird, P.A. Gravil, Surf. Sci. 377–379 (1997) 555.
[433] T. Zambelli, Ph. D. Thesis, Freie Universität Berlin, 1996.
[434] R. Wang, K. Fichthorn, Phys. Rev. B 48 (1993) 18288.
[435] B.C. Stipe, M.A. Rezai, W. Ho, Science 279 (1998) 1907.

[436] J.L. Brand, M.V. Arena, A.A. Deckert, S.M. George, J. Chem. Phys. 92 (1990) 5136.
[437] M.V. Arena, A.A. Deckert, J.L. Brand, S.M. George, J. Phys. Chem. 94 (1990) 6792.
[438] M.V. Arena, E.D. Westre, S.M. George, J. Chem. Phys. 94 (1991) 4001.
[439] E.D. Westre, M.V. Arena, A.A. Deckert, J.L. Brand, S.M. George, Surf. Sci. 233 (1990) 293.
[440] S. Ichihara, J. Yoshinobu, H. Ogasawara, M. Nantoh, M. Kawai, K. Domen, J. Electron Spectrosc. Relat. Phenom. 88–91 (1998) 1003.
[441] J.C. Dunphy, M. Rose, S. Behler, D.F. Ogletree, M.B. Salmeron, P. Sautet, Phys. Rev. B 57 (1998) 12705.
[442] J. Yoshinobu, H. Tanaka, T. Kawai, M. Kawai, Phys. Rev. B 53 (1996) 7492.
[443] M. Fujisawa, T. Sekitani, Y. Morikawa, M. Nishijima, J. Phys. Chem. 95 (1991) 7415.
[444] J. Weckesser, J.V. Barth, K. Kern, J. Chem. Phys. 110 (1999) 5351.
[445] J. Weckesser, J.V. Barth, K. Kern, unpublished.
[446] L.J. Lauhon, W. Ho, J. Chem. Phys. 111 (1999) 5663.
[447] J.S. Raut, D.S. Sholl, K.A. Fichthorn, Surf. Sci. 389 (1998) 88.
[448] T. Ala-Nissila, S. Herminghaus, T. Hjelt, P. Leiderer, Phys. Rev. Lett. 76 (1996) 4003.
[449] T. Hjelt, T. Ala-Nissila, Surf. Sci. 454–456 (2000) 562.
[450] T. Hjelt, I. Vattulainen, J. Chem. Phys. 112 (2000) 4731.
[451] J.M. Lahtinen, T. Hjelt, T. Ala-Nissila, Surf. Sci. 454–456 (2000) 598.
[452] T.A. Jung, R.R. Schlittler, J.K. Gimzewski, Nature 386 (1997) 696.
[453] S.J. Stranick, M.M. Kamna, P.S. Weiss, Surf. Sci. 338 (1995) 41.
[454] J. Weckesser, J.V. Barth, C. Cai, B. Müller, K. Kern, Surf. Sci. 431 (1999) 268.
[455] J.V. Barth, J. Weckesser, C. Cai, L. Bürgi, O. Jeandupeux, P. Günter, K. Kern, Angew. Chem. Int. Ed. 39 (2000) 1230.
[456] T. Kawai, H. Tanaka, T. Nakagawa, Surf. Sci. 386 (1997) 124.
[457] M. Böhringer, K. Morgenstern, W.-D. Schneider, R. Berndt, F. Mauri, A. De Vita, R. Car, Phys. Rev. Lett. 83 (1999) 324.
[458] J. Weckesser, Ph.D. Thesis, EPF Lausanne, 2000.
[459] B.C. Stipe, M.A. Rezai, W. Ho, Phys. Rev. Lett. 81 (1998) 1263.
[460] J.K. Gimzewski, C. Joachim, R.R. Schlittler, V. Langlais, H. Tang, I. Johannsen, Science 281 (1998) 531.
[461] J.A. Barker, D.J. Auerbach, Surf. Sci. Rep. 4 (1984) 1.
[462] M. Grunze, H.J. Kreuzer (Eds.), Kinetics of Interface Reactions, Springer Series in Surface Science, Vol. 8, Springer, Berlin, 1987.
[463] S.T. Ceyer, Ann. Rev. Phys. Chem. 39 (1988) 479.
[464] C.R. Arumainayagam, R.J. Madix, Prog. Surf. Sci. 38 (1991) 1.
[465] C.T. Rettner, M.N.R. Ashfold (Eds.), Dynamics of Gas–Surface Interactions, Royal Society of Chemistry, London, 1991.
[466] J.A. Becker, C.D. Hartmann, J. Phys. Chem. 57 (1953) 157.
[467] G. Ehrlich, J. Chem. Phys. 59 (1955) 473.
[468] P.J. Kisliuk, J. Phys. Chem. Sol. 3 (1957) 95.
[469] P.J. Kisliuk, J. Phys. Chem. Sol. 5 (1958) 78.
[470] A. Cassuto, D.A. King, Surf. Sci. 102 (1981) 388.
[471] W.H. Weinberg, in: M. Grunze, H.J. Kreuzer (Eds.), Kinetics of Interface Reactions, Springer Series in Surface Science, Vol. 8, Springer, Berlin, 1987, p. 94.
[472] J.C. Tully, C.W. Muhlhausen, L.R. Ruby, Ber. Bunsenges. Phys. Chem. 86 (1982) 433.
[473] R. Sedlmeier, W. Brenig, Z. Phys. B 36 (1980) 245.
[474] K. Schönhammer, O. Gunnarsson, J. Electron Spectrosc. Relat. Phenom. 29 (1983) 91.
[475] F. Sols, N. Garcia, F. Flores, Surf. Sci. 146 (1984) L577.
[476] H. Metiu, J.W. Gadzuk, J. Chem. Phys. 74 (1981) 2641.
[477] T. Greber, Surf. Sci. Rep. 28 (1997) 1.
[478] J.C. Tully, Surf. Sci. 111 (1981) 461.
[479] J. Harris, B. Kasemo, Surf. Sci. 105 (1981) L281.
[480] J.C. Tully, Surf. Sci. 299/300 (1994) 667.
[481] D.J. Doren, J.C. Tully, J. Chem. Phys. 94 (1991) 8428.
[482] A. Gross, S. Wilke, M. Scheffler, Phys. Rev. Lett. 75 (1995) 2718.

[483] A. Eichler, J. Hafner, Phys. Rev. Lett. 79 (1997) 4481.
[484] G. Ertl, in: J.R. Andersen, M. Boudart (Eds.), Catalysis, Science and Technology, Springer, Berlin, 1987, p. 257.
[485] W.H. Weinberg, in: C.T. Rettner, M.N.R. Ashfold (Eds.), Dynamics of Gas–Surface Interactions, Royal Society of Chemistry, Cambridge, 1991, p. 171.
[486] J.L. Morrison, J.K. Roberts, Proc. R. Soc. London A 173 (1939) 13.
[487] I. Langmuir, Trans. Faraday Soc. 17 (1921) 607.
[488] M.W. Roberts, Appl. Surf. Sci. 52 (1991) 133.
[489] M.W. Roberts, Surf. Sci. 299/300 (1994) 769.
[490] C.T. Rettner, D.J. Auerbach, J.C. Tully, A.W. Kleyn, J. Phys. Chem. 100 (1996) 13021.
[491] W.F. Eglhoff, I. Jacob, Phys. Rev. Lett. 62 (1989) 921.
[492] S.C. Wang, G. Ehrlich, J. Chem. Phys. 94 (1991) 4071.
[493] D.E. Sanders, A.E. DePristo, Surf. Sci. 254 (1991) 341.
[494] M. Head-Gordon, J.C. Tully, C.T. Rettner, C.B. Mullins, D.J. Auerbach, J. Chem. Phys. 94 (1991) 1516.
[495] J. Strömquist, L. Bengtsson, M. Persson, B. Hammer, Surf. Sci. 397 (1998) 382.
[496] S. Caratzoulas, B. Jackson, M. Persson, J. Chem. Phys. 107 (1997) 6420.
[497] D.V. Shalashilin, B. Jackson, J. Chem. Phys. 109 (1998) 2856.
[498] C. Engdahl, G. Wahnström, Surf. Sci. 312 (1994) 429.
[499] G. Wahnström, A.B. Lee, J. Strömquist, J. Chem. Phys. 105 (1996) 326.
[500] S.P. Singh-Boparai, M. Bowker, D.A. King, Surf. Sci. 53 (1975) 55.
[501] T. Matsushima, Surf. Sci. 127 (1983) 403.
[502] W.D. Mieher, W. Ho, J. Chem. Phys. 91 (1989) 2755.
[503] W.D. Mieher, W. Ho, J. Chem. Phys. 99 (1993) 9279.
[504] T. Yamanaka, Y. Inoue, T. Matsushima, J. Chem. Phys. 119 (1999) 2597.
[505] J. Boh, G. Eilmsteiner, K.D. Rendulic, A. Winkler, Surf. Sci. 395 (1998) 98.
[506] S. Wehner, J. Küppers, J. Chem. Phys. 109 (1998) 294.
[507] T. Kammler, S. Wehner, J. Küppers, J. Chem. Phys. 109 (1998) 4071.
[508] H. Pölzl, G. Strohmeier, A. Winkler, J. Chem. Phys. 110 (1999) 1154.
[509] J.-Y. Kim, J. Lee, Phys. Rev. Lett. 82 (1999) 1325.
[510] S. Wehner, J. Küppers, J. Chem. Phys. 111 (1999) 3225.
[511] A.N. Artsykhovich, I. Harrison, Surf. Sci. 350 (1996) L199.
[512] Q.-S. Xin, X.-Y. Zhu, Surf. Sci. 347 (1996) 346.
[513] M. Sano, Y. Ohno, T. Yamanaka, T. Matsushima, E.B. Quinay, T. Matsushima, J. Chem. Phys. 108 (1998) 10231.
[514] P.S. Weiss, D.M. Eigler, Phys. Rev. Lett. 69 (1992) 2240.
[515] M.J. Abrams, P.S. Weiss, Surf. Sci. 312 (1994) 1.
[516] J.H. Ferris, J.G. Kushmerick, J.A. Johnson, P.S. Weiss, Surf. Sci. 446 (2000) 112.
[517] P. Zeppenfeld, J. George, M. Büchel, R. David, G. Comsa, Surf. Sci. 318 (1994) L1187.
[518] L. Vattuone, M. Rocca, C. Boragno, U. Valbusa, J. Chem. Phys. 101 (1994) 713.
[519] L. Vattuone, C. Boragno, M. Pupo, P. Restelli, M. Rocca, U. Valbusa, Phys. Rev. Lett. 72 (1994) 510.
[520] K.C. Prince, G. Paolucci, A.M. Bradshaw, Surf. Sci. 175 (1986) 101.
[521] F. Bartolucci, R. Franchy, J.C. Barnard, R.E. Palmer, Phys. Rev. Lett. 80 (1998) 5224.
[522] J.V. Barth, T. Zambelli, J. Wintterlin, G. Ertl, Chem. Phys. Lett. 270 (1997) 152.
[523] A. Raukema, A.W. Kleyn, Phys. Rev. Lett. 74 (1995) 4333.
[524] B. Briner, M. Doering, H.-P. Rust, A.M. Bradshaw, Phys. Rev. Lett. 78 (1997) 1516.
[525] A.C. Luntz, J. Grimblot, D.E. Fowler, Phys. Rev. B 39 (1989) 12903.
[526] C.T. Rettner, C.B. Mullins, J. Chem. Phys. 94 (1991) 1626.
[527] C. Puglia, A. Nilsson, B. Hernnäs, O. Karis, P. Bennich, N. Mårtensson, Surf. Sci. 342 (1995) 119.
[528] T. Zambelli, J.V. Barth, J. Wintterlin, G. Ertl, Nature 390 (1997) 495.
[529] H. Steininger, S. Lehwald, H. Ibach, Surf. Sci. 123 (1982) 1.
[530] B.C. Stipe, M.A. Rezai, W. Ho, J. Chem. Phys. 107 (1997) 6443.
[531] A.N. Artsykhovich, I. Harrison, Surf. Sci. 347 (1996) 303.
[532] H.S. Taylor, Proc. R. Soc. London A 108 (1925) 105.
[533] C. Astaldi, P. Geng, K. Jacobi, J. Electron Spectrosc. Relat. Phenom. 44 (1987) 175.

[534] L. Österlund, L. Zoric, B. Kasemo, Phys. Rev. B 55 (1999) 15452.
[535] T. Sasaki, T. Ohno, Surf. Sci. 433–435 (1998) 172.
[536] T. Sasaki, T. Ohno, Phys. Rev. B 60 (1999) 7824.
[537] K. Honkala, K. Laasonen, Phys. Rev. Lett. 84 (2000) 705.
[538] H. Brune, J. Wintterlin, R.J. Behm, G. Ertl, Phys. Rev. Lett. 68 (1992) 624.
[539] H. Brune, J. Wintterlin, J. Trost, G. Ertl, J. Wiechers, R.J. Behm, J. Chem. Phys. 99 (1993) 2128.
[540] D.S. Sholl, J. Chem. Phys. 106 (1997) 289.
[541] U. Diebold, W. Hebenstreit, G. Leonardelli, M. Schmid, P. Varga, Phys. Rev. Lett. 81 (1998) 405.
[542] B.C. Stipe, M.A. Rezaei, W. Ho, S. Gao, M. Persson, B.I. Lundqvist, Phys. Rev. Lett. 78 (1997) 4410.
[543] L. Bartels, M. Wolf, G. Meyer, K.H. Rieder, Chem. Phys. Lett. 291 (1998) 573.
[544] S. Schintke, S. Messerli, K. Morgenstern, J. Nieminen, W.-D. Schneider, submitted for publication.